

Bucknell University

## Bucknell Digital Commons

---

Master's Theses

Student Theses

---

Fall 2019

### Solar Powered Atmospheric Water Generation

Ben Conser

*Bucknell University*, bsc011@bucknell.edu

Follow this and additional works at: [https://digitalcommons.bucknell.edu/masters\\_theses](https://digitalcommons.bucknell.edu/masters_theses)



Part of the [Heat Transfer, Combustion Commons](#)

---

#### Recommended Citation

Conser, Ben, "Solar Powered Atmospheric Water Generation" (2019). *Master's Theses*. 228.  
[https://digitalcommons.bucknell.edu/masters\\_theses/228](https://digitalcommons.bucknell.edu/masters_theses/228)

This Masters Thesis is brought to you for free and open access by the Student Theses at Bucknell Digital Commons. It has been accepted for inclusion in Master's Theses by an authorized administrator of Bucknell Digital Commons. For more information, please contact [dcadmin@bucknell.edu](mailto:dcadmin@bucknell.edu).

I, Benjamin S. Conser, do grant permission for my thesis to be copied.



# Solar Powered Atmospheric Water Generation

by


Benjamin Scott Conser

A Thesis

Presented to the Faculty of  
Bucknell University

In Partial Fulfillment of the Requirements for the Degree of  
Master of Science in the Department of Mechanical Engineering

Approved:

  
Nate Siegel  
Thesis Advisor  
Constance Ziemian  
Chair, Department of Mechanical Engineering  
José Madero  
Engineering Thesis Committee  
Kevin Gilmore  
Engineering Thesis Committee

December 13, 2019

Date

## Acknowledgements

I would like to express my great appreciation to my research advisor Prof. Nate Siegel for his mentorship throughout the research process. His guidance has helped me grow as a problem solver and critical thinker.

I would also like to thank my thesis committee members, Prof. José Madero and Prof. Kevin Gilmore, for their assistance in reviewing my thesis.

The assistance provided by Hugh Weber regarding the hardware involved in the desiccant and prototype tests was greatly valued.

I wish to acknowledge the assistance provided by Daniel Johnson, Tim Baker, and Aaron Clark with the design and machining of several hardware components involved in the desiccant and prototype tests.

Thank you to Monica Hoover for her assistance in using the IC and ICP-MS systems when conducting tests on the condensate.

My special thanks are extended the staff of the Bucknell Mechanical Engineering Department for their continuous support throughout the research process.

Thanks to the Office of Graduate Studies for their support of my research.

Lastly, I would like to thank my parents for their endless love and support throughout my education at Bucknell University.

## Table of Contents

Acknowledgements.....	ii
List of Tables .....	v
List of Figures .....	vi
Nomenclature.....	viii
Abstract.....	ix
Chapter 1: Introduction.....	1
AWG Background .....	1
The Thermodynamics of AWG .....	4
AWG System Configurations .....	6
Refrigerated Atmospheric Water Generation .....	6
Compression and Condensation.....	8
Atmospheric Water Generation with Solid Desiccants.....	8
Atmospheric Water Generation with Liquid Desiccants .....	10
Multi-Stage Flash.....	11
Scope of Thesis.....	12
Chapter 2: Techno-Economic Modelling.....	14
Thermodynamic Modelling .....	14
Refrigerated Atmospheric Water Generation .....	14
Compression and Condensation.....	19
Atmospheric Water Generation with Solid Desiccants.....	21
Atmospheric Water Generation with Liquid Desiccants .....	24
Multi-Stage Flash.....	25
Thermodynamic Modelling Results Summary .....	30
Economic Modelling.....	31
Hardware Levelized Costs .....	31
LCOW Analyses .....	35
Optimal System Configuration .....	41
Chapter 3: Desiccant Evaluation.....	43
Testing Setup .....	46
Desiccant Tests .....	47
Effect of fan speed on water absorption .....	47
Effect of desiccant type on water absorption .....	49
Effect of mixing on water absorption .....	51
Effect of solution depth on water absorption.....	53
Effect of solution surface area on water absorption.....	55
Verification of equilibrium desiccant solution properties.....	55
Optimizing water absorption.....	57
Chapter 4: Prototype Development.....	58
First System Prototype.....	58
Status of the First Prototype.....	61
Second System Prototype .....	62
Chapter 5: Prototype Evaluation and Modeling Validation.....	75
Convection Losses Testing .....	75
Prototype Testing – Atmospheric Pressure.....	76
Testing Procedure .....	77

Testing Results.....	84
Prototype Testing – Sub-Atmospheric Pressure .....	86
Testing Procedure .....	86
Testing Results.....	88
Modeling Validation .....	89
Evaluation of Desiccant Loss.....	90
Condensate Contaminant Testing .....	92
Chapter 6: Conclusions and Future Work.....	94
References.....	96

## List of Tables

<b>Table 1:</b> RAWG system operation for different operating times .....	19
<b>Table 2:</b> SEC for RAWG system with continuous operation.....	19
<b>Table 3:</b> SEC of a CC system.....	20
<b>Table 4:</b> Performance of a DAWG batch-style system at atmospheric pressure.....	23
<b>Table 5:</b> SEC of a DAWG batch-style system at atmospheric pressure.....	23
<b>Table 6:</b> Performance of a DAWG batch-style system at sub-atmospheric pressure.....	23
<b>Table 7:</b> SEC of a DAWG batch-style system at sub-atmospheric pressure.....	23
<b>Table 8:</b> Performance of a DAWG batch-style system with latent energy recovery .....	24
<b>Table 9:</b> SEC of a DAWG batch-style system with latent energy recovery.....	24
<b>Table 10:</b> Performance of a DAWG continuous-style system with no energy recovery .....	25
<b>Table 11:</b> SEC of a DAWG continuous-style system with no energy recovery.....	25
<b>Table 12:</b> Performance of a DAWG continuous-style system with sensible and latent energy recovery .....	25
<b>Table 13:</b> SEC of a DAWG continuous-style system with sensible and latent energy recovery ..	25
<b>Table 14:</b> Minimum SEC estimates for several AWG system configurations .....	30
<b>Table 15:</b> Refrigeration compressor specifications [43] [44].....	32
<b>Table 16:</b> Baseboard heater specifications [48] .....	33
<b>Table 17:</b> Heat pump specifications [50] .....	34
<b>Table 18:</b> System configurations with no energy recovery analyzed in economic analysis .....	36
<b>Table 19:</b> System configurations with energy recovery analyzed in economic analysis .....	37
<b>Table 20:</b> Minimum LCOW breakdown for batch-style DAWG system with latent energy recovery .....	39
<b>Table 21:</b> Minimum LCOW breakdown for a continuous-style DAWG system with latent and sensible energy recovery using minimum PV electricity cost .....	40
<b>Table 22:</b> LCOW breakdown for a continuous-style DAWG system with latent and sensible energy recovery using current PV electricity cost .....	41
<b>Table 23:</b> Water absorption versus solution surface area.....	55
<b>Table 24:</b> Theoretical and experimental equilibrium desiccant mass fractions.....	56
<b>Table 25:</b> Test matrix for tests conducted at atmospheric pressure.....	77
<b>Table 26:</b> Comparison of final desiccant mass fraction measurement methods.....	84
<b>Table 27:</b> Test matrix for tests conducted at sub-atmospheric pressure.....	86
<b>Table 28:</b> Comparison of condensate contaminant concentrations (ppb) to contaminant limits from literature .....	92



## List of Figures

<b>Figure 1:</b> AWG Design Types Overview [5] .....	2
<b>Figure 2:</b> Water Scarcity Map [11] .....	3
<b>Figure 3:</b> Regions with good solar resources and physical water stress .....	4
<b>Figure 4:</b> Psychrometric Chart [12].....	5
<b>Figure 5:</b> RAWG system using cooled air to reduce the temperature of the refrigerant in the condenser .....	7
<b>Figure 6:</b> RAWG system with sensible energy recovery .....	7
<b>Figure 7:</b> Compression and Condensation AWG with energy recovery .....	8
<b>Figure 8:</b> Batch-style DAWG system using a solid desiccant .....	9
<b>Figure 9:</b> Batch-style DAWG system using a solid desiccant and incorporating latent energy recovery .....	10
<b>Figure 10:</b> Continuous operation liquid desiccant AWG system with sensible and latent energy recovery .....	11
<b>Figure 11:</b> Multi-Stage Flash system using liquid desiccant.....	12
<b>Figure 12:</b> Thermal energy breakdown of moist air cooling for a RAWG system without a precooler .....	16
<b>Figure 13:</b> Thermal energy breakdown of moist air cooling for a RAWG system with a precooler .....	16
<b>Figure 14:</b> Annual water and ice production from a continuous operation RAWG system .....	17
<b>Figure 15:</b> Annual water generation of a RAWG system versus the condenser operating temperature .....	18
<b>Figure 16:</b> SEC of an MSF AWG system as a function of inlet desiccant temperature .....	27
<b>Figure 17:</b> SEC of an MSF AWG system as a function of top brine temperature .....	28
<b>Figure 18:</b> Relation of minimum free energy, SEC, system efficiency, and top brine temperature for an MSF AWG system .....	29
<b>Figure 19:</b> LCOW breakdown for a desalination plant [52] .....	34
<b>Figure 20:</b> LCOW of a DAWG batch-style system with no energy recovery at atmospheric pressure .....	38
<b>Figure 21:</b> LCOW of a DAWG batch-style system with no energy recovery at sub-atmospheric pressure .....	38
<b>Figure 22:</b> LCOW of a batch-style DAWG system with latent energy recovery.....	39
<b>Figure 23:</b> LCOW of a continuous-style DAWG system with latent and sensible energy recovery .....	40
<b>Figure 24:</b> Plot showing relationship between desiccant mass fraction, dry bulb temperature, and relative humidity for $\text{CaCl}_2$ solutions at one atmosphere [36].....	44
<b>Figure 25:</b> Plot showing relationship between desiccant mass fraction, dry bulb temperature, and relative humidity for $\text{LiCl}$ desiccant solutions at one atmosphere [36] .....	45
<b>Figure 26:</b> Schematic of the experimental setup for desiccant testing [53] [54].....	46
<b>Figure 27:</b> Experimental setup for desiccant testing .....	46
<b>Figure 28:</b> Mass of water absorbed over time, comparing low and high fan speeds .....	47
<b>Figure 29:</b> Desiccant mass fraction over time, comparing low and high fan speeds .....	48
<b>Figure 30:</b> Water absorption rate over time, comparing low and high fan speeds.....	48
<b>Figure 31:</b> Mass of water absorbed over time, comparing $\text{CaCl}_2$ and $\text{LiCl}$ .....	49
<b>Figure 32:</b> Desiccant mass fraction over time, comparing $\text{CaCl}_2$ and $\text{LiCl}$ .....	50

<b>Figure 33:</b> Water absorption rate, comparing $\text{CaCl}_2$ and $\text{LiCl}$ .....	51
<b>Figure 34:</b> Mass of water absorbed over time, comparing mixing and no mixing.....	52
<b>Figure 35:</b> Desiccant mass fraction over time, comparing mixing and no mixing .....	52
<b>Figure 36:</b> Water absorption rate, comparing mixing and no mixing .....	53
<b>Figure 37:</b> Desiccant mass fraction over time, comparing 1/4" and 1/2" solution depths .....	54
<b>Figure 38:</b> Water absorption rate over time, comparing 1/4" and 1/2" solution depths.....	54
<b>Figure 39:</b> Regenerator Solidworks assembly model.....	58
<b>Figure 40:</b> Schematic of first system prototype during water absorption .....	59
<b>Figure 41:</b> Schematic of first system prototype during regeneration .....	59
<b>Figure 42:</b> Positioning of sensors within the regenerator of the first system prototype.....	60
<b>Figure 43:</b> Correlation between resistance heating power and time to perform a regeneration test using the first system prototype .....	62
<b>Figure 44:</b> AWG system test setup schematic.....	63
<b>Figure 45:</b> Regenerator desiccant pan wire handle .....	64
<b>Figure 46:</b> Regenerator layout.....	64
<b>Figure 47:</b> Ambient moist air flow through the system when the desiccant is absorbing moisture .....	65
<b>Figure 48:</b> Fan setup with the acrylic lid used when the regenerator is absorbing moisture .....	65
<b>Figure 49:</b> Aluminum regenerator lid with foam insulation and data collection hardware installed .....	66
<b>Figure 50:</b> Bare aluminum lid with Swagelok port connectors exposed.....	67
<b>Figure 51:</b> Aluminum lid with a Dragon Skin™ silicone gasket .....	68
<b>Figure 52:</b> Condenser shape and orientation.....	69
<b>Figure 53:</b> Storage vessel and condenser positioning .....	70
<b>Figure 54:</b> Welch DuoSeal 1400 Vacuum Pump [56] .....	71
<b>Figure 55:</b> Temperature controller box .....	72
<b>Figure 56:</b> Temperature controller electrical schematic .....	73
<b>Figure 57:</b> DAQ system electrical schematic.....	74
<b>Figure 58:</b> Cylindrical heat transfer model of the regenerator .....	76
<b>Figure 59:</b> Diagram showing the process of water vapor absorption.....	77
<b>Figure 60:</b> Diagram showing the process of water vapor regeneration.....	78
<b>Figure 61:</b> Othmer chart showing relation between solution temperature, vapor pressure, and desiccant mass fraction for $\text{CaCl}_2$ solutions [36] .....	80
<b>Figure 62:</b> Othmer chart showing relation between solution temperature, vapor pressure, and desiccant mass fraction for $\text{LiCl}$ solutions [36] .....	81
<b>Figure 63:</b> Desiccant crystalizing after a regeneration test .....	83
<b>Figure 64:</b> Experimental SEC breakdown for $\text{CaCl}_2$ at atmospheric pressure.....	84
<b>Figure 65:</b> Experimental SEC breakdown for $\text{LiCl}$ at atmospheric pressure .....	85
<b>Figure 66:</b> Experimental SEC breakdown for $\text{CaCl}_2$ at sub-atmospheric pressure .....	88
<b>Figure 67:</b> Experimental SEC breakdown for $\text{LiCl}$ at sub-atmospheric pressure .....	89

## Nomenclature

**AWG:** atmospheric water generation; process by which liquid water is extracted from the water vapor in ambient air

**CC:** compression and condensation-based atmospheric water generation

**DAQ:** data acquisition system

**DAWG:** desiccant-based atmospheric water generation

**Desiccant:** hygroscopic material used to absorb water vapor out of ambient air

**Desiccant Mass Fraction ( $\beta$ ):** ratio of the mass of desiccant in a solution to the total solution mass

**GHI:** global horizontal irradiance; total amount of solar radiation incident on a horizontal surface

**IC:** ion chromatograph

**ICP-MS:** inductively coupled plasma mass spectrometer

**LCOE:** levelized cost of energy; monetary cost per unit of electric or work energy

**LCOH:** levelized cost of heating; monetary cost per unit of thermal energy

**LCOW:** levelized cost of water; monetary cost required to produce a unit of water

**MSF:** multi-stage flash distillation

**PV:** photovoltaics

**RAWG:** refrigeration-based atmospheric water generation

**Regeneration:** process of vaporizing and capturing previously absorbed water vapor from a desiccant material

**Regenerator:** hardware associated with DAWG processes where regeneration occurs

**SEC:** specific energy consumption; energy required to produce a unity of water

**TMY:** typical meteorological year; meteorological dataset with data values for every hour in a year for a given geographical location

**Water Stress:** situation where the local demand for water exceeds the water available

## Abstract

Several atmospheric water generation (AWG) system configurations were analyzed to determine the feasibility of AWG as a method to combat water stress. In order to best combat water stress, AWG must be implemented in such a way which minimizes the energetic and monetary cost of water production. Thermodynamic and economic analyses were used to compare the performance of several AWG system configurations. Metrics such as specific energy consumption (SEC) and levelized cost of water (LCOW), which measure the energetic and monetary cost of water production respectively, were used to compare each system. Using this approach, the optimal system configuration was found to be a batch-style desiccant-based AWG system which utilizes latent energy recovery. The minimum theoretical SEC and LCOW for this system are 210 kWh/m<sup>3</sup> and 3.34 \$/m<sup>3</sup> (12.64 \$/Kgal). A prototype of a batch-style desiccant-based AWG system with no energy recovery was developed and tested. The evaluation of this system validated the approach used in the thermodynamic analyses for predicting the system's performance. Future work will involve implementing latent energy recovery and redesigning some of the system components in order to further decrease the system's SEC.

# Chapter 1: Introduction

## AWG Background

Atmospheric water generation (AWG) is the process by which liquid water is extracted from the water vapor in ambient air. The significance of AWG is that it can combat physical water scarcity by supplying freshwater to locations where the local liquid water resource is physically lacking. Passive AWG processes do not require an energy input and include methods such as fog harvesting [1], dew collection [2], and controlled convection [3]. Passive techniques are constrained to operate when there is high humidity or a large enough temperature swing to allow for spontaneous condensation. Because of these constraints, the locations where passive AWG may be implemented are limited and typically do not align with locations experiencing physical water scarcity, which tend to have low humidity.

Active AWG processes require an energy input to operate, in the form of either electricity or heat. Active processes include refrigerated surface cooling (RAWG), compression and condensation (CC), or a temperature and pressure swing in conjunction with solid or liquid desiccants (DAWG). Several AWG technologies have been presented previously in literature [4] [5]. These AWG technologies are given in Figure 1 [5].

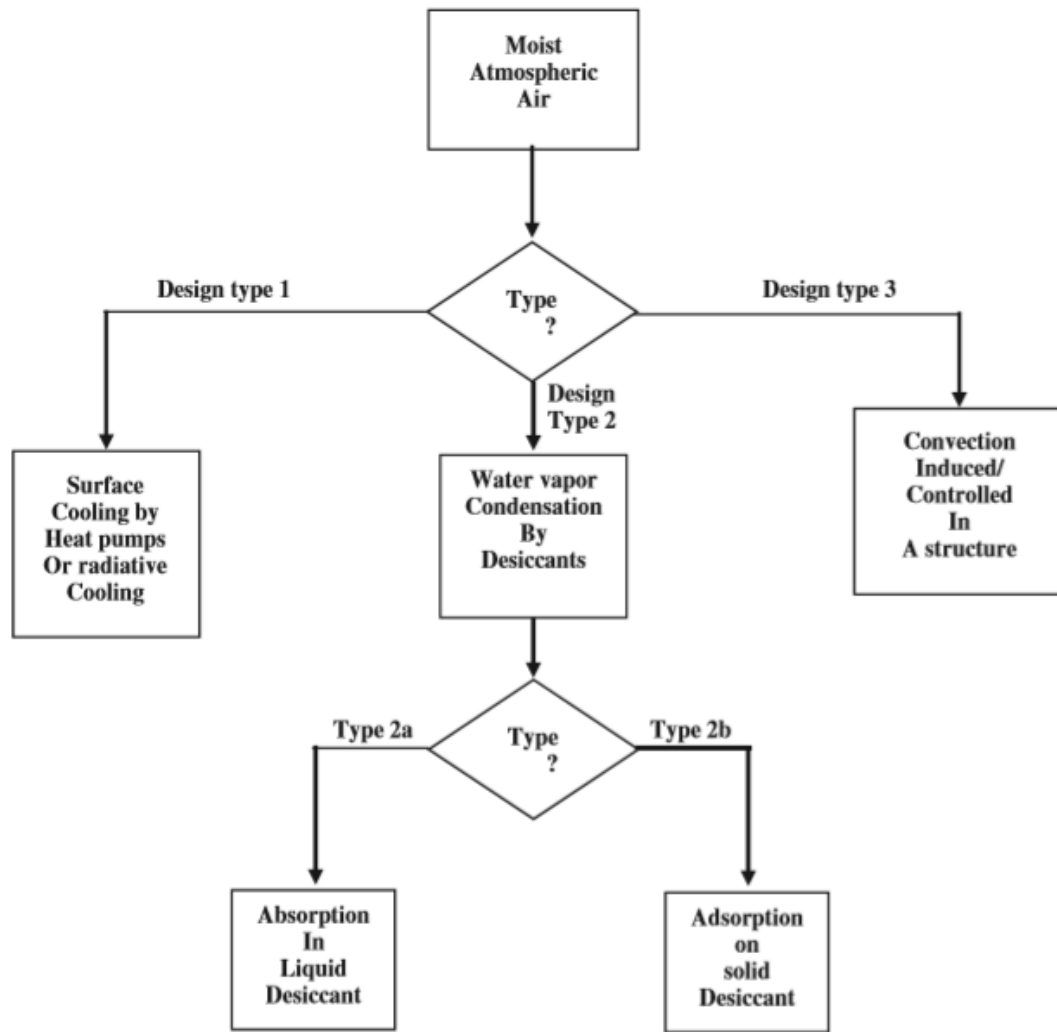


**Figure 1:** AWG Design Types Overview [5]

While an AWG system could be implemented anywhere in the world, it would provide the most benefit being implemented in locations with water stress. Water stress describes a situation where the local demand for water exceeds the water available [6]. Water stress could be driven due to a limited resource availability (physical water scarcity) or due to a poor local economy and infrastructure (economic water scarcity). Solutions to physical water scarcity require the development and implementation of new technologies and water capture methods, such as AWG.

There are several different methods and metrics that can be used to analyze physical water scarcity. One method [7] looks at the most basic water requirements for survival, which include drinking water, sanitation, bathing, cooking, and natural ecosystem requirements. Gleick's estimate for the average water requirements is 50 liters per day per capita. Other water needs such as agriculture and power generation were not considered with this method.

Another population-based water scarcity index [8] does take these additional water needs into account. This index compares the number of people dependent on a volume of water used on an annual basis. Falkenmark describes the threshold for water stress as 600 – 1000 persons per  $10^6 \text{ m}^3$

per year ( $1000 - 1700 \text{ m}^3$  per capita per year). A location above  $2000 \text{ persons per } 10^6 \text{ m}^3$  per year (below  $500 \text{ m}^3$  per capita per year) is described as having absolute water scarcity.

The International Water Management Institute (IWMI) [9] developed a criterion for water scarcity based on the water resources in a country. IWMI defines physical water scarcity as when the ratio of the primary water supply to utilizable water supply is greater than 60%. The primary water supply is the water used by the local population, while the utilizable water supply is the total water available to be used in a region. Another IWMI study [10] grouped countries into several groupings of water scarcity levels, based on the projected percent increase in water withdrawals and the projected total water withdrawals as a percentage of annual water resources. A water scarcity map using this area-based metric is shown in Figure 2 [11].

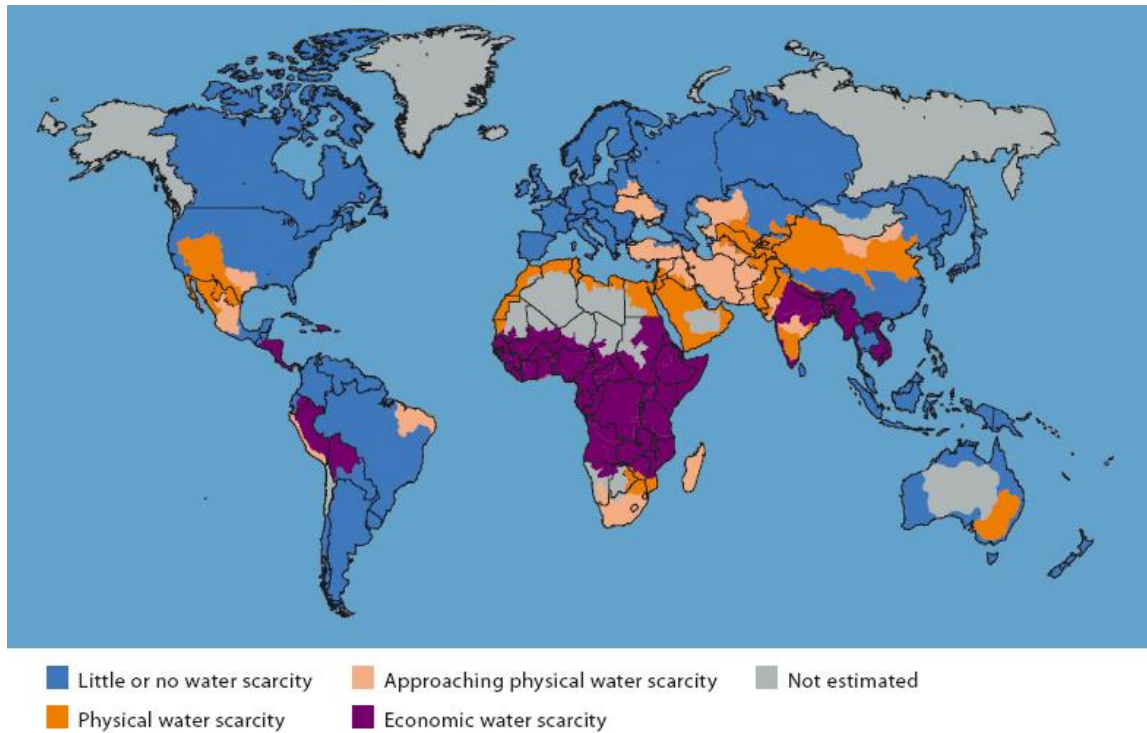


**Figure 2:** Water Scarcity Map [11]

One way to ensure that AWG provides the most benefit is to have the ability to operate off-grid. Off-grid capabilities can be achieved if the system requires no external water or power from the grid. One way to provide off-grid electric power is with solar electricity. This would require that the operating region has exceptional annual solar resource availability. Figure 3 highlights regions experiencing physical water scarcity as well as exceptional annual solar resource availability (annual global horizontal irradiance (GHI)  $> 4.5 \text{ kWh/m}^2/\text{day}$ ).



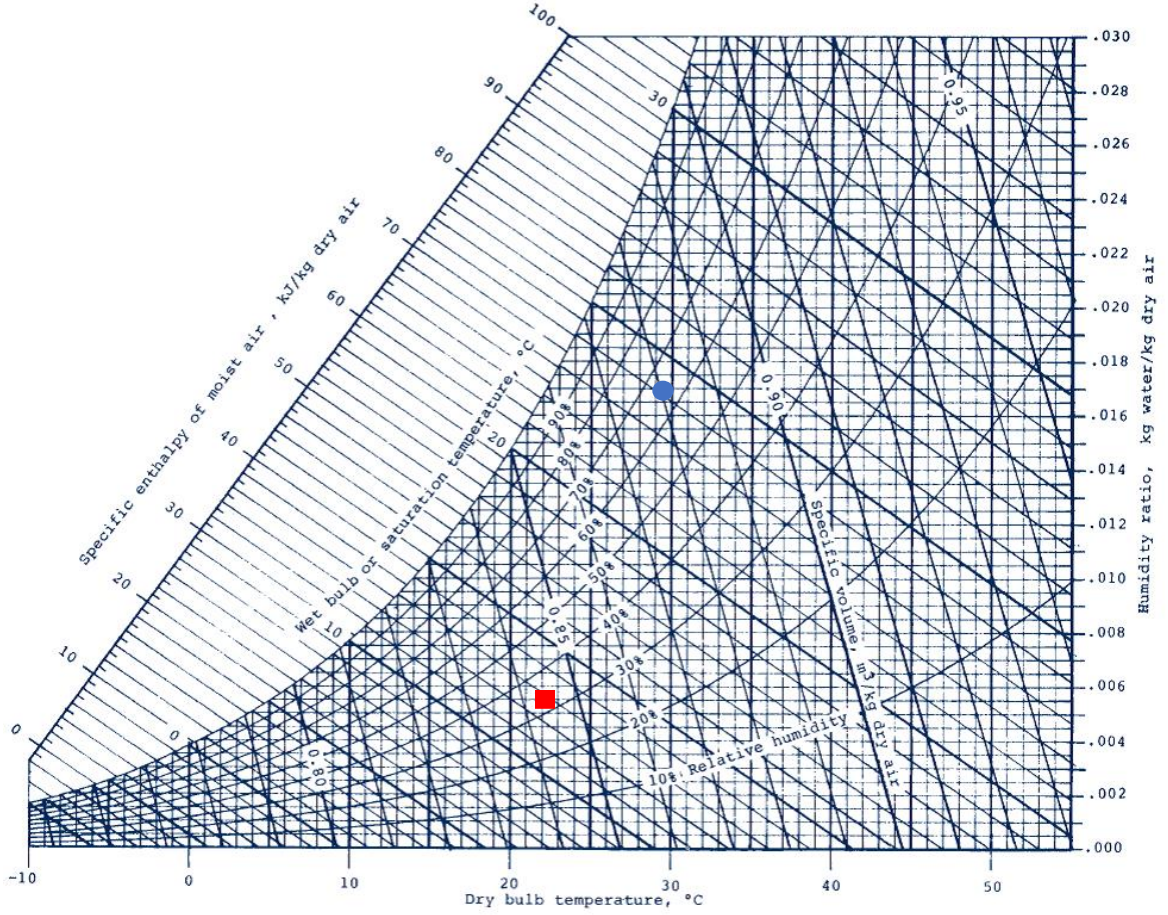
**Figure 3:** Regions with good solar resources and physical water stress

Figure 3 shows that there are several regions experiencing physical water scarcity and excellent solar resources. This means that external water or power from the grid would not be required in these regions, allowing for a standalone solar-driven AWG unit to be implemented. This means that solar powered AWG would be most valuable in these regions.

### The Thermodynamics of AWG

When considering the thermodynamics of AWG, there is a correlation between the energy consumption and the amount of water in the air. The amount of water in the air is related to the dry bulb temperature and relative humidity. This relationship can be seen using a psychrometric chart, such as that in Figure 4 [12].





**Figure 4:** Psychrometric Chart [12]

The typical conditions of a dry location (Daggett, CA) is highlighted by the square, whereas the typical conditions of a more humid location (U.S. Virgin Islands) is highlighted by the circle. For water to be extracted, first the moist air must reach its saturation point, which is indicated by the 100% relative humidity curve on the psychrometric chart. This can be done in one of two ways. The first method is to cool the moist air to the saturation temperature. The second method is to compress the moist air to the saturation pressure. Once at the saturation point, the enthalpy of vaporization must be extracted to condense the saturated water vapor. This is typically facilitated using a heat exchanger.

When using the cooling method, the minimum required energy for AWG can be modelled using Eq. 1

$$Q_{min} \left[ \frac{kJ}{kg_{water\ vapor}} \right] = \frac{\Delta h_{sat}}{\omega} + \Delta h_{vap} \quad (1)$$

$\Delta h_{sat}$  is the required enthalpy change of the air to reach its saturation temperature,  $\Delta h_{vap}$  is the enthalpy of vaporization of water vapor at the saturation temperature, and  $\omega$  is the absolute humidity ratio. The value for  $\Delta h_{sat}$  is 16 kJ/kg<sub>dry air</sub> and 6 kJ/kg<sub>dry air</sub> for Daggett, CA and the U.S. Virgin Islands respectively. The value for  $\Delta h_{vap}$  can be taken as 2442 kJ/kg<sub>water vapor</sub>. The absolute humidity ratio is 0.0055 and 0.017 for Daggett, CA and the U.S. Virgin Islands

respectively. These values give a minimum energy of 5351  $\text{kJ}/\text{kg}_{\text{water vapor}}$  for Daggett, CA and 2795  $\text{kJ}/\text{kg}_{\text{water vapor}}$  for the U.S. Virgin Islands.

When using the compression method, the enthalpy change required to reach the saturation pressure can be represented by the isothermal compression work required by a compressor to compress the air to the saturation pressure from ambient pressure. When using the compression method, the minimum energy required for AWG can be modelled using Eq. 2

$$E_{\min} \left[ \frac{\text{kJ}}{\text{kg}_{\text{water vapor}}} \right] = \frac{RT_{\infty}}{\omega} \ln \frac{P_{\text{sat}}}{P_{\infty}} + \Delta h_{\text{vap}} \quad (2)$$

where  $R$  is the ideal gas constant,  $T_{\infty}$  is the ambient temperature, and  $P_{\text{sat}}$  and  $P_{\infty}$  are the saturation and ambient pressures respectively. The value of the compressive work is 25  $\text{kJ}/\text{kg}_{\text{dry air}}$  and 16  $\text{kJ}/\text{kg}_{\text{dry air}}$  for Daggett, CA and the U.S. Virgin Islands respectively. Using the same values as before for  $\Delta h_{\text{vap}}$  and  $\omega$ , the minimum energy is 6897  $\text{kJ}/\text{kg}_{\text{water vapor}}$  for Daggett, CA and 3383  $\text{kJ}/\text{kg}_{\text{water vapor}}$  for the U.S. Virgin Islands.

In order to attain 100% relative humidity and decrease the minimum energy requirement, a separator such as a membrane may be implemented in the system. A separator would be optimal for the compression method since the compressor can act as a vacuum pump to draw the dry air through the separator while capturing the water vapor. The advantage to this approach is that the work required to compress the air can be avoided. However, a work input will be required to draw the collected water vapor through the separator. Once at the outlet of the separator, the water vapor will be saturated. If heat transfer is facilitated from the water vapor, then the water vapor will spontaneously condense.

## AWG System Configurations

There are several different methods that can be used to produce water from atmospheric humidity. These can be split into active and passive processes. Active processes require energy input in the form of either electricity or heat, whereas passive processes do not require energy input. Active processes can be coupled to a solar energy resource. The solar energy resource may provide energy directly via a thermal collector, or indirectly via photovoltaics or concentrating solar power. Passive processes include fog harvesting [1], dew collection [2], and controlled convection [3]. Passive processes are constrained to operate only under high humidity or large enough temperature swings to allow for spontaneous condensation. Because of this constraint, passive processes were not considered in system analyses.

Several active AWG processes were considered for the techno-economic analyses. These systems include a refrigeration system, a compression and condensation system, a desiccant-based system. Desiccant systems have several potential operating configurations, including the utilization of a pressure and/or temperature swing. Thermal desalination methods such as a multi-stage flash system using liquid desiccants were also considered.

## Refrigerated Atmospheric Water Generation

In refrigerated atmospheric water generation (RAWG) humid air is cooled to the dew point temperature. Once this temperature is reached, water condenses on the heat transfer surfaces of the

refrigeration hardware, which typically utilizes vapor compression technology. Some systems have been deployed commercially [13] which can produce water on the order of liters/day. Schematics showing a RAWG system both without / with sensible energy recovery are shown in Figures 5 and 6 respectively.

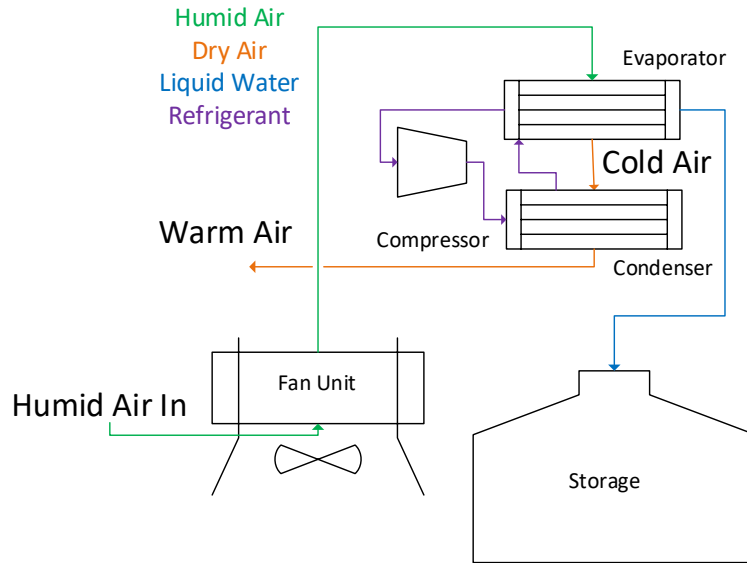


**Figure 5:** RAWG system using cooled air to reduce the temperature of the refrigerant in the condenser

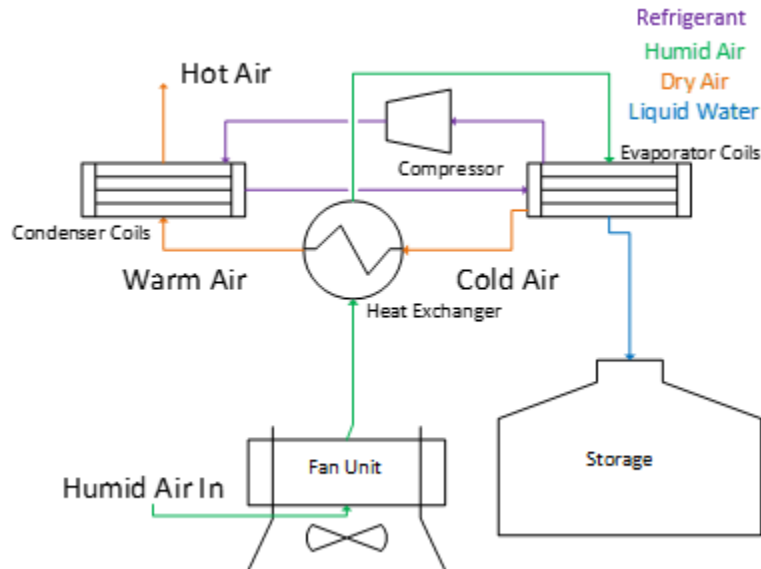


**Figure 6:** RAWG system with sensible energy recovery

In operation, a fan blows humid ambient air through a refrigerated heat exchanger (evaporator), so that enough thermal energy is extracted from the humid air to cool it to the dewpoint temperature or slightly below. This enables a portion of the humidity in the air to condense on the walls of the evaporator. The condensate is then collected and stored in a storage tank.

Two methods for improving the RAWG system's performance are shown in Figures 5 and 6. In Figure 5, the cold air exiting the evaporator is subsequently passed through another refrigerated heat exchanger (condenser). The purpose of this is to further cool the refrigerant before it is used again in the evaporator. This increases the heat transfer in the evaporator and possibly improves the coefficient of performance ( $COP_R$ ).

In order to recover sensible heat, a heat exchanger (precooler) may be incorporated between the fan and the evaporator, as seen in Figure 6. The cool air exiting the evaporator may be used to precool the humid air before it enters the evaporator, thereby reducing the evaporator's cooling load. Because the thermal capacity of the dry air and the humid air are very similar, the amount of sensible energy that can be recovered can be relatively high when compared to the thermal load on the evaporator.

### Compression and Condensation

In a compression and condensation AWG system (CC), humid air is compressed to a pressure above the saturation pressure, causing the water vapor to condense. While no systems which use this approach are currently commercially available, this method has been proposed in literature [14] [15]. A schematic of a CC AWG system is given in Figure 7.

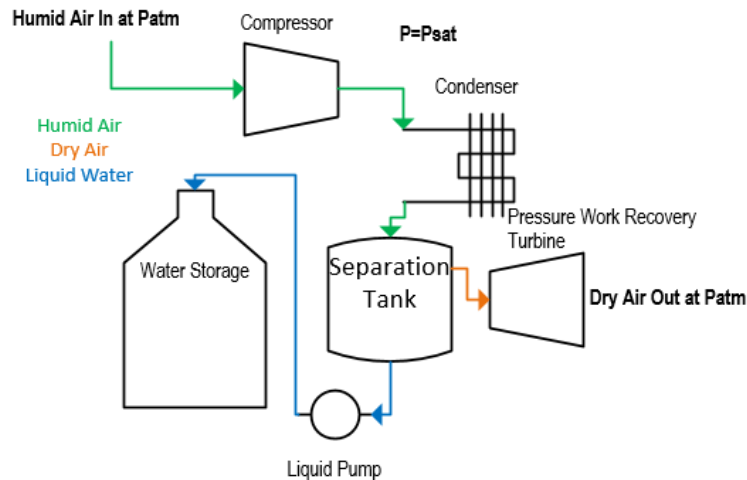


**Figure 7:** Compression and Condensation AWG with energy recovery

In a CC system, humid air is compressed by a compressor, which increases the water vapor pressure above the water vapor's saturation pressure at ambient temperature. The saturated water vapor is then forced across a condenser, where the water vapor spontaneously condenses. At the outlet of the condenser is condensate and pressurized air. This pressurized air may be moved across a turbine in order to recover a portion of the compression work. The condensate is pumped out of the separation tank and into storage.

### Atmospheric Water Generation with Solid Desiccants

A desiccant-based AWG system (DAWG) uses a deliquescent desiccant material which absorbs water from the air. Once the desiccant has become saturated, it undergoes a temperature and/or pressure swing, allowing for the water vapor to be desorbed and the desiccant to be regenerated.

The product water vapor is then collected and condensed. The cycle of water vapor absorption and desorption by the desiccant continues over the system's operation. Since the water absorption and desorption occur at separate times while creating multiple batches of condensate, this type of operation is sometimes referred to as a batch-style operation. A schematic of a simple batch-style DAWG system is shown in Figure 8.

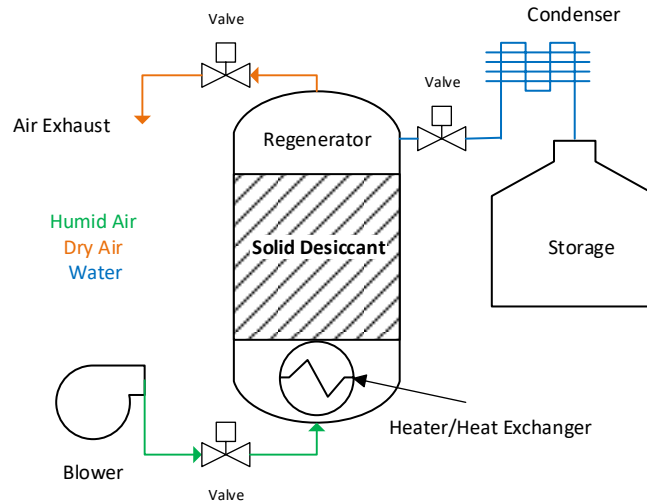


**Figure 8:** Batch-style DAWG system using a solid desiccant

The batch-style DAWG system uses a solid or fixed desiccant material. These may include metal organic frameworks (MOFs) [16] [17] [18], zeolites [19], silica gel [20] [21], or salts [22] [23]. In operation, a fan or blower blows humid air across the desiccant in the regenerator, where a portion of the humid air's water vapor is absorbed by the desiccant. Once it is time for regeneration, the intake and exhaust valves are closed. The heater is turned on, raising the temperature within the regenerator and heating the desiccant. As water vapor is desorbed from the desiccant, it is condensed and stored in a storage vessel. The condenser may use natural convection to condense the water at atmospheric temperature if it is long enough to have enough heat transfer surface area. Alternatively, another blower may also be used to blow ambient air across the condenser to increase the convective heat loss across the condenser and allow a smaller condenser to be used. However, this does come at an increased energetic cost since an additional blower would consume energy.

A batch-style DAWG system may be modified to incorporate the recovery of the latent heat of vaporization. A system incorporating latent heat recovery is shown in Figure 9.

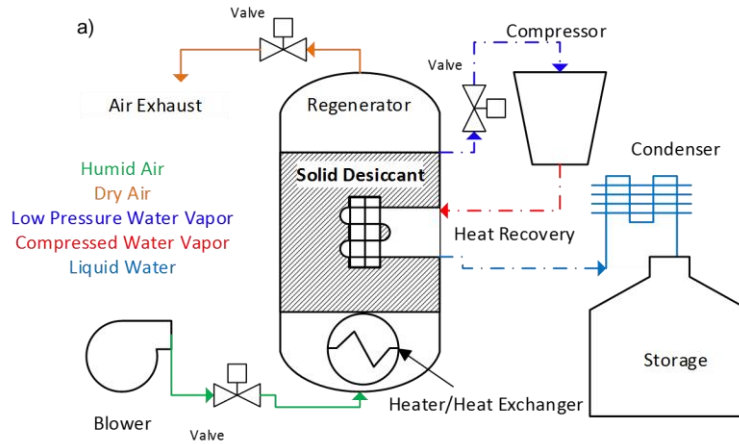


**Figure 9:** Batch-style DAWG system using a solid desiccant and incorporating latent energy recovery

To recover latent heat, the water vapor initially exiting the regenerator undergoes isentropic compression. This causes the water vapor to become superheated and allows for the condensation of water vapor at a temperature higher than the regenerator temperature. The compressed water vapor then flows through a heat exchanger embedded within the regenerator. This allows the compressed water vapor to transfer sensible heat (superheat) and latent heat to the desiccant. This causes a portion of the water vapor to condense and drives the vaporization of additional water vapor from the desiccant. The condensate and water vapor mixture then flow through a condenser in order to be cooled to ambient temperature and condense any remaining water vapor before going into a storage tank.

### Atmospheric Water Generation with Liquid Desiccants

A liquid desiccant-based AWG system may be configured to produce water either continuously or as a batch system [24] [25] [26] [27] [28], using a system configuration like that in Figures 8 or 9. Types of liquid desiccants include calcium chloride, triethylene glycol, lithium chloride and lithium bromide [25] [26]. In a continuous operation configuration, the water uptake and regeneration occur simultaneously and at different temperatures, allowing for the recovery of sensible energy. A schematic of a liquid desiccant system with continuous water production is shown in Figure 10.



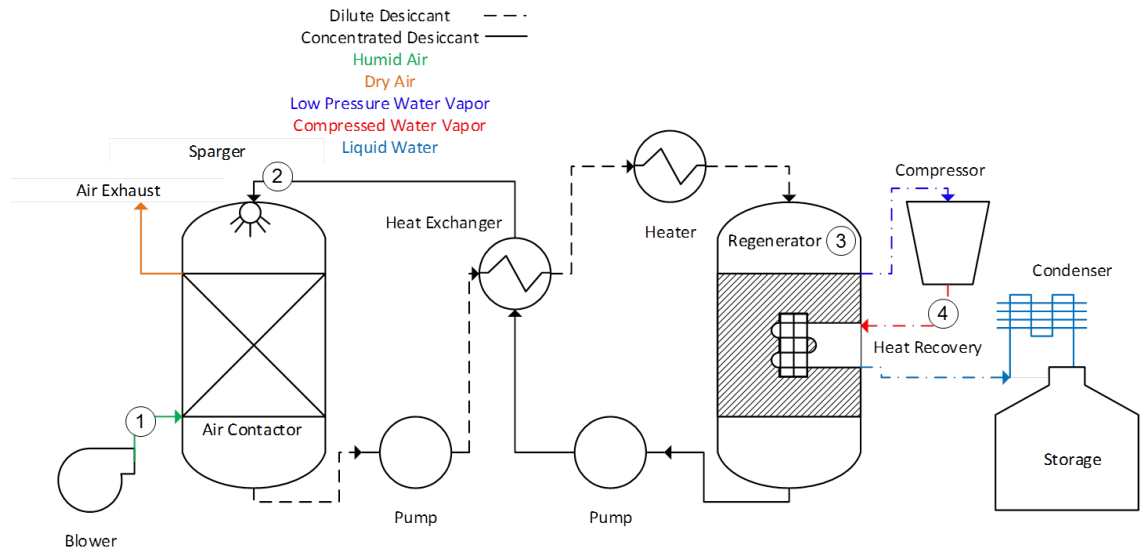


**Figure 10:** Continuous operation liquid desiccant AWG system with sensible and latent energy recovery

In operation, a sparger sprays concentrated desiccant through an air contactor. A fan or blower blows humid air through the air contactor. When the humid air encounters the desiccant, some of the water vapor is absorbed into the desiccant. This interaction occurs at ambient temperature. Dry air is exhausted, while the dilute desiccant is pumped out of the air contactor and to the rest of the system. The dilute desiccant is heated up to the regenerator temperature before entering the regenerator. Within the regenerator, water vapor is regenerated, and the concentrated desiccant solution exits the regenerator. Latent energy may be recovered using a compressor and internal heat exchanger, using the same latent energy recovery process described in the solid-desiccant system. The hot concentrated desiccant solution may pass through a heat exchanger in order to preheat the dilute desiccant, allowing for a portion of the sensible energy to be recovered. The cooled concentrated desiccant solution then enters the sparger in the air contactor, allowing the cycle to continue.

### Multi-Stage Flash

For the continuous operation liquid desiccant AWG system, the latent energy recovery may be done using a multi-stage flash (MSF) process rather than the regenerator and compressor. Each flashing stage consists of a sparger, condenser, and brine reservoir. A system utilizing MSF is shown in Figure 11.

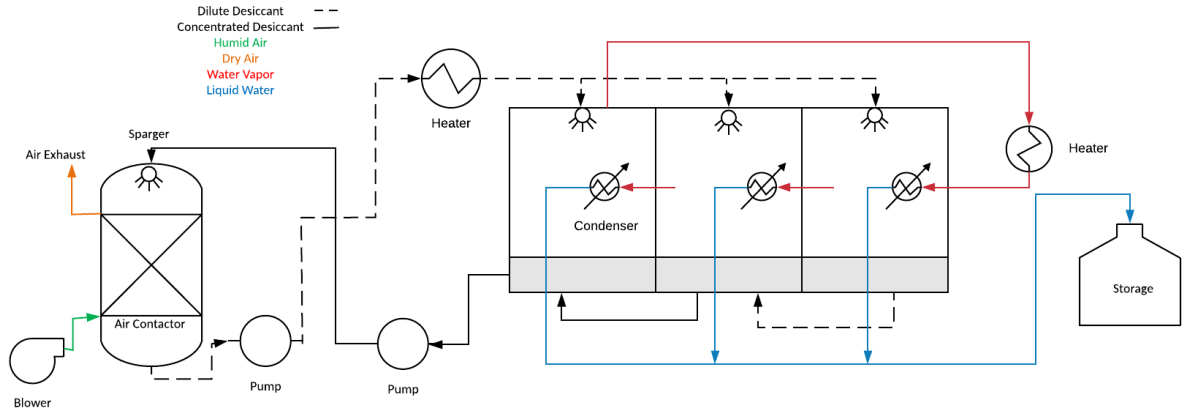


**Figure 11:** Multi-Stage Flash system using liquid desiccant

In operation, dilute desiccant enters each stage through a sparger. The desiccant then collects in a reservoir of brine solution at the bottom of each stage. Pre-heated water vapor enters the first stage (the stage farthest to the right in Figure 11). It passes through a condenser, releasing its latent heat to the desiccant in the brine reservoir and causing some of the dilute brine to vaporize. This vapor then enters the condenser of the next stage, while the more concentrated brine solution is also allowed to flow to the next stage. The next stage operates at a lower pressure than the previous, allowing for the condensation of water vapor in the condenser, as well as the vaporization of additional water vapor from the brine solution. Temperature decreases with each stage as well, meaning that the brine in the first stage has the highest temperature. This temperature is called the top brine temperature. While Figure 11 shows a system with three stages, a system with more stages is also possible. In the final stage, the vapor is reheated and cycled back to the first stage. The concentrated brine solution is pumped back to the air contactor to absorb more moisture and recirculate in the system.

## Scope of Thesis

The goal of the thesis is to determine the feasibility of AWG as a method of water production. For AWG to be an attractive option for water production, the energetic and monetary cost of water production must be minimized. In order to quantify the energetic cost of water, thermodynamic analyses were conducted to find the specific energy consumption (SEC), or energy required to produce a unit of water, for the previously described AWG systems. The effect of adding energy recovery methods on a system's SEC was also analyzed. The SEC of these systems were compared to current water generation techniques such as seawater reverse osmosis, which requires between 3-4 kWh/m<sup>3</sup>. Once the system configurations with the lowest SEC values were identified, economic analyses were conducted to determine the levelized cost of water (LCOW), or monetary cost required to produce a unit of water. Using the SEC and LCOW for each system configuration, an optimal configuration was chosen. An AWG system utilizing the optimal system configuration was designed with the capability of operating both with and without energy recovery. Material testing was performed to verify material properties from literature, as well as gain information on how to optimize the rate of water uptake. Finally, the system was constructed and run under several different operating conditions. The water collection and energetics of the system were measured in order to calculate the SEC value of the system. These SEC values were then compared to those



from the thermodynamic analyses to verify the modelling. Finally, the SEC values of AWG were compared to those of current water production methods to determine if and when AWG would be a feasible option.

## Chapter 2: Techno-Economic Modelling

The techno-economic modelling comprised of both thermodynamic and economic analyses. A thermodynamic analysis was performed to determine the SEC for each AWG system configuration. Once the optimal system configuration on an energetic basis was determined, an economic analysis was performed to determine the best way to provide the energy to the system such that the LCOW of the system is minimized. Based on the SEC and LCOW for each system configuration, the ideal AWG system configuration was determined.

### Thermodynamic Modelling

Several thermodynamic analyses were conducted to determine the SEC for several AWG system configurations. The analyses were structured around hourly Typical Meteorological Year (TMY) data. TMY data models a year's worth of meteorological data for a particular location. The location chosen for the analyses was Daggett, CA due to its level of water stress and excellent solar resource. Meteorological data used in the analyses included dry bulb temperature ( $^{\circ}\text{C}$ ), percent relative humidity, dew point temperature ( $^{\circ}\text{C}$ ), absolute pressure (Pa), and global horizontal irradiance ( $\text{W}/\text{m}^2$ ). The energy consumption and water production were calculated for every hour of the year. The annual energy consumption and annual water production were used to calculate the SEC for each AWG system configuration.

Below are the results of thermodynamic analyses for several AWG configurations. These configurations include refrigerated atmospheric water generation (RAWG), compression and condensation based atmospheric water generation (CC), as well as several desiccant-based atmospheric water generation techniques. The desiccant-based approaches include the use of solid desiccants, or the use of liquid desiccants with several different system configurations.

### Refrigerated Atmospheric Water Generation

Several different system operating modes were considered such as the use of a precooler heat exchanger, restricting operation to daytime (6 AM – 6 PM) or nighttime (6 PM – 6 AM), and allowing water to freeze on the evaporator. The results of this analysis were used to see whether changes to the system's operation enable a reduction in SEC.

An energy balance was performed to determine the amount of thermal energy that must be removed to condense water vapor. When there is no precooler heat exchanger (as seen in Figure 6), the cooling condenser must be sized to extract enough energy from the air to cool it to the dew point temperature and enable the condensation of a portion of the water vapor. The thermal power,  $\dot{Q}_{cond}$ , required by the condenser is given in Eq. 3. The power,  $\dot{W}_{RAWG}$ , to operate the RAWG system is given in Eq. 4.

$$\dot{Q}_{cond}[\text{W}] = \dot{m}_{H_2O} \left( h_{fg} + c_{p_{H_2O,v}}(T_{\infty} - T_c) \right) + \dot{m}_{air} (c_{p_{air}} + \omega_2 c_{p_{H_2O,v}})(1 - \epsilon)(T_{\infty} - T_c) \quad (3)$$

$$\dot{W}_{RAWG}[\text{W}] = \dot{W}_{fan} + \frac{\dot{Q}_{cond}}{COP_R} \quad (4)$$

$\dot{W}_{fan}$  is the power required by the fan to move a flow of dry air,  $\dot{m}_{air}$ , water product,  $\dot{m}_{H_2O}$ , and water vapor exhaust,  $\omega_2 \dot{m}_{air}$ , initially at ambient temperature,  $T_\infty$ , through an evaporator operating at  $T_c$ . The heat capacity of water vapor is  $cp_{H_2O,v}$ , the heat capacity of dry air is  $cp_{air}$ , and the coefficient of performance is  $COP_R$ . Performance data for refrigerated heat exchangers shows that the  $COP_R$  typically range between 2 and 5 [29], so a constant  $COP_R$  value of 3.5 was used for the analysis. The heat exchanger effectiveness,  $\epsilon$ , is assumed to be 80% or more based on the typical performance of gas-gas heat exchangers [30]. The flow rate of extracted water is given in Eq. 5.

$$\dot{m}_{H_2O} = \dot{m}_{air}(\omega_1 - \omega_2) = \dot{m}_{air}\Delta\omega \quad (5)$$

$\omega_1$  and  $\omega_2$  are the absolute humidity of the air flow at the inlet and outlet of the evaporator. The specific energy consumption,  $SEC_{RAWG}$ , may be found by dividing Equations 4 and 5 and is given in Eq. 6.

$$SEC_{RAWG} \left[ \frac{J}{kg_{H_2O}} \right] = \frac{\Delta P}{\rho_{air}\Delta\omega} + \frac{(h_{fg} + cp_{H_2O}(T_\infty - T_c) + \frac{(1-\epsilon)(cp_{air} + \omega_2 cp_{H_2O,v})(T_\infty - T_c)}{\Delta\omega})}{COP_R} \quad (6)$$

When performing sensible energy recovery, the sensible energy of the exhaust air may be used to precool the incoming moist air before the evaporator. The precooling could be performed by implementing a crossflow heat exchanger. The rejected moist air coming into the precooler is assumed to be heated in the precooler to the dry bulb temperature. It was also assumed that the precooler hardware is large for the temperature of the exhaust moist air to reach the dry bulb temperature. The thermal power,  $\dot{Q}_{pc}$ , being transferred within the precooler is given in Eq. 7.

$$\dot{Q}_{pc}[W] = \omega_2 \dot{m}_{air} cp_{H_2O,v}(T_\infty - T_c) + \dot{m}_{air} cp_{air}(T_\infty - T_c) \quad (7)$$

The heat transfer between the incoming and rejected moist air causes the incoming moist air to be precooled to a new temperature,  $T_{pc}$ . This temperature may be calculated using Eq. 8.

$$T_{pc}[K] = \frac{\dot{m}_{air} cp_{air} T_\infty + \omega_1 \dot{m}_{air} T_\infty - \dot{Q}_{pc}}{\dot{m}_{air} cp_{air} + \omega_1 \dot{m}_{air} cp_{H_2O,v}} \quad (8)$$

The specific energy consumption with a precooler is like that without a precooler. The difference is that the evaporator needs to cool the incoming moist air from the precooler outlet temperature rather than from the dry bulb temperature. The specific energy consumption when using a precooler,  $SEC_{RAWG,pc}$ , is given in Eq. 9.

$$SEC_{RAWG,pc} \left[ \frac{J}{kg_{H_2O}} \right] = \frac{\Delta P}{\rho_{air}\Delta\omega} + \frac{(h_{fg} + cp_{H_2O}(T_{pc} - T_c) + \frac{(1-\epsilon)(cp_{air} + \omega_2 cp_{H_2O,v})(T_{pc} - T_c)}{\Delta\omega})}{COP_R} \quad (9)$$

Power required by the fan to move moist air through the system is a function of the flow pressure drop,  $\Delta P$ , and air density,  $\rho_{air}$ . The performance of a RAWG system is best when fan power is minimized and sensible energy recovery, coefficient of performance, and water extraction,  $\Delta\omega$ , are maximized. In an optimal system with nearly complete sensible energy recovery, the minimum SEC can be approximated by the heat of vaporization of water and the  $COP_R$  of the refrigeration hardware.

When performing the analysis of the RAWG system with a precooler, the thermal energy extracted from the moist air was broken down into sensible cooling energy in the precooler, sensible cooling energy in the evaporator, and latent energy in the evaporator. The breakdown of thermal energies

during the heat extraction process both without and with a precooling are shown in Figures 12 and 13 respectively.

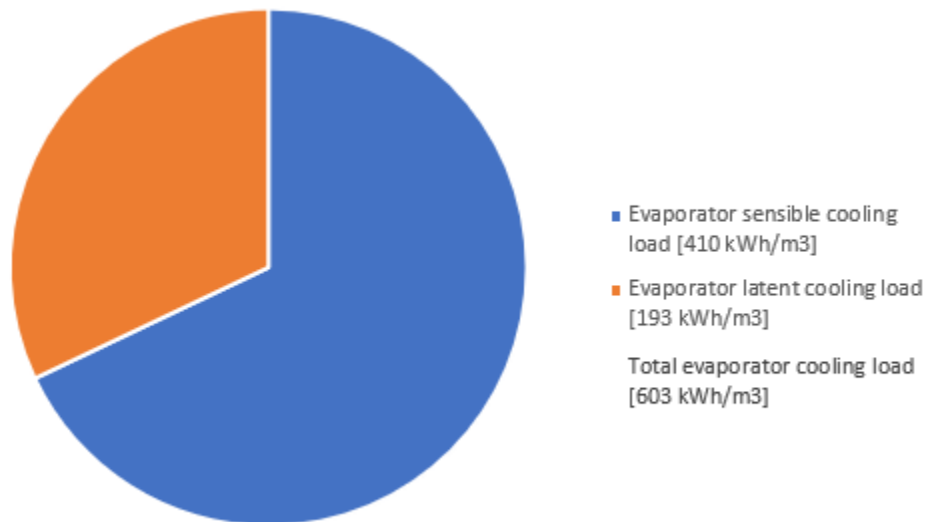


**Figure 12:** Thermal energy breakdown of moist air cooling for a RAWG system without a precooling

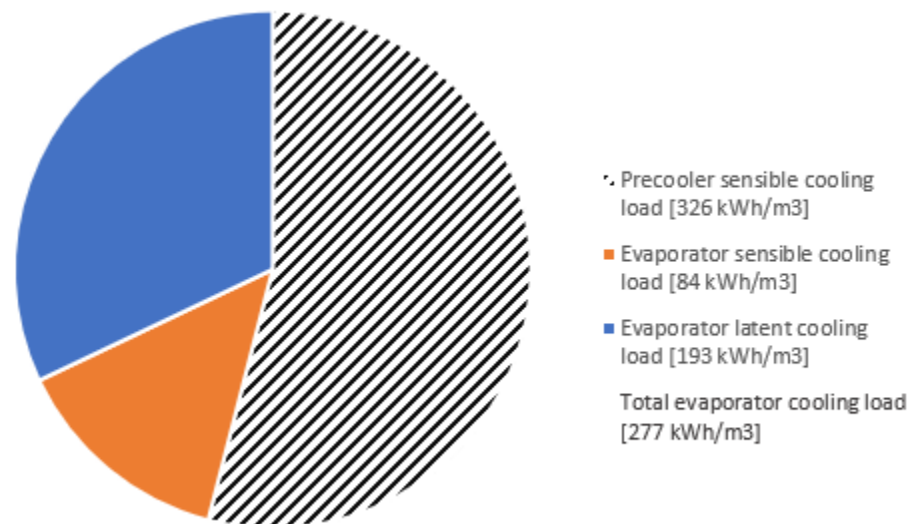


**Figure 13:** Thermal energy breakdown of moist air cooling for a RAWG system with a precooling

When there is no precooling, the sensible energy load is the largest cooling load. When a precooling is added to the system, the precooling provides most of the sensible energy load. The sensible energy provided by the precooling does not account for an energetic cost during the SEC evaluation, since this sensible energy was provided using the cooled outlet air from the evaporator rather than an

external energy source. The sensible energy of the evaporator is reduced when the precoolers is used. However, the latent energy cooling remains constant.

If a condenser was used as in Figure 5, the thermal energy breakdown would look similar to that in Figure 12. This is because the condenser increases the thermal energy transfer of the system, which increases the coefficient of performance. Equation 6 shows that if the fan power is negligible, the SEC scales with the coefficient of performance. However, the percentages of the SEC taken up by latent and sensible energy will remain unchanged.

The amount of water produced was calculated by first assuming that a fan was blowing moist air through the system at a flow rate of 100 m<sup>3</sup>/min. Scaling this flow rate will proportionally scale the amount of water produced by the system. It was further assumed that half of the inlet moisture condensed in the condenser, and the remaining water vapor left the condenser with the exhaust air. Finally, it was also assumed that if the dew point temperature fell below 1 °C, then the moisture would freeze on the evaporator coils rather than condense as liquid water. The plot of normalized annual water production of a system operating continuously under these assumptions in Daggett, CA is shown in Figure 14.

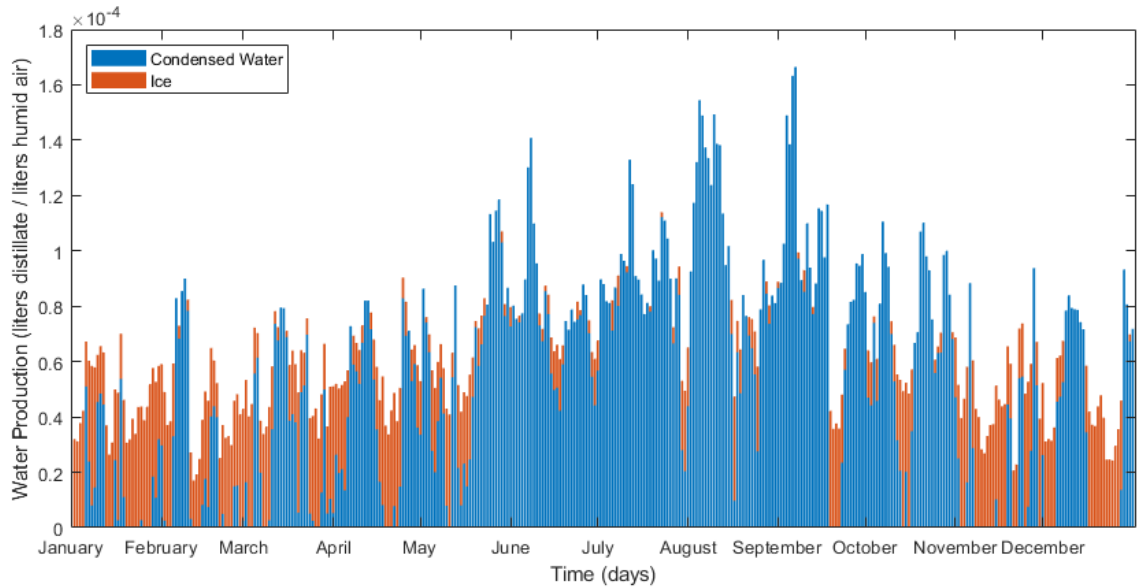


**Figure 14:** Annual water and ice production from a continuous operation RAWG system

Figure 14 shows that the Summer months are the most humid and therefore have the potential to generate the most water. Additionally, the Summer months have higher dew point temperatures, so less ice is generated during the Summer months than in the Winter months.

The evaporator can be run at different operating temperatures. This temperature is the minimum temperature to which the moist air can be cooled, assuming the heat exchanger hardware is large enough. If the dew point temperature is below the operating temperature, then the heat exchanger won't be able to cool the moist air enough to either condense any water or freeze any ice. Thus, the lower the operating temperature, the more water that would be expected to be collected. However, once the operating temperature falls below -5 °C, the annual water production is within 5% of the maximum expected water production. This optimal evaporator temperature will vary depending on the system operating location. This trend is seen in Figure 15.

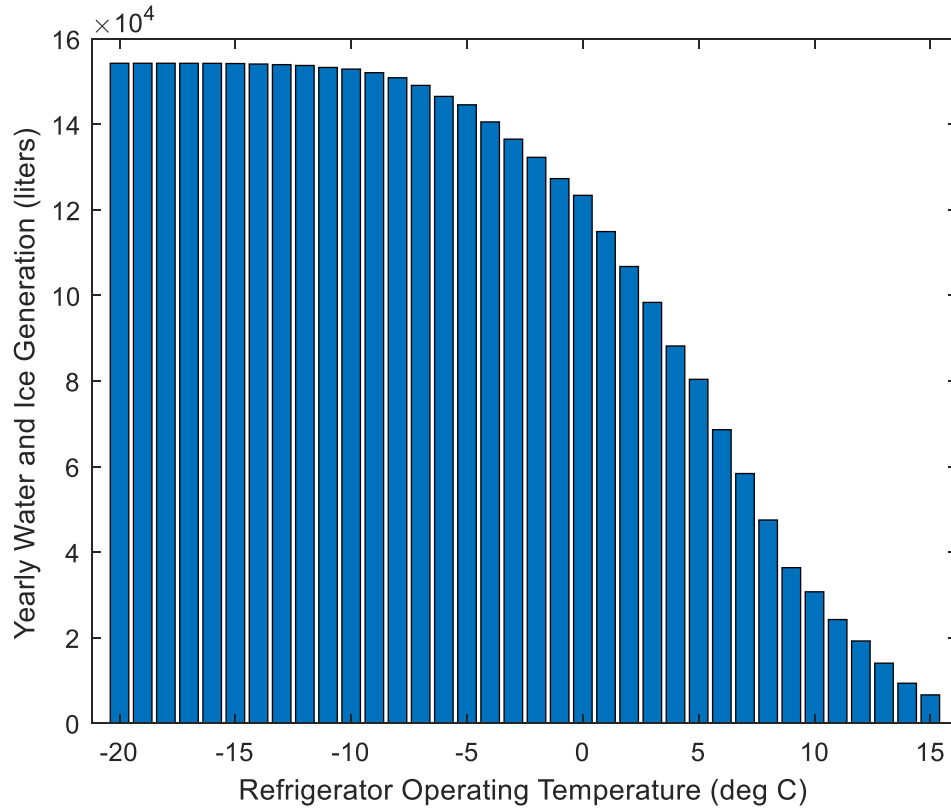


**Figure 15:** Annual water generation of a RAWG system versus the condenser operating temperature

Previous studies have analyzed the effect of frost formation on heat exchanger performance [31] [32]. These studies have shown that the formation of ice causes a decrease in heat exchanger efficiency. This is because the frost creates an insulating layer which reduces heat transfer. This reduction in heat exchanger performance would lead to an increase in SEC. Because of this, a RAWG system operating with ice harvesting was not further explored.

If the operation of the system is restricted to only during the day or only during the night, the system would perform differently. Nighttime is typically cooler than daytime. This means that nighttime operation has lower dry bulb temperatures. Additionally, the relative humidity at nighttime is higher than at daytime. Lower dry bulb temperatures mean that less energy is required to cool the moist air to the dew point temperature. Higher relative humidity means that more water can be generated at nighttime since there is more moisture in the air. Because of these two characteristics, the performance of the system at nighttime would be better than during the daytime. To determine how the performance of the system at different times compare, the data was split up between daytime hours (6 AM – 6 PM) and nighttime hours (6 AM – 6 PM).

**Table 1:** RAWG system operation for different operating times

	Daily Water Production [ $\frac{\text{liters}}{\text{day}}$ ]	SEC [ $\frac{\text{kWh}}{\text{m}^3}$ ]
Nighttime Operation	158.2	262.1
Daytime Operation	156.7	292.9
Continuous Operation	314.9	277.4

Table 1 shows that nighttime operation results in slightly better performance than daytime operation due to its lower SEC. Therefore, if the system can only operate for a portion of the day, nighttime would be the optimal time. However, one of the challenges of operating at night using solar energy is the requirement of generating and storing enough energy for the system to operate. This issue is not as pertinent to daytime operation since solar energy may be generated and immediately be used by the system.

The SEC of the RAWG system may be calculated using Eqs. 6 and 9 for systems without and with sensible energy recovery respectively. These systems were assumed to operate without ice harvesting. The SEC values for these RAWG systems operating continuously in Daggett, CA are given in Table 2.

**Table 2:** SEC for RAWG system with continuous operation

	SEC [ $\frac{\text{kWh}}{\text{m}^3}$ ]
RAWG without sensible energy recovery	603.2
RAWG with sensible energy recovery	277.4

## Compression and Condensation

A compression and condensation (CC) system was analyzed to determine its SEC. In a CC system, moist air is compressed to its saturation pressure. The saturated water vapor then flows through a heat exchanger where the water vapor condenses as it releases its latent energy. This type of system is shown in Figure 7.

An energy balance was performed to determine the compressive work required to operate the CC system. When operating ideally, the only required energy input is the compressive work required to compress the water vapor from its ambient vapor pressure to a value slightly above the saturation pressure. Since the water vapor at the exit of the compressor is already at the saturation pressure, only the latent energy load needs to be transferred from the water vapor to the surroundings for the water vapor to start spontaneously condensing. The compression and expansion processes were modeled as isentropic processes for an ideal gas with efficiencies of  $\eta_c$  and  $\eta_T$  respectively. The compressive work may be split into that required to compress air and water. The power requirement,  $\dot{W}_{net}$ , for a CC system is given in Eqs. 10-12.

$$\dot{W}_{net} = \dot{m}_{air}W_{c,air} + \dot{m}_{H_2O,v}W_{c,H_2O} - \dot{m}_{air}W_{T,air} \quad (10)$$

$$W_C = \frac{cp \cdot T_\infty \left( PR^{\frac{\gamma-1}{\gamma}} - 1 \right)}{\eta_c} \quad (11)$$

$$W_T = \eta_T \cdot cp \cdot T_H \left( PR^{\frac{\gamma-1}{\gamma}} - 1 \right) \quad (12)$$

$W_{c,air}$  is the work required to compress dry air,  $W_{c,H_2O}$  is the work required to compress water vapor, and  $W_{T,air}$  is the work that may be recovered across the turbine. The specific heat ratio is  $\gamma$ . At the outlet of the condenser, the flow rate of compressed air is much greater than that of compressed water vapor. Because of this, it was assumed that only the flow or compressed dry air is used during energy recovery. The mass flow rate of water vapor entering the compressor is given in Eq. 13. It is assumed that all the water vapor is condensed in the system. The pressure ratio across the compressor and turbine is the pressure needed to raise the water vapor partial pressure to the saturation temperature, which is the reciprocal of relative humidity. The pressure ratio is given in Eq. 14.

$$\dot{m}_{H_2O} = \omega_1 \dot{m}_{air} \quad (13)$$

$$PR = \frac{P_{sat,\infty}}{P_{H_2O,\infty}} = \frac{1}{Rh} \quad (14)$$

When calculating the SEC, it was assumed that the air exiting the compressor equilibrates quickly to the dry bulb temperature,  $T_\infty = T_H$ . Additionally, it was assumed that the isentropic compression and expansion efficiencies are equal,  $\eta_c = \eta_T = \eta$ . With these assumptions, the SEC for a CC system is given in Eq. 15.

$$SEC_{CC} \left[ \frac{kJ}{kg_{H_2O}} \right] = \frac{cp_{air}T_\infty}{\omega_\infty} \left( \frac{1}{RH} \frac{\gamma_{air}^{-1}}{\gamma_{air}} - 1 \right) \left( \frac{1}{\eta} - \eta \right) + \frac{cp_{H_2O}T_\infty}{\eta} \left( \frac{1}{RH} \frac{\gamma_{H_2O}^{-1}}{\gamma_{H_2O}} - 1 \right) \quad (15)$$

The performance of a CC system is best when there is a high isentropic efficiency or relative humidity. One way to ensure there is high relative humidity air entering the compressor is to separate the water vapor from the air upstream of the compressor. This process may be performed by implementing separators, such as membranes, upstream of the compressor [33] [34] [35]. The compressor then acts as a vacuum pump to draw the moist air through the separator. While the work to compress air would be reduced, this would come at the cost of the work required to draw water vapor through the separator.

The SEC for a CC system with no separator may be calculated using Eq. 15. The SEC may be split into the SEC due to compressing dry air and due to compressing water vapor. The SEC for a CC system operating continuously in Daggett, CA with no separator is given in Table 3.

**Table 3:** SEC of a CC system

Portion of SEC, Dry Air Compression $\left[ \frac{kWh}{m^3} \right]$	Portion of SEC, Water Vapor Compression $\left[ \frac{kWh}{m^3} \right]$	SEC $\left[ \frac{kWh}{m^3} \right]$
446	37	483



Table 3 shows that while the SEC for CC system may be higher than a RAWG system, most of the SEC is due to the compression of dry air. The resulting SEC due to water vapor compression is very small. If the inlet stream to the compressor were pure water vapor rather than moist air, then the SEC of a CC system would be 37 kWh/m<sup>3</sup>.

### Atmospheric Water Generation with Solid Desiccants

An energy balance was performed on a DAWG system with batch operation to determine its SEC. The system was assumed to be operating using the desiccants lithium chloride, LiCl, or calcium chloride, CaCl<sub>2</sub>. These desiccants have been studied previously and several of their material properties have been documented [36]. These material properties allow for the state of the desiccant solution to be determined when performing the SEC analysis.

For the analysis, it was assumed that the desiccant absorbed water for twelve hours at night and regenerated water for twelve hours during the day. This daily process was repeated for an entire operating year. It was assumed that during the water absorption stage, enough water was absorbed for the desiccant to become saturated to its equilibrium desiccant concentration based upon the ambient nighttime dry bulb temperature and water vapor pressure. During regeneration, a range of final concentrated desiccant mass fractions,  $\beta$ , were analyzed. The final concentrated desiccant mass fraction is the desiccant mass fraction at the end of the water regeneration process when all of the absorbed water vapor has been boiled out of the desiccant solution and the concentration of desiccant is at its highest. It was assumed that the desiccant mass fraction moved between its equilibrium mass fraction and the final concentrated mass fraction for each regeneration cycle. By choosing a more concentrated final desiccant mass fraction, it means more water was absorbed and desorbed during each batch cycle.

When regenerating the water from the dilute desiccant solution, one of two methods may be used. Using the first method, the desiccant may be heated up to its saturation temperature while at atmospheric pressure. This saturation temperature is determined by the final concentrated mass fraction and the ambient pressure. This saturation temperature is the temperature the regenerator must operate at to ensure that enough water vapor is desorbed to reach the final concentrated desiccant mass fraction. The second operation method involves regenerating the water vapor while at sub-atmospheric pressure. By operating at lower pressure, a lower regenerator temperature is required to desorb the water vapor.

In a DAWG system with solid desiccants, the system may be operated with no energy recovery, or with latent energy recovery. It is assumed that the desiccant is fixed in place while the system is operating. This means that the desiccant cannot be pumped or moved across a heat exchanger to efficiently recover sensible energy. The thermal energy requirement to operate a DAWG system is given in Eq. 16. This equation assumes that the energy required by the pump or blower is negligible. Additionally, when there is no energy recovery in the system, this equation gives the SEC of the system.

$$Q_{DAWG} \left[ \frac{kJ}{kg_{H2O}} \right] = \frac{\beta_2}{\beta_2 - \beta_1} * c_{p,s1} * (T_{reg} - T_{\infty}) + h_{fg} \quad (16)$$

The thermal energy requirement is a function of the regenerator temperature,  $T_{reg}$ , ambient dry bulb temperature,  $T_{\infty}$ , the specific heat of the desiccant/water solution,  $c_{p,s1}$ , the dilute desiccant concentration,  $\beta_1$ , the concentrated desiccant concentration,  $\beta_2$ , and the latent load,  $h_{fg}$ . In order

to minimize the required thermal load, a desiccant with a high water carrying capacity should be used, allowing for the dilute desiccant concentration to be very low relative to the concentrated desiccant concentration. The mass of water produced,  $M_{H2O}$ , is the difference between the desiccant solution masses before and after regeneration,  $M_{s1}$  and  $M_{s2}$  respectively. This relationship is shown in Eq. 17. It is assumed that while the system is operating, the change in mass is due solely due to a change in water in the desiccant solution, with the mass of desiccant in the solution,  $M_{des}$ , remaining fixed. This allows the desiccant solution concentrations to be expressed as in Eq. 18.

$$M_{H2O} = M_{s1} - M_{s2} \quad (17)$$

$$\beta_1 = \frac{M_{des}}{M_{s1}}, \beta_2 = \frac{M_{des}}{M_{s2}} \quad (18)$$

If latent energy is recovered, then a term must be added to Eq. 16 to account for the work of the compressor,  $W_c$ . The specific energy becomes a sum of thermal energy inputs and work inputs. The SEC equation for a DAWG system with latent energy recovery is given in Eq. 19.

$$SEC_{DAWG} \left[ \frac{kJ}{kg_{H2O}} \right] = \frac{\beta_2}{\beta_2 - \beta_1} * c_{p,s1} * (T_{Reg} - T_\infty) - c_{p,vap} (T_{isen} - (T_{reg} + \Delta T_{s,comp})) + \Delta h_{fg} + W_c \quad (19)$$

$$W_c = \frac{c_{p,vap} \cdot T_{Reg} \left( PR^{\frac{\gamma-1}{\gamma}} - 1 \right)}{\eta_c} \quad (20)$$

$$PR = \frac{P_{comp}}{P_{Reg}} \quad (21)$$

The regenerator operates at a pressure  $P_{reg}$  and temperature  $T_{reg}$ . The desiccant with specific heat  $c_{p,s1}$  is regenerated between mass fractions  $\beta_1$  and  $\beta_2$ . When analyzing the system,  $\beta_1$  corresponded to the saturated desiccant mass fraction at the ambient temperature and pressure, while a range for final concentrated mass fractions,  $\beta_2$ , were analyzed ranging from 0.4 – 0.65. The desiccant is sensibly heated from the ambient temperature  $T_\infty$  to the regenerator temperature. As the water vapor exits the desiccant it flows across a compressor where it is compressed isentropically.

The compressor has an isentropic efficiency  $\eta_c$ . The water vapor is compressed from the regenerator pressure to a higher pressure  $P_{comp}$ , resulting in a pressure ratio  $PR$  across the compressor. The pressure ratio helps determine the compressor work  $W_c$ . The compressor outlet pressure was chosen such that  $P_{comp}$  is the saturation pressure corresponding to a saturation temperature which is  $\Delta T_{s,comp}$  hotter than the regenerator temperature. Several saturation temperature increases across the compressor were analyzed, ranging between 2 – 5 °C. While in theory a negligible increase in saturation temperature may work, this would result in a very large embedded heat exchanger in the regenerator, as seen in Figure 9. In practice, there would need to be a large enough saturation temperature increase to allow enough heat transfer to occur when using a heat exchanger of manageable size. Since the compressor is assumed to operate isentropically, the water vapor is superheated to a temperature  $T_{isen}$ . Because of this, some sensible energy may be recovered as the compressed water vapor cools between  $T_{isen}$  and its saturation temperature,  $(T_{reg} + \Delta T_{s,comp})$ .

Nearly all the latent load can be recovered in the regenerator. Only a small latent load is required,  $\Delta h_{fg}$ , which corresponds to the change in the water vapor's enthalpy of vaporization. The enthalpy

of vaporization decreases as the saturation temperature increases. This means that the latent energy to vaporize the water vapor from the desiccant is slightly higher than the latent load released from the water vapor as it condenses at a slightly higher temperature.

Several different operating states were analyzed for the DAWG system. The final concentrated mass fraction,  $\beta_2$ , was analyzed over a range from 0.4 – 0.65. A range of saturation temperature increases across the compressor were analyzed, ranging from 2 – 5 °C. A range of regenerator temperatures were analyzed, with the regenerator being set to operate between 5 – 20 °C above the ambient dry bulb temperatures. All the different combinations of the system parameters were tested in order to determine the minimum SEC for the DAWG system.

Using the previously described analysis, the optimal system parameters and minimum SEC were calculated for a DAWG batch-style system with solid desiccants. The performance breakdown for a DAWG batch-style system with the regenerator at atmospheric pressure is given in Table 4, while the breakdown of its SEC is given in Table 5. The performance of a DAWG batch-style system with the regenerator at sub-atmospheric pressure is given in Table 6, while the breakdown of its SEC is given in Table 7. The performance of a DAWG batch-style system with latent energy recovery is given in Table 8, while the breakdown of its SEC is given in Table 9.

**Table 4:** Performance of a DAWG batch-style system at atmospheric pressure

Desiccant	$T_{reg}$ [K]	$P_{reg}$ [Pa]	$MF_{conc}$	SEC $\left[\frac{kWh}{m^3}\right]$
CaCl <sub>2</sub>	421.92	101325	0.62	886.01
LiCl	451.72	101325	0.65	925.65

**Table 5:** SEC of a DAWG batch-style system at atmospheric pressure

Desiccant	SEC $\left[\frac{kWh}{m^3}\right]$	SEC <sub>sensible</sub> $\left[\frac{kWh}{m^3}\right]$	SEC <sub>latent</sub> $\left[\frac{kWh}{m^3}\right]$	SEC <sub>work</sub> $\left[\frac{kWh}{m^3}\right]$
CaCl <sub>2</sub>	886.01	203.86	682.05	0
LiCl	925.65	243.77	681.89	0

**Table 6:** Performance of a DAWG batch-style system at sub-atmospheric pressure

Desiccant	$T_{reg}$ [K]	$P_{reg}$ [Pa]	$MF_{conc}$	SEC $\left[\frac{kWh}{m^3}\right]$
CaCl <sub>2</sub>	292.36	894	0.60	731.03
LiCl	311.28	1360	0.51	768.59

**Table 7:** SEC of a DAWG batch-style system at sub-atmospheric pressure

Desiccant	SEC $\left[\frac{kWh}{m^3}\right]$	SEC <sub>sensible</sub> $\left[\frac{kWh}{m^3}\right]$	SEC <sub>latent</sub> $\left[\frac{kWh}{m^3}\right]$	SEC <sub>work</sub> $\left[\frac{kWh}{m^3}\right]$
CaCl <sub>2</sub>	731.03	45.97	685.06	0
LiCl	768.59	85.09	683.50	0

**Table 8:** Performance of a DAWG batch-style system with latent energy recovery

Desiccant	$T_{reg}$ [K]	$T_{comp}$ [K]	$P_{reg}$ [Pa]	$P_{comp}$ [Pa]	$MF_{conc}$	SEC $\left[\frac{kWh}{m^3}\right]$
CaCl <sub>2</sub>	408.51	410.51	88481	101325	0.44	209.99

**Table 9:** SEC of a DAWG batch-style system with latent energy recovery

Desiccant	SEC $\left[\frac{kWh}{m^3}\right]$	SEC <sub>sensible</sub> $\left[\frac{kWh}{m^3}\right]$	SEC <sub>latent</sub> $\left[\frac{kWh}{m^3}\right]$	SEC <sub>work</sub> $\left[\frac{kWh}{m^3}\right]$
CaCl <sub>2</sub>	209.99	199.25	1.61	9.13

Tables 5 and 7 show that the latent load takes up most of the SEC when operating both at atmospheric and sub-atmospheric pressure. Therefore, it makes sense that when latent energy recovery is incorporated, the latent load is nearly eliminated. While this does come at the cost of compressor work, the reduction in latent energy more than makes up for this additional energetic cost.

### Atmospheric Water Generation with Liquid Desiccants

An energy balance was performed on a DAWG system using liquid desiccants with both batch-style and continuous operation. The analysis was like that of a DAWG system using solid desiccants. Eqs. 16-21 may be used to calculate the performance of a liquid desiccant DAWG system with no energy recovery and with latent energy recovery.

When analyzing the system with continuous operation, it was assumed that the desiccant solution entering the regenerator has the equilibrium mass fraction corresponding to the ambient dry bulb temperature and water vapor pressure. A range of concentrated desiccant mass fractions were analyzed exiting the regenerator. The regeneration may occur at atmospheric pressure and a high saturation temperature, or at sub-atmospheric pressure and a low saturation temperature. When the regenerated condensate exits the condenser at sub-atmospheric pressure, it must be pressurized up to atmospheric pressure before entering the storage tank. This is because the system is operating continuously, so the system operation cannot be stopped to let the condensate equilibrate to atmospheric pressure.

Since the DAWG system is operating continuously and using liquid desiccants, sensible energy recovery may also be implemented. Adding sensible heat recovery can be modelled using a recovery factor,  $\epsilon$ , which represents the fraction of sensible heat that may be recovered. There is also a compressive work term,  $W_{pdp}$ , associated with a positive displacement pump for compressing the condensate back to atmospheric pressure. When using a DAWG system with both latent and sensible energy recovery, the SEC equation may be modified as in Eq. 22.

$$SEC_{DAWG} \left[ \frac{kJ}{kg_{H_2O}} \right] = \frac{(1-\epsilon)\beta_2}{\beta_2-\beta_1} * c_{p,s1} * (T_{Reg} - T_{\infty}) - c_{p,vap}(T_{isen} - (T_{reg} + \Delta T_{s,comp})) + \Delta h_{fg} + W_c + W_{pdp} \quad (22)$$

Using the previously described analysis, the optimal system parameters and minimum SEC were calculated for a DAWG continuous-style system with liquid desiccants. The performance of a continuous-style DAWG system with no energy recovery is given in Table 10, while the breakdown

of the SEC is given in Table 11. The performance of a continuous-style DAWG system implementing both sensible and latent energy recovery is given in Table 12, and the breakdown of the SEC is given in Table 13. For this system, it was assumed that the outlet pressure of the compressor is atmospheric pressure, thereby eliminating the work required to pressurize the condensate while collecting the water from the storage tank.

**Table 10:** Performance of a DAWG continuous-style system with no energy recovery

Desiccant	$T_{reg}$ [K]	$P_{reg}$ [K]	$MF_{conc}$	$SEC$ $\left[\frac{kWh}{m^3}\right]$
CaCl <sub>2</sub>	333.51	2023	0.65	674.26

**Table 11:** SEC of a DAWG continuous-style system with no energy recovery

Desiccant	$SEC$ $\left[\frac{kWh}{m^3}\right]$	$SEC_{sensible}$ $\left[\frac{kWh}{m^3}\right]$	$SEC_{latent}$ $\left[\frac{kWh}{m^3}\right]$	$SEC_{work}$ $\left[\frac{kWh}{m^3}\right]$
CaCl <sub>2</sub>	674.26	19.53	654.67	0.06

**Table 12:** Performance of a DAWG continuous-style system with sensible and latent energy recovery

Desiccant	$T_{reg}$ [K]	$T_{comp}$ [K]	$P_{reg}$ [Pa]	$P_{comp}$ [Pa]	$MF_{conc}$	$SEC$ $\left[\frac{kWh}{m^3}\right]$
CaCl <sub>2</sub>	333.51	335.51	9457	101325	0.6	185.64

**Table 13:** SEC of a DAWG continuous-style system with sensible and latent energy recovery

Desiccant	$SEC$ $\left[\frac{kWh}{m^3}\right]$	$SEC_{sensible}$ $\left[\frac{kWh}{m^3}\right]$	$SEC_{latent}$ $\left[\frac{kWh}{m^3}\right]$	$SEC_{work}$ $\left[\frac{kWh}{m^3}\right]$
CaCl <sub>2</sub>	185.64	8.86	1.37	175.42

When energy recovery methods are implemented in the DAWG system, there is a significant reduction in SEC. When there is no energy recovery, the latent load is responsible for the majority of the SEC. When energy recovery is implemented, latent energy recovery account for most of the SEC reduction when compared to the reduction in SEC due to sensible energy recovery. This reduction in latent and sensible load comes at the cost of compressor work. When both sensible and latent energy are recovered, the compressor work becomes the largest contributor to SEC. The compressor load with both sensible and latent energy recovery is much larger than the compressor load when only latent energy is recovered, as seen in Tables 9 and 13.

### Multi-Stage Flash

Multi-stage flash distillation is a decades-old approach to water desalination. This approach is typically used in the desalination of seawater, particularly in the Arab Gulf countries [37]. This approach splits salty seawater into a freshwater stream and a salty brine stream. A dilute desiccant solution may operate in the same way where the desiccant solution is split into a freshwater stream

and a brine stream of concentrated desiccant solution. This type of AWG system is shown in Figure 11.

An energy analysis was performed on a multi-stage flash thermal desalination to determine its SEC. This analysis was based on the approach used in other desalination analyses [38] [39]. The initial and final brine salinity were assumed for the analysis. The SEC was calculated as a function of inlet desiccant temperature and again as a function of top brine temperature.

The SEC of an MSF AWG system was analyzed by looking at the states of the desiccant solution entering and exiting the MSF section of the system. The minimum free energy required per volume of water produced is given by Eq. 23.

$$MFE \left[ \frac{kWh}{m^3} \right] = \frac{-RT_{TBT}}{(v_1 - v_2)\bar{v}} \int_{v_1}^{v_2} \ln(a) dv \quad (23)$$

$R$  is the gas constant,  $T_{TBT}$  is the top brine temperature,  $\bar{v}$  is the molar volume of water,  $v_1$  and  $v_2$  are the initial and final brine solution volumes, and  $a$  is the solution activity. To perform the integration, the activity must be defined in terms of solution volume. Activity is given in Eq. 24.

$$a = \frac{p}{p_0} \quad (24)$$

$p_0$  and  $p$  are the equilibrium vapor pressure of pure water and the brine solution respectively. Activity is a function of desiccant mass fraction. Activity vs. mass fraction data for LiCl brine solution was fit using a parabolic equation, given by Eq. 25.

$$a = 1 - 1.172\beta - 1.562\beta^2 \quad (25)$$

Since none of the salt leaves the brine solution, the mass of the salt in the inlet and outlet brine solution must be constant. The mass of salt can be related using Eq. 26.

$$\beta v = \beta_1 v_1 \quad (26)$$

Substituting Eqs. 25 and 26 into Eq. 23, the minimum free energy per volume of water may be expressed as in Eq. 27.

$$MFE \left[ \frac{kWh}{m^3} \right] = \frac{-RT}{(v_1 - v_2)\bar{v}} \int_{v_1}^{v_2} \ln \left( 1 - 1.172 \left( \frac{\beta_1 v_1}{v} \right) - 1.562 \left( \frac{\beta_1 v_1}{v} \right)^2 \right) dv \quad (27)$$

The system efficiency relates the 2<sup>nd</sup> Law efficiency and the Carnot efficiency. The system efficiency is given by Eq. 28.

$$\eta = \left( 1 - \frac{T_L}{T_{TBT}} \right) \left( \frac{\Delta T_{BP}}{\Delta T_{BP} + \Delta T_{MED}} \right) \quad (28)$$

$T_L$  is the inlet desiccant temperature,  $\Delta T_{BP}$  is the difference in the saturation temperature of pure water and the inlet desiccant solution, and  $\Delta T_{MED}$  is the temperature difference across each stage. The SEC, also known as the least heat of separation, is given by relating the minimum free energy per volume of water and the system efficiency. This relationship is given by Eq. 29.

$$SEC \left[ \frac{kWh}{m^3} \right] = \frac{MFE}{\eta} \quad (29)$$

The analysis assumed an inlet and outlet desiccant salinity of 400 g/kg and 440 g/kg respectively. LiCl desiccant was used for this analysis. When analyzing the effect of inlet desiccant temperature

on SEC, the top brine temperature was held at 100 °C (389 K). The results of this analysis are shown in Figure 16.

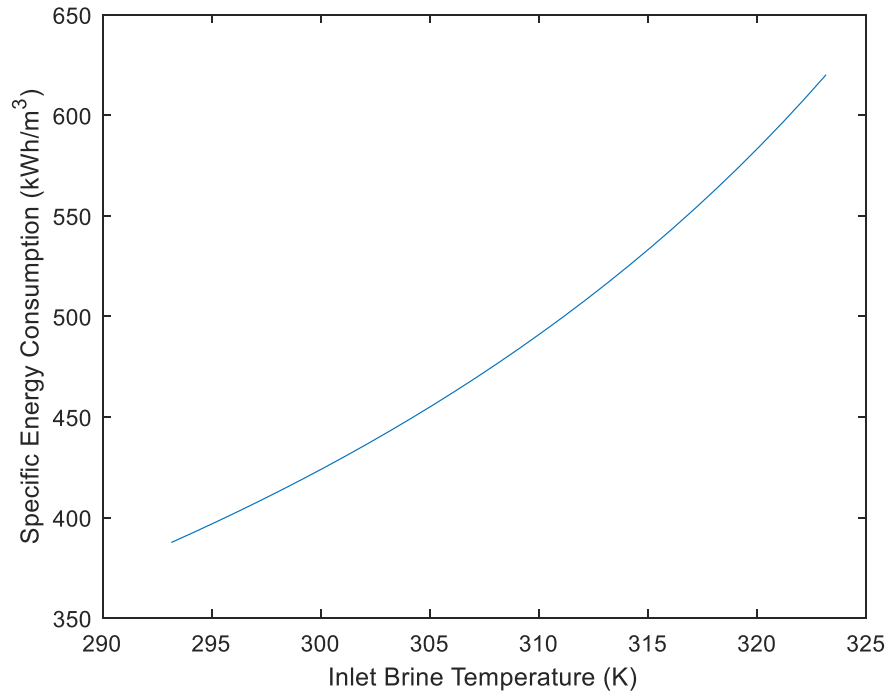


**Figure 16:** SEC of an MSF AWG system as a function of inlet desiccant temperature

For the next analysis, the inlet desiccant temperature was held at 25 °C (298 K) while the top brine temperature could vary. The results of this analysis are shown in Figure 17.

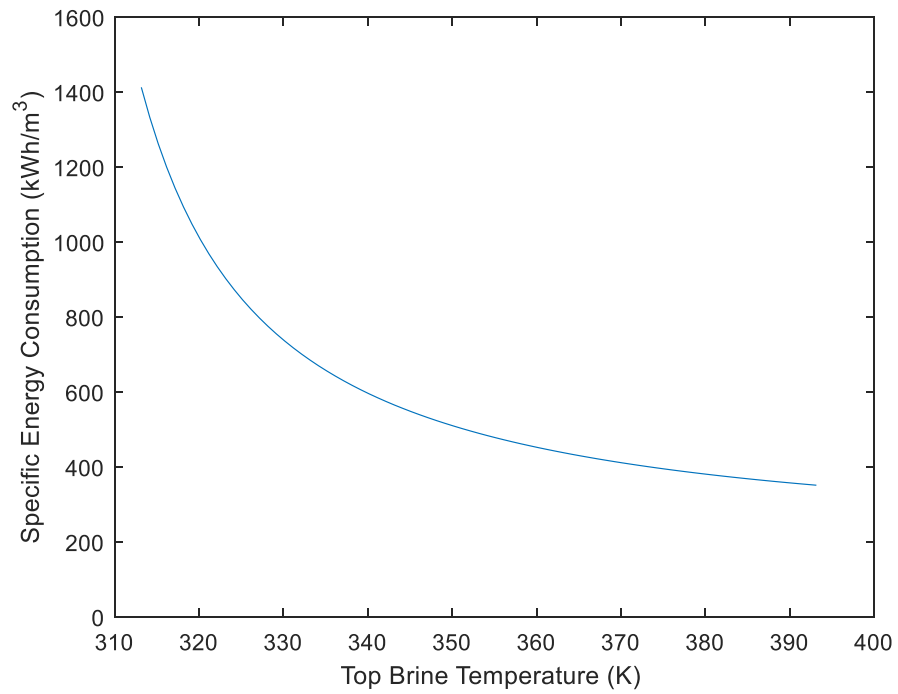


**Figure 17:** SEC of an MSF AWG system as a function of top brine temperature

The previous two figures show that the SEC can be minimized by minimizing the inlet desiccant temperature and maximizing the top brine temperature. This is because the system efficiency increases with top brine temperature. The relation between minimum free energy, SEC, system efficiency, and top brine temperature is shown in Figure 18.



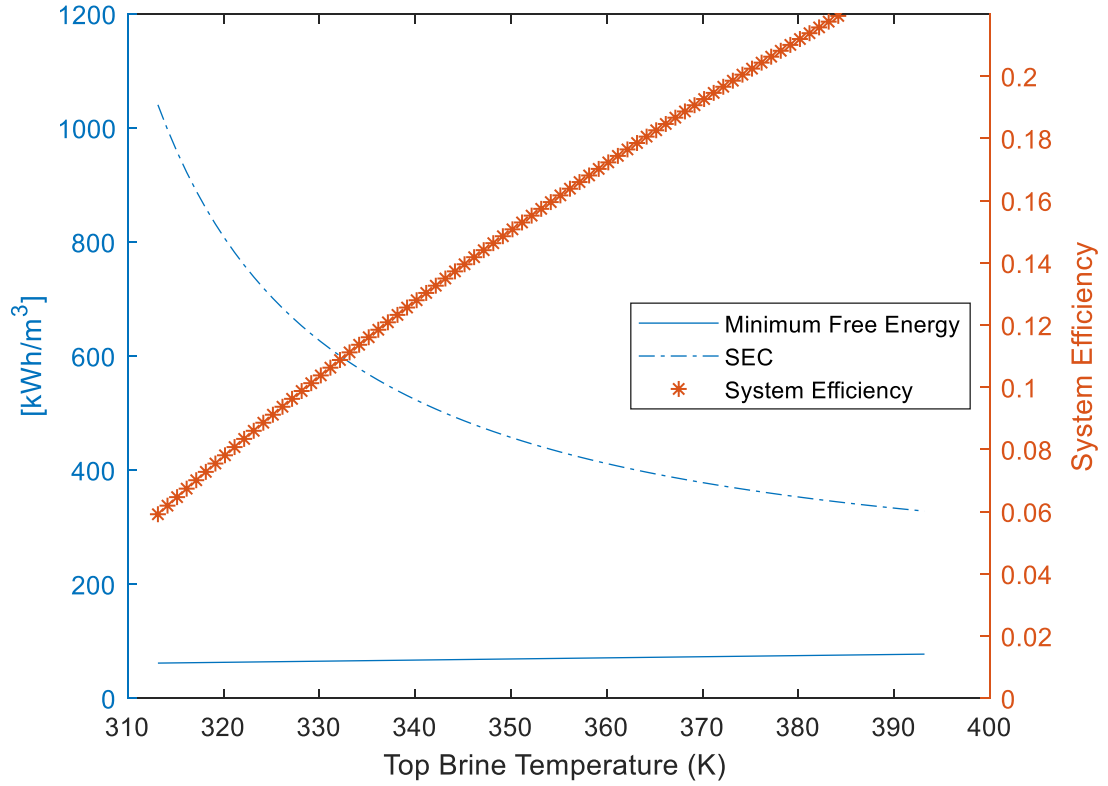


**Figure 18:** Relation of minimum free energy, SEC, system efficiency, and top brine temperature for an MSF AWG system

The SEC, also known as the least heat of separation, is given by relating the minimum free energy and system efficiency, as given in Equation 29. To find the minimum SEC, the inlet brine temperature was set to 20 °C and the top brine temperature to 120 °C. Using these temperatures, the minimum SEC is 334.1 kWh/m<sup>3</sup>. This figure shows that the inlet desiccant should not be preheated before the MSF section. To reach a high top brine temperature, a large temperature change across each stage or many stages would be required.

The effectiveness of MSF AWG is limited since the SEC is a function of the vapor pressure of water in equilibrium with the desiccant, which is a strong function of salinity. The salinity of the desiccant solution used in MSF AWG is typically at least 400 g/kg. The salinity of seawater, for which MSF is used as a desalination approach, is an order of magnitude less at 35 g/kg. Because the salinity of LiCl desiccant solution is nearly an order of magnitude larger than that of seawater, the SEC of LiCl desiccant solution is also nearly an order of magnitude greater than that of seawater (5 kWh/m<sup>3</sup>).

When comparing an MSF AWG system to a batch or continuous-style DAWG system, a DAWG system is better on an SEC basis if latent energy recovery is performed. Additionally, an MSF system has much more complex hardware than a batch-style DAWG system. This is because several effects are required by an MSF system for it to perform optimally. Because of the additional energetic costs and hardware complexities, a batch or continuous-style DAWG system would be better than an MSF AWG system.

## Thermodynamic Modelling Results Summary

Thermodynamic analyses were conducted for several AWG system configurations to determine their average annual SEC. The analyses were each conducted using TMY data from Daggett, CA. By analyzing the system performance at a shared geographical location with the same meteorological conditions, each system could be commonly compared. Each analysis resulted in an SEC value, which is a metric that allows for an impartial comparison of the energetic performance of different system configurations. The results of the thermodynamic analyses are summarized in Table 14.

**Table 14:** Minimum SEC estimates for several AWG system configurations

Configuration	$SEC_{sensible} \left[ \frac{kWh_{th}}{m^3} \right]$	$SEC_{latent} \left[ \frac{kWh_{th}}{m^3} \right]$	$SEC_{work} \left[ \frac{kWh_e}{m^3} \right]$	$SEC \left[ \frac{kWh}{m^3} \right]$
RAWG ( $COP_R = 3.5$ ), ( $\varepsilon = 0.8$ )	84	193	n/a	277
CC	n/a	n/a	446 (air) 37 ( $H_2O_v$ )	483
DAWG no energy recovery, 1 atm	204	682	n/a	886
DAWG no energy recovery, <1 atm	46	685	n/a	731
DAWG with latent recovery	199	2	9	210
DAWG with latent and sensible recovery	9	1	175	185
MSF	n/a	n/a	334	334

Desiccant-based AWG has the best SEC relative to other AWG configurations, but only when sensible and/or latent energy recovery is used. Another interesting note is that for a CC system, the energy requirement is used nearly entirely for the processing of dry air. By ensuring that the inlet air to the compressor has a high relative humidity, perhaps through the use of efficient upstream separation, then the amount of work required to process the water could be estimated to be a minimum of 37 kWh/m<sup>3</sup>, which is lower than any other AWG configuration.

When considering DAWG configurations, they typically require some sort of thermal load. This may be supplied directly via solar thermal heating, or indirectly using an electric heat pump. When using a heat pump, the energy load may be reduced by a factor equal to the coefficient of performance of the heat pump. While a heat pump may be used, it was not considered in the analysis due to uncertainty in the achievable performance and the additional economic cost the heat pump

hardware. If a heat pump with a high COP ( $>6$ ) were used in a DAWG system, it could make DAWG without energy recovery look appealing on an SEC basis.

When operating a DAWG system, especially one with a batch-style configuration, it is optimal to perform the water absorption process at night and the regeneration during the day. Nighttime typically has higher relative humidity and lower dry bulb temperature, which corresponds to a lower equilibrium mass fraction. A lower equilibrium mass fraction means that more water vapor can be absorbed during each absorption cycle. The regeneration process, which requires a large thermal load, takes place during the day when there is the greatest amount of solar insolation available.

## Economic Modelling

The purpose of the economic analysis for AWG is to determine the cost per unit of water, also called the levelized cost of water (LCOW). An LCOW will be determined for several different operating configurations. Since DAWG systems were deemed the optimal configuration on an SEC basis, only DAWG systems were considered for the economic analysis. The operating points of each system configuration are those with the minimum SEC, which was previously determined in the thermodynamic analyses.

Each operating configuration needs energy provided for the system to operate, either in the form of electricity or thermal energy. Electric energy was provided using photovoltaics (PV). The thermal energy was provided using either an electric resistance heater, a solar thermal unit such as a parabolic trough solar collector, or a heat pump. The levelized cost of energy (LCOE) for each energy source, as well as the SEC values associated with the sensible, latent, and compressor work, were used to determine the LCOW for each combination of DAWG operating configuration and energy delivery method. The general equation for LCOW is given in Eq. 30.

$$LCOW \left[ \frac{\$}{m^3} \right] = \frac{\sum cost}{\sum water} = \frac{Total\ cost\ of\ hardware,\ operation,\ and\ maintenance}{Total\ life\ cycle\ water\ production} \quad (30)$$

## Hardware Levelized Costs

The levelized cost of several pieces of hardware were found. The levelized cost of energy (LCOE), describes the cost per unit of electric or work energy. The levelized cost of heating (LCOH) is the cost per unit of thermal energy. The levelized cost of water (LCOW) gives the cost per unit of water.

The levelized cost of energy were found for PV ( $LCOE_{pv}$ ), compressors ( $LCOE_{comp}$ ), and positive displacement pumps ( $LCOE_{pdp}$ ).  $LCOE_{pv}$  describes the cost of any electric energy provided by photovoltaics. This energy is used to operate the compressors in AWG systems with latent energy recovery and the positive displacement pump in continuous-style AWG systems. Electricity is also used to provide the thermal load when using resistive heaters.  $LCOE_{comp}$  describes the hardware cost associated with compressive work in AWG system with latent energy recovery.  $LCOE_{pdp}$  describes the hardware cost associated with compressive work of the positive displacement pump in continuous-style AWG systems.

The levelized cost of heating were found for solar thermal hardware ( $LCOH_{st}$ ), resistance heaters ( $LCOH_{rh}$ ), and heat pumps ( $LCOH_{hp}$ ). These levelized costs describe the hardware cost associated

with the thermal load in each AWG system. The thermal load is only ever delivered using one of these three methods.

The levelized cost of water was found for thermal desalination hardware ( $LCOW_{desal}$ ). This cost is associated with the desalination and storage of water. These costs are mainly associated with the regenerator and storage vessel.

#### *LCOE PV*

The LCOE for thin film solar PV is given to be between 36-44 \$/MWh, or 0.036-0.044 \$/kWh [40]. With subsidies, it is projected that the LCOE of thin fin solar PV is between 32-41 \$/MWh, or 0.032-0.041 \$/kWh. As PV prices continue to fall, the LCOE for PV may fall as low as 0.01 \$/kWh. While this minimum price of PV electricity may not be currently attainable, future improvements in PV technology such as the use of low-cost multi-junction solar cells [41] and multi-exciton generation [42] may allow this price of PV electricity to be achieved. The effect of varying the price of PV between 0.01 – 0.05 \$/kWh was analyzed.

#### *LCOE Compressor Hardware*

When the system operates with latent energy recovery, a compressor is added to the system. The retail cost and power consumption for several refrigeration compressors were found [43]. The typical compressor lifetime was found to be approximately 50,000 hours [44]. Using these three values, the average levelized cost of compressor hardware is 0.0267 \$/kWh. The tabulated values of several compressor are given in Table 15. The derivation of the LCOE is given in Equation 31.

**Table 15:** Refrigeration compressor specifications [43] [44]

Power (hp)	Power (kW)	Cost (\$)	Lifetime (hours)	LCOE (\$/kWh)
0.1	0.07457	144.95	50000	0.038876224
0.125	0.0932125	139.95	50000	0.030028161
0.16666667	0.12428333	199.95	50000	0.032176478
0.2	0.14914	244.95	50000	0.03284833
0.2	0.14914	185.95	50000	0.024936301
0.2	0.14914	425.95	50000	0.057120826
0.25	0.186425	334.95	50000	0.035934022
0.25	0.186425	229.95	50000	0.024669438
0.25	0.186425	165.95	50000	0.017803406
0.25	0.186425	194.95	50000	0.020914577
0.33333333	0.24856667	244.95	50000	0.019708998
0.33333333	0.24856667	229.95	50000	0.018502079
0.33333333	0.24856667	319.95	50000	0.025743597
0.5	0.37285	384.95	50000	0.020649055
0.75	0.559275	414.95	50000	0.014838854
0.75	0.559275	355.95	50000	0.012728979

$$LCOE_{comp} = average(LCOE) = 0.0267 \frac{\$}{kWh} \quad (31)$$

#### *LCOE Positive Displacement Pump*

When the system is operating continuously, a positive displacement pump is needed to pressurize the collected water back up to ambient pressure. The retail price and power consumption of a positive displacement pump was found [45]. While pump life expectancy may vary due to a variety of factors, a pump lifetime of 10,000 hours was assumed [46]. Using these values, the levelized cost of positive displacement pump hardware is 0.500 \$/kWh. The derivation of this value is given in Equation 32.

$$LCOE_{pdp} = \left( \frac{184.60 \$}{0.05 hp} \right) \left( \frac{1 hp}{0.7547 kW} \right) \left( \frac{1 lifetime}{10000 hr} \right) = 0.500 \frac{\$}{kWh} \quad (32)$$

#### *LCOH Solar Thermal Hardware*

The current levelized cost of heating for low-cost solar thermal energy hardware is given to be 0.027 \$/kWh [47]. The Department of Energy is looking to improve this technology such that the LCOH is 0.01 \$/kWh and 0.015 \$/kWh for large- and small-scale systems, respectively. The effect of varying the levelized cost of solar thermal heating between 0.01-0.05 \$/kWh was analyzed.

#### *LCOH Resistance Heater*

The retail price and power consumption of several baseboard resistance heaters were found [48]. Based on an operating time of 8 hours/day and a typical resistance heater lifetime of 20 years [49], the levelized cost of resistance heating hardware is 0.000695 \$/kWh. The tabulated values for several baseboard heaters are given in Table 16. This gives the average levelized cost of power to be 0.041 \$/W. The derivation of this value is given in Equation 33.

**Table 16:** Baseboard heater specifications [48]

Cost (\$)	Power (W)	Heater Length (in.)	Levelized Cost of Power (\$/W)
87.86	2500	96	0.0351
58.78	1500	72	0.0392
82.44	2500	96	0.0330
44.58	1000	48	0.0446
38.19	750	36	0.0509

$$LCOH_{rh} = \left( \frac{\$ 0.041}{W} \right) \left( \frac{1}{20 years} \right) \left( \frac{1 year}{365 days} \right) \left( \frac{1 day}{8 operating hours} \right) \left( \frac{1000 Wh}{1 kWh} \right) = 0.000695 \frac{\$}{kWh} \quad (33)$$

#### *LCOH Heat Pump*

The retail price and power consumption of several heat pumps were found [50]. Based on an operating time of 8 hours/day and a typical heat pump lifetime of 15 years [51], the levelized cost of heat pump hardware is 0.0298 \$/kWh. This value takes into account the hardware cost and the heating power input. The heating power input refers to the electric power consumed by the heat

pump when operating in standard conditions. Because this refers to the power consumption of the heat pump, the coefficient of performance (COP) doesn't need to be taken into account when calculating the LCOH value. However, the COP does need to be considered when relating the LCOH to the thermal energy load provided by the heat pump. The tabulated values for several heat pumps are given in Table 17, which gives an average levelized cost of heating power of 1.306 \$/W. The derivation of the levelized cost of heating is given in Equation 34.

**Table 17:** Heat pump specifications [50]

Cost (\$)	Heating Power Input (W)	Levelized Cost of Power (\$/W)
1310.40	720	1.8200
1468.80	1100	1.3353
1800.00	1600	1.1250
2091.60	1680	1.2450
2354.40	2340	1.0062

$$LCOH_{hp} = \left( \frac{1.306 \$}{W} \right) \left( \frac{1}{15 \text{ years}} \right) \left( \frac{1 \text{ year}}{365 \text{ days}} \right) \left( \frac{1 \text{ day}}{8 \text{ operating hours}} \right) \left( \frac{1000 \text{ Wh}}{1 \text{ kWh}} \right) = 0.0298 \frac{\$}{kWh} \quad (34)$$

#### *LCOW Thermal Desalination Hardware*

Previous studies have analyzed the levelized cost of water for desalination hardware [52]. This value is given to be 0.855 \$/m<sup>3</sup> of water. This value is based off the operation of a thermal desalination plant. A breakdown of levelized cost of water for a thermal desalination plant is shown in Figure 19.

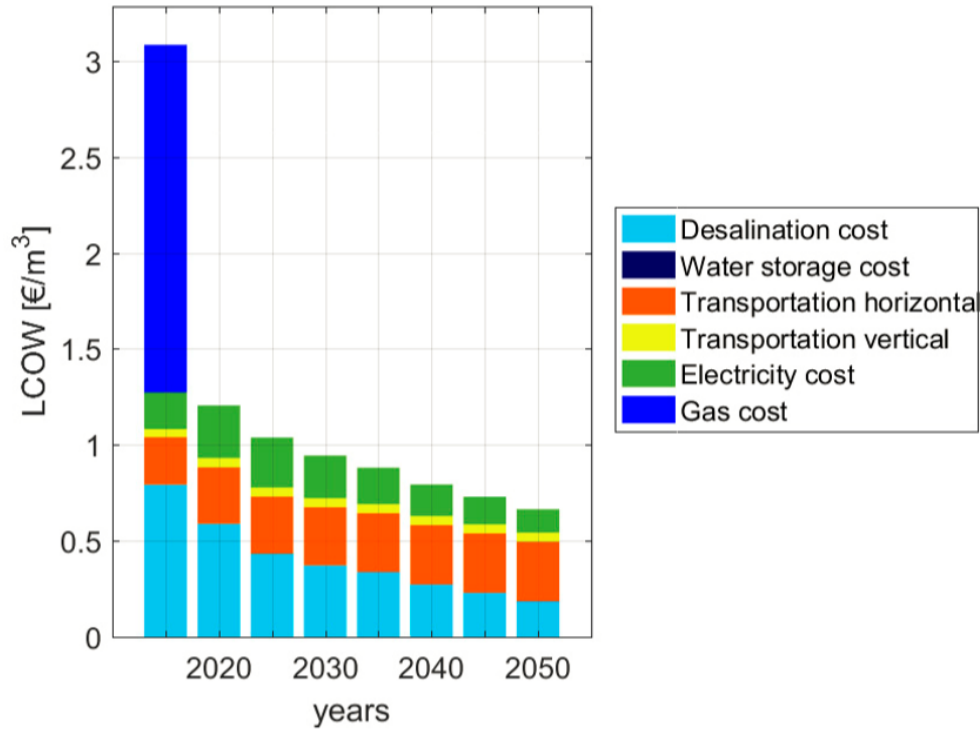


**Figure 19:** LCOW breakdown for a desalination plant [52]

Figure 19 shows that the largest projected decrease in LCOW is due to a reduction in gas and electricity consumption. There will also be incremental increases in system efficiency over time which will further reduce the LCOW. The LCOW cost relevant to the AWG system is the desalination cost. The 2015 desalination cost is shown in Figure 19 to be approximately 0.75 €/m<sup>3</sup>. The conversion of this value to the U.S. dollar used in the AWG analyses is shown in Equation 35.

$$LCOW_{desal} = \left( \frac{0.75 \text{ €}}{1 \text{ m}^3} \right) \left( \frac{1.14 \$}{1 \text{ €}} \right) = 0.855 \frac{\$}{\text{m}^3 \text{ water}} \quad (35)$$

### Neglected Costs

Not all the life cycle costs of the system were accounted for in this economic analysis. These include system emissions and emission controls, environmental and human health impacts, condensate purification, raw material collection, and system disposal.

Some levelized hardware costs were neglected during the analysis. These include the heat exchangers for heat recovery, as well as pumps required to circulate the liquid desiccant for continuous operation system configurations.

Heat recovery heat exchangers were neglected because the heat transfer they facilitate utilizes thermal energy already in the AWG system and does not require an external energy supply to operate. If the AWG system were massively scaled up, then the cost of energy to operate the system would dominate the hardware cost of the heat exchangers. Thus, by neglecting these types of hardware costs, the LCOW of a certain system configuration will be constant no matter how much the system is scaled up.

Pump work for moist air circulation was not taken into consideration in the analysis. Because of this, the hardware cost associated with the pump was also neglected for a similar reason to the heat recovery heat exchangers. If the AWG system were scaled up, then the hardware cost of the pump would become negligible when compared to the cost of energy for system operation. Additionally, different systems would have different piping networks for the moist air. Each piping network would have different piping losses which may drastically affect the pumping work from system to system, especially when scaling up the systems. In order to maintain a common comparison of different AWG systems, these piping losses and subsequently the pumping work associated with these losses were not considered.

### LCOW Analyses

The levelized cost of water was found for several different types of DAWG system configurations and different sources of thermal energy. The first two systems analyzed were batch-style DAWG systems operating at atmospheric and sub-atmospheric pressure with no energy recovery. Three different thermal energy sources were considered: resistance heating, solar thermal hardware, and heat pumps. The LCOW using these thermal energy sources are given in Eqs. 36-38 respectively. The configurations analyzed using these equations are shown in Table 18.

$$LCOW_{rh} = LCOE_{pv} * SEC + LCOH_{rh} * (SEC_{sensible} + SEC_{latent}) + LCOW_{desal} \quad (36)$$

$$LCOW_{st} = LCOE_{pv} * SEC_{work} + LCOH_{st} * (SEC_{sensible} + SEC_{latent}) + LCOW_{desal} \quad (37)$$

$$LCOW_{hp} = \left( \frac{LCOE_{pv}}{COP} + \frac{LCOH_{hp}}{COP} \right) * (SEC_{sensible} + SEC_{latent}) + LCOE_{pv} * SEC_{work} + LCOW_{desal} \quad (38)$$

**Table 18:** System configurations with no energy recovery analyzed in economic analysis

System Configuration	Energy Recovery Method	System Pressure	Heat Source	Equation Number
Batch-Style DAWG	None	Atmospheric	Resistance Heating	36
Batch-Style DAWG	None	Atmospheric	Solar Thermal	37
Batch-Style DAWG	None	Atmospheric	Heat Pump	38
Batch-Style DAWG	None	Sub-Atmospheric	Resistance Heating	36
Batch-Style DAWG	None	Sub-Atmospheric	Solar Thermal	37
Batch-Style DAWG	None	Sub-Atmospheric	Heat Pump	38

$SEC_{sensible}$ ,  $SEC_{latent}$ , and  $SEC_{work}$  are the portion of the SEC due to the sensible, latent, and compressive work loads respectively, while  $SEC$  refers to the total energy load. The third and fourth systems analyzed were a batch-style DAWG system with latent energy recovery and a continuous-style DAWG system with both latent and sensible energy recovery. Both system configurations utilize compressors and positive displacement pumps. Therefore, additional terms must be added to the LCOW expressions for the costs associated with the additional hardware. The LCOW for these systems can be found using Eqs. 39-41. The configurations analyzed using these equations are shown in Table 19.

$$LCOW_{rh} = LCOE_{pv} * SEC + LCOH_{rh} * (SEC_{sensible} + SEC_{latent}) + LCOE_{pdp} * SEC_{work,pdp} + LCOE_{comp} * SEC_{work,comp} + LCOW_{desal} \quad (39)$$

$$LCOW_{st} = LCOE_{pv} * SEC_{work} + LCOH_{st} * (SEC_{sensible} + SEC_{latent}) + LCOE_{pdp} * SEC_{work,pdp} + LCOE_{comp} * SEC_{work,comp} + LCOW_{desal} \quad (40)$$

$$LCOW_{hp} = \left( \frac{LCOE_{pv}}{COP} + \frac{LCOH_{hp}}{COP} \right) * (SEC_{sensible} + SEC_{latent}) + LCOE_{pdp} * SEC_{work,pdp} + LCOE_{comp} * SEC_{work,comp} + LCOW_{desal} \quad (41)$$



**Table 19:** System configurations with energy recovery analyzed in economic analysis

System Configuration	Energy Recovery Method	System Pressure	Heat Source	Equation Number
Batch-Style DAWG	Latent	Atmospheric	Resistance Heating	39
Batch-Style DAWG	Latent	Atmospheric	Solar Thermal	40
Batch-Style DAWG	Latent	Atmospheric	Heat Pump	41
Continuous-Style DAWG	Sensible and Latent	Sub-Atmospheric	Resistance Heating	39
Continuous-Style DAWG	Sensible and Latent	Sub-Atmospheric	Solar Thermal	40
Continuous-Style DAWG	Sensible and Latent	Sub-Atmospheric	Heat Pump	41

In these expressions, the SEC due to compressive work is further split up into that due to the positive displacement pump,  $SEC_{work,pdp}$ , and due to the compressor,  $SEC_{work,comp}$ .

Using Eqs. 36-38, the LCOW for a batch-style DAWG system with no energy recovery operating at atmospheric and sub-atmospheric pressure were found. The results of this analysis are shown in Figures 20 and 21, where LCOW is plotted versus the cost of either PV electricity or solar thermal heating, depending on the system configuration being analyzed. For systems with PV and solar thermal heating, the cost being varied is noted in the plot legend.

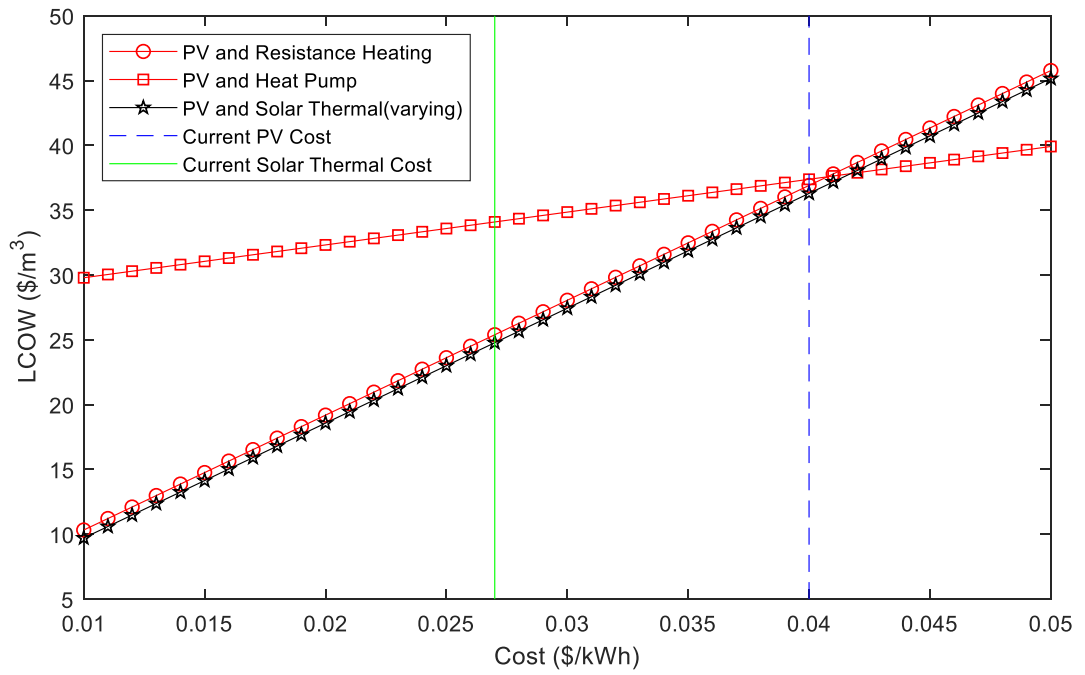


**Figure 20:** LCOW of a DAWG batch-style system with no energy recovery at atmospheric pressure

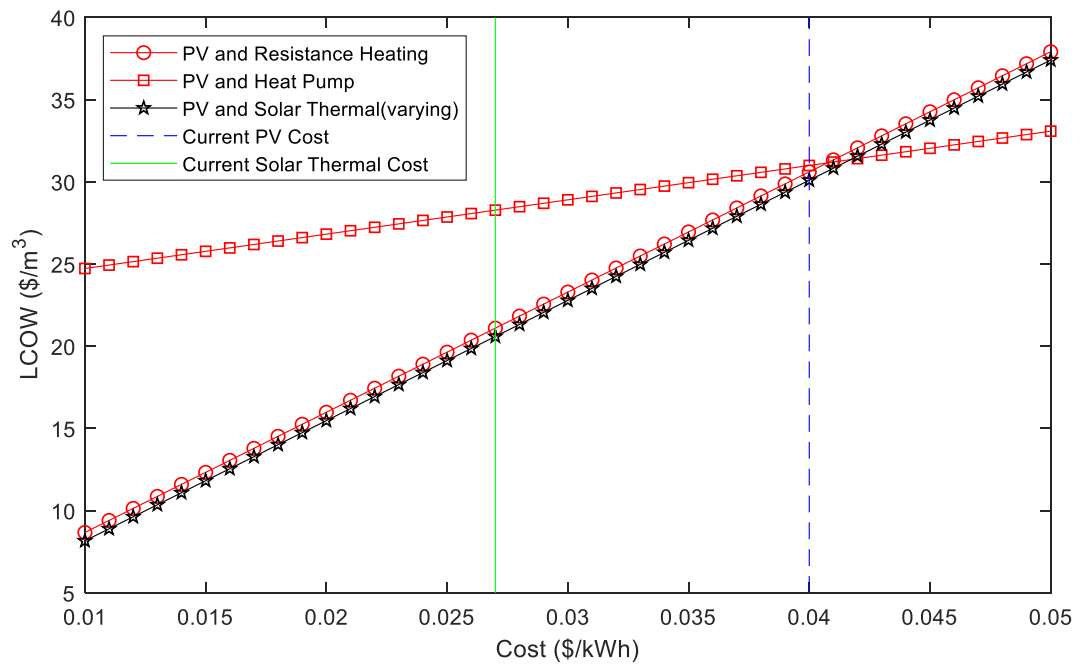


**Figure 21:** LCOW of a DAWG batch-style system with no energy recovery at sub-atmospheric pressure

These figures show that when the cost of PV electricity and solar thermal heat is high, it makes most sense to operate the system with a heat pump. Based off the current cost of PV electricity and

solar thermal heat, it would make the most sense to operate the system using solar thermal heating since Figures 20 and 21 shows solar thermal heating has the lowest LCOW at the current PV electricity cost. Additionally, if the price of PV electricity falls much lower than the cost of solar heating, then it makes then most sense to operate the system using resistance heating since Figures 20 and 21 show resistance heating has the lowest LCOW when the cost of PV electricity falls to 0.01 \$/kWh.

Using Eqs. 39-41, the LCOW was found for DAWG systems with energy recovery. The LCOW for a batch-style DAWG system with latent energy recovery is given in Figure 22. It was found that this system's lowest LCOW could be attained when the energy loads were provided using PV and resistance heaters when PV electricity costs 0.01 \$/kWh. The breakdown of the levelized cost of water for this PV electricity price point is provided in Table 20.

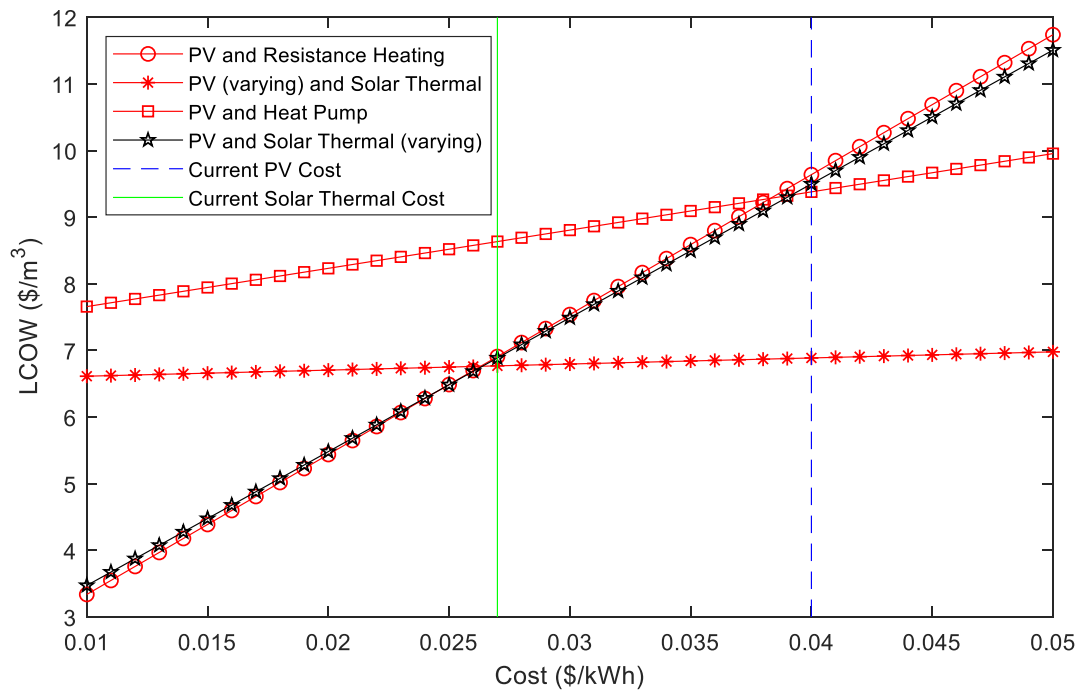


**Figure 22:** LCOW of a batch-style DAWG system with latent energy recovery

**Table 20:** Minimum LCOW breakdown for batch-style DAWG system with latent energy recovery

	PV	Resistance Heating	Distillation Hardware	Compressor	Total
LCOW [\$/m³]	2.100	0.140	0.855	0.244	3.339
Percentage of Total LCOW	62.9%	4.2%	25.6%	7.3%	N/A

The LCOW for a continuous-style DAWG system with latent and sensible energy recovery is given in Figure 23. It was found that this system's lowest LCOW could be attained when the energy loads

were provided using PV and resistance heaters when PV electricity costs 0.01 \$/kWh. Additionally, using PV and a heat pump has nearly the same LCOW at the same PV electricity cost, while deviating much less from this minimum LCOW value over the entire range of PV electricity costs analyzed. The breakdown of the levelized cost of water for this PV electricity price point is provided in Table 21. The breakdown of the levelized cost of water for the current PV electricity price point is provided in Table 22.

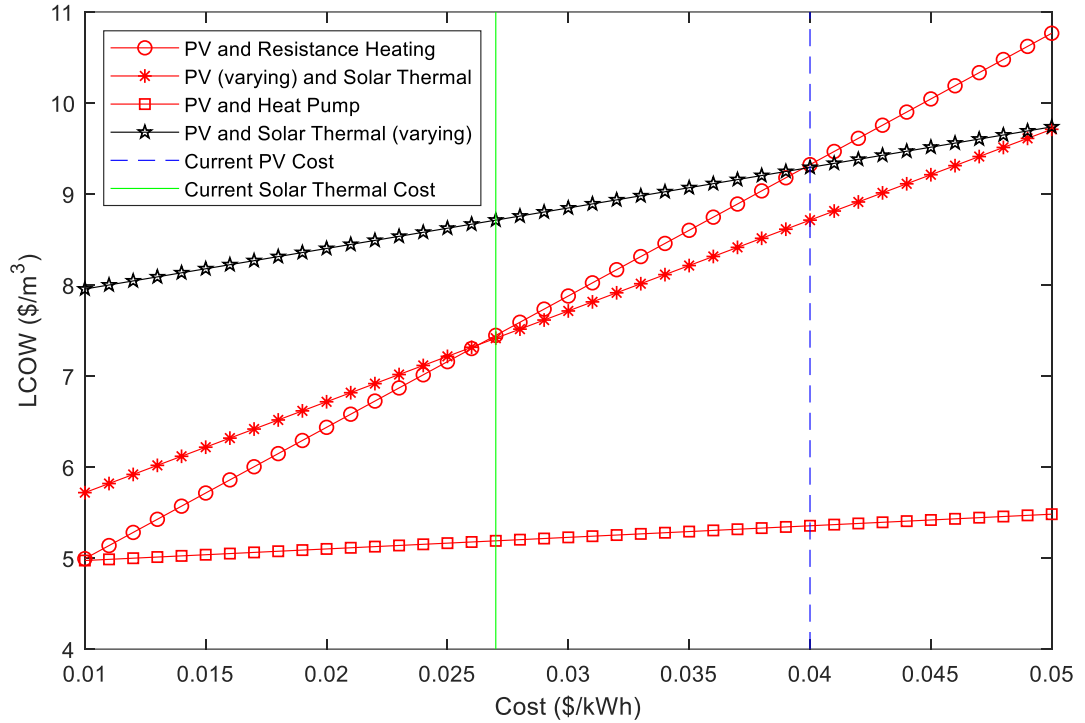


**Figure 23:** LCOW of a continuous-style DAWG system with latent and sensible energy recovery

**Table 21:** Minimum LCOW breakdown for a continuous-style DAWG system with latent and sensible energy recovery using minimum PV electricity cost

	PV	Resistance Heating	Distillation Hardware	Compressor	Positive Displacement Pump	Total
LCOW [\$/m <sup>3</sup> ]	1.443	0.031	0.855	2.664	0	4.993
Percentage of LCOW	28.9%	0.6%	17.1%	53.4%	0%	N/A

**Table 22:** LCOW breakdown for a continuous-style DAWG system with latent and sensible energy recovery using current PV electricity cost

	PV	Resistance Heating	Distillation Hardware	Compressor	Positive Displacement Pump	Total
LCOW [\$/m <sup>3</sup> ]	5.772	0.031	0.855	2.664	0	9.322
Percentage of LCOW	61.9%	0.3%	9.2%	28.6%	0%	N/A

Tables 21 and 22 show that for a continuous-style DAWG system with latent and sensible energy recovery using resistance heating, the cost of PV electricity is the greatest contributor to the LCOW at the current price of PV electricity. As the cost of PV electricity decreases from its current price of 0.04 \$/kWh to 0.01 \$/kWh, the cost of the compressor hardware becomes the greatest contributor to LCOW.

If the cost of PV electricity can fall to a cost of 0.01 \$/kWh, then a batch-style DAWG system with latent energy recovery is able to provide water at the lowest monetary cost. The reason for this is because when compared the a continuous-style DAWG system with both latent and sensible energy recovery, the batch-style system uses much less compressor work. Compressor work is a more expensive form of energy than thermal energy provided by resistance heaters. Therefore, even though the continuous-style system utilizes less energy, the energy it uses is more expensive, which drives up the LCOW.

If the price of PV electricity does not fall much lower than its current price, then Figure 23 shows that the thermal energy should be supplied using a heat pump. This is because the LCOW for a continuous-style DAWG system using a heat pump doesn't change much as the price of PV electricity varies. If PV electricity costs more than 0.02 \$/kWh, then the LCOW is minimized by using a continuous-style DAWG system utilizing sensible and latent energy recovery and a heat pump rather than a batch-style DAWG system with latent energy recovery and a resistive heater.

### Optimal System Configuration

When choosing the optimal system configuration, the results of both the thermodynamic and economic modeling must be considered. Table 14 shows that when latent energy is implemented in a DAWG system, the SEC may be as low as 210 kWh/m<sup>3</sup>, while when both latent and sensible energy are implemented in a DAWG system, the SEC may be as low as 185 kWh/m<sup>3</sup>.

When considering the LCOW of these systems, the DAWG system with latent energy recovery provides water at 3.34 \$/m<sup>3</sup>, while the DAWG system with both latent and sensible energy recovery provides water at 4.99 \$/m<sup>3</sup>. The reason the cost of water is higher with the system with both types of energy recovery is that the LCOW was calculated for the operating point with the lowest SEC. The operating point with lowest SEC using both latent and sensible energy recovery uses much more compressive work compared to the system operating with only latent energy recovery, as seen

when comparing Tables 20 and 21. Since energy provided by a compressor is a more expensive form of energy than heat provided by a resistance heater, the cost of the energy required to make the water increases, which in turn increases the water's cost. Another type of analysis could have been to search for the operating point with the lowest LCOW, but this new operating point would not be operating with the smallest possible SEC.

Due to its lower LCOW, it was decided that a DAWG system with latent energy recovery is the optimal AWG system configuration. This is due to having the lowest LCOW and only a slightly higher SEC value than a system with latent and sensible energy recovery. With the current cost of PV electricity and system hardware, latent energy recovery is recommended. In the future, if certain hardware costs drastically decrease, then energy recovery may not be recommended. For example, if the cost of PV electricity decreased so much that it was essentially free, then it would be cheaper to run the system using as much PV electricity and decreasing the cost of the total system hardware. This would consist of eliminating any hardware associated with energy recovery and using a system with just the desalination hardware and the cheapest thermal energy supply, which from the analysis would be resistance heaters.

## Chapter 3: Desiccant Evaluation

Several tests were conducted on different desiccants to better understand the effects of different desiccant characteristics on total water absorption and water absorption rate. The initial desiccant was mixed to a known initial solution mass, solution volume, and desiccant mass fraction. During the test, the total solution mass, ambient dry bulb temperature, and relative humidity were recorded using a DAQ system. The desiccant characteristics tested to understand their effect on water absorption included the type of desiccant, mixing or not mixing the desiccant, the depth of the desiccant solution, fan speed, and the surface area of the desiccant. To test each of these characteristics, a single desiccant characteristic was altered between tests in order to isolate the effect of a single dependent variable on water absorption. Additionally, the tests were used to verify the theoretical desiccant solution equilibrium property data which was used in the thermodynamic analyses [36]. The theoretical relationship between dry bulb temperature, desiccant mass fraction, and relative humidity for desiccant solutions at one atmosphere is shown in Figures 24 and 25. Figure 24 shows the relationship for calcium chloride solutions, while Figure 25 shows the relationship for lithium chloride solutions. In the figures, the crystallization line is shown in black, while the lines of constant relative humidity are shown in red. If the operating point corresponding to the ambient dry bulb temperature and relative humidity lies above the crystallization line, then the desiccant solution will absorb water vapor until the corresponding equilibrium desiccant mass fraction is reached.

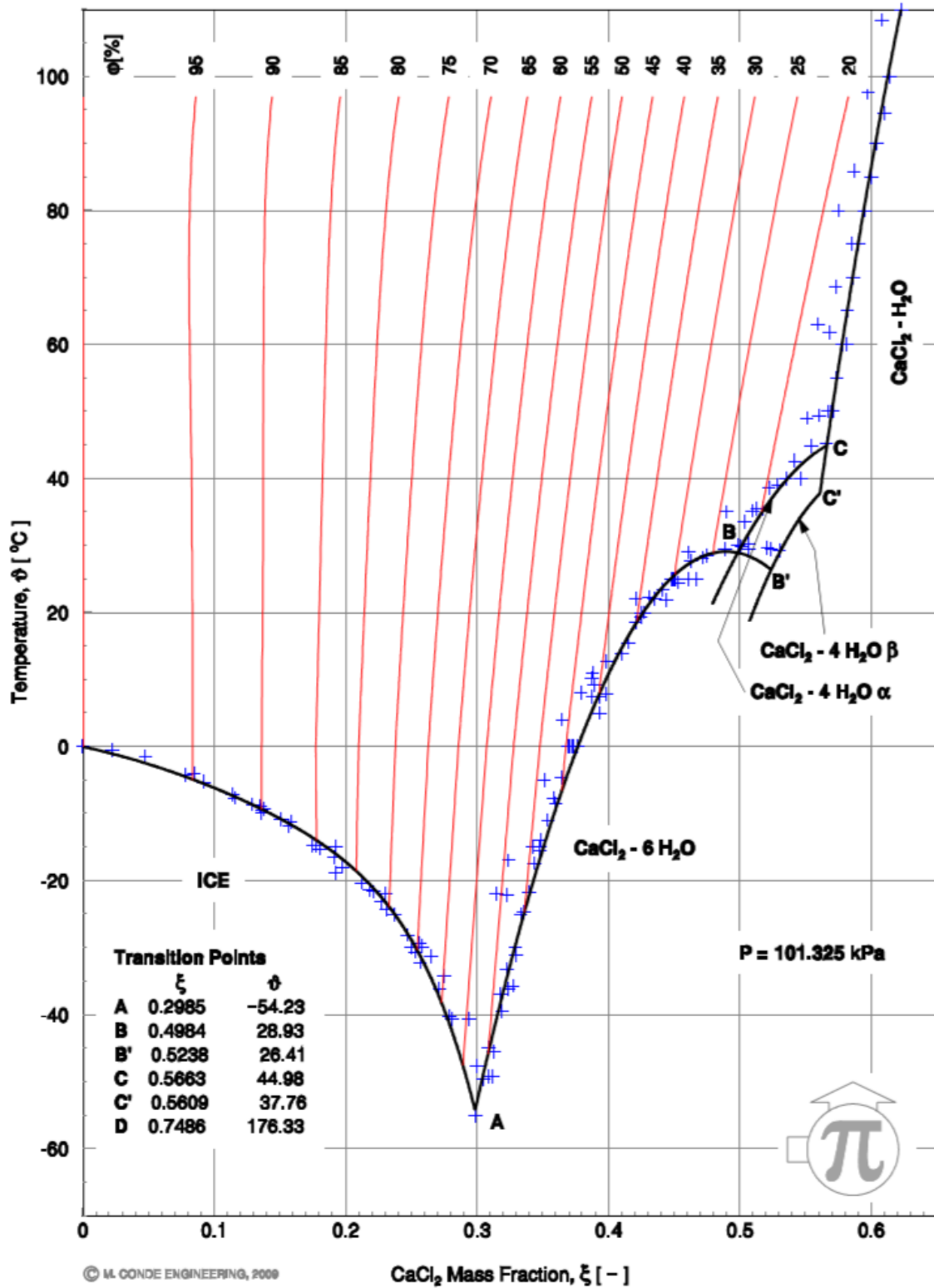


**Figure 24:** Plot showing relationship between desiccant mass fraction, dry bulb temperature, and relative humidity for  $\text{CaCl}_2$  solutions at one atmosphere [36]



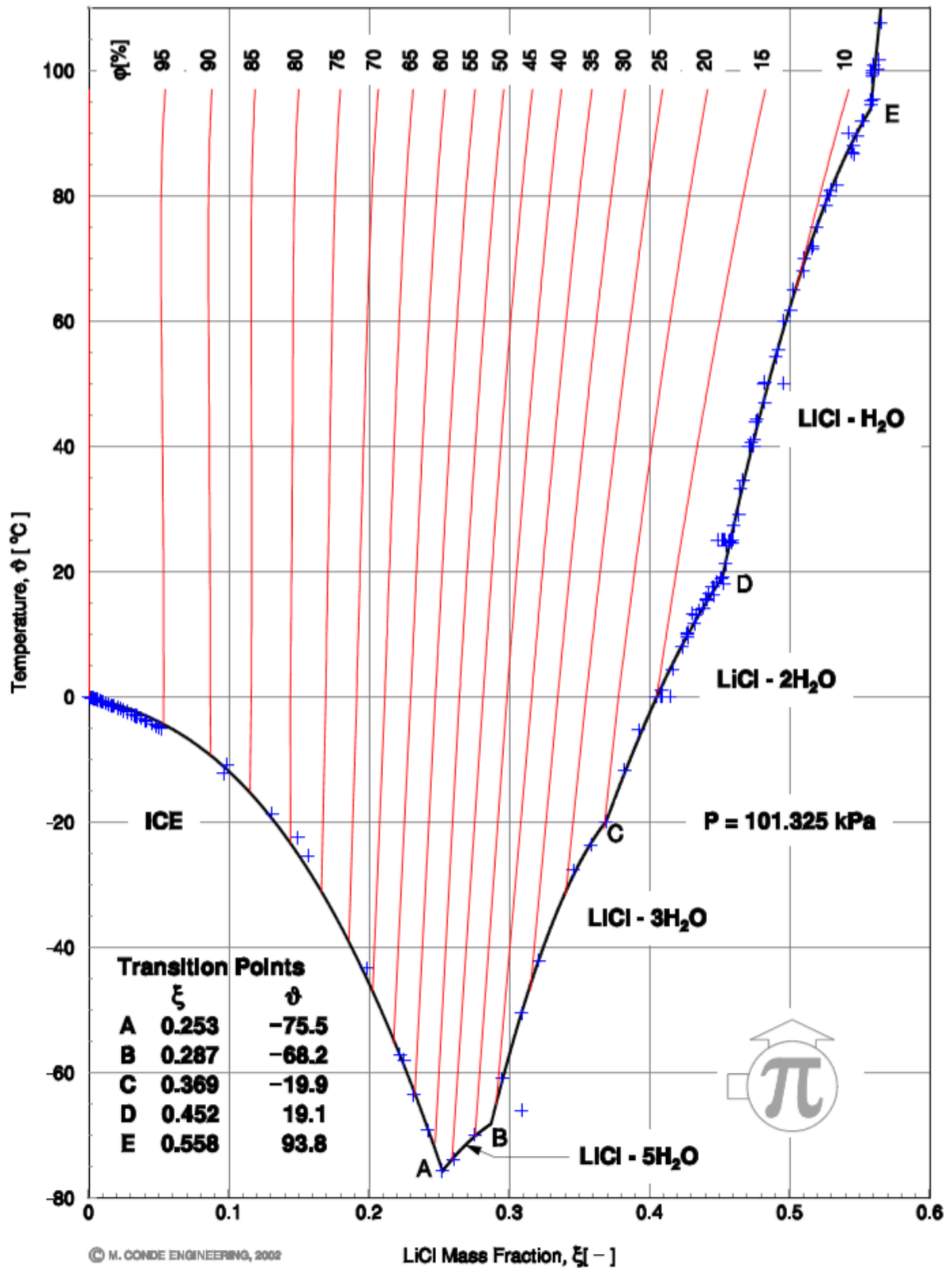


**Figure 25:** Plot showing relationship between desiccant mass fraction, dry bulb temperature, and relative humidity for LiCl desiccant solutions at one atmosphere [36]

## Testing Setup

A schematic of the experimental setup is shown in Figure 26. Air is blown into a lidded box using a fan. While moving through the box, the air moves across the desiccant solution in the petri dish before leaving the box out the sides. The desiccant solution absorbs some of the water vapor out of the air, causing the solution's mass and volume to increase. The solution mass would start out between 30 – 60 grams and increase over the course of the test. An Ohaus scale is used to measure the system's mass and send it to a DAQ system. Since the box would overload the scale, it is propped up around the scale using external supports. A dish support extends through the bottom of the box to hold the petri dish below the fan. The total mass of the dish support, petri dish, and desiccant solution is measured by the scale. When testing the effect of mixing the desiccant, a mixer was suspended above the test to agitate the desiccant solution. The equipment for this setup is shown in Figure 27.

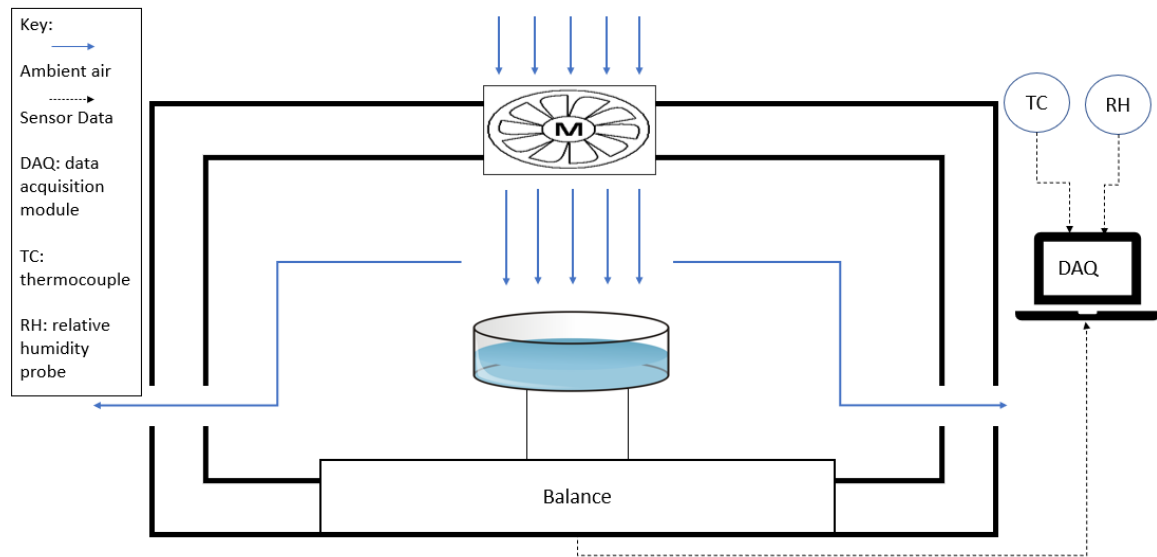


**Figure 26:** Schematic of the experimental setup for desiccant testing [53] [54]

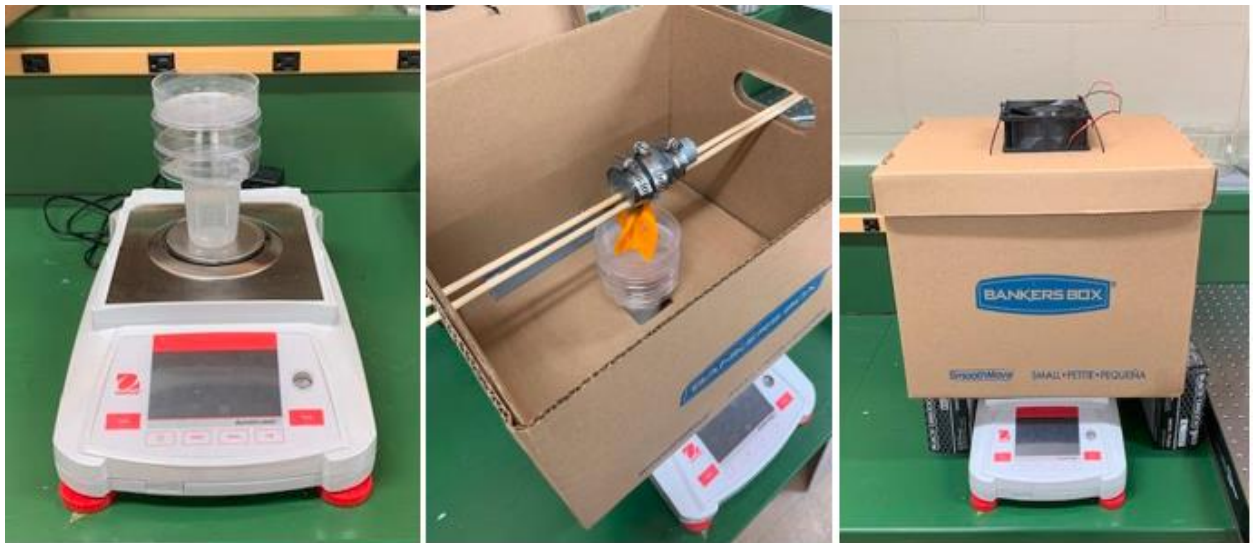


**Figure 27:** Experimental setup for desiccant testing

## Desiccant Tests

### Effect of fan speed on water absorption

The effect of fan speed on water absorption was tested. A high and low fan speed were tested, corresponding to air speeds of 16 mph and 4 mph respectively. A calcium chloride desiccant solution with an initial solution depth of  $\frac{1}{4}$ " and an initial desiccant mass fraction of 0.6 was used. A petri dish with a 3.5" diameter was used to house the desiccant solution. The solution was mixed during the test. During the testing process, water vapor was absorbed by the desiccant increasing its mass. This mass was recorded on a DAQ system. The tests were each conducted in a temperature-controlled room. A separate DAQ system was used to record the ambient dry bulb temperature and relative humidity. The dry bulb temperature and relative humidity were used to determine the theoretical equilibrium concentration of the desiccant solution, and thus the expected uptake of water. The tests were run until the mass readings stabilized, at which point the solution was assumed to be at equilibrium. These stabilization processes many times took several days.

One issue that occurred during testing was that the DAQ system responsible for measuring dry bulb temperature and relative humidity would often run out of memory, leaving these data sets incomplete. While the daily temperature and relative humidity was recorded by hand, many times a more complete set of data was not available. In order to compensate for this, minimum and maximum error bars were set to the theoretical limits for the mass of water absorbed and equilibrium mass fraction. These error bars were based on the known range of relative humidity and temperature over the span of the testing period. Error bars were required when plotting all the desiccant property evaluation results in Chapter 3.

The results of these tests are given in Figures 28, 29, and 30. Figure 28 shows the mass of water absorbed over time. Figure 29 shows the desiccant mass fraction over time. Figure 30 shows the rate of water absorption over time.

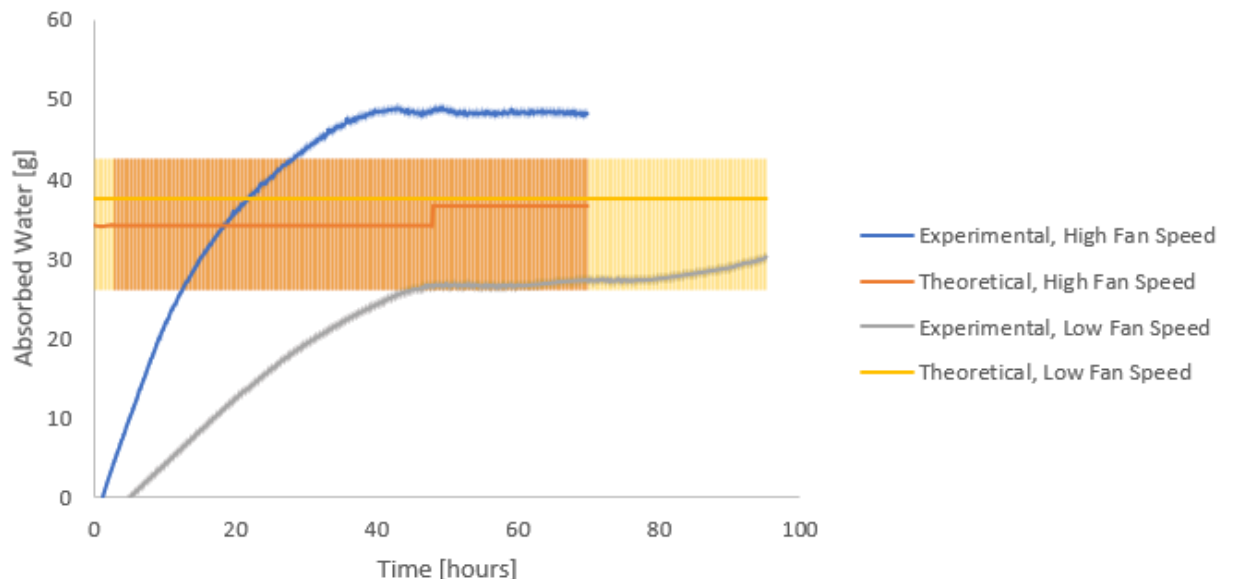


**Figure 28:** Mass of water absorbed over time, comparing low and high fan speeds

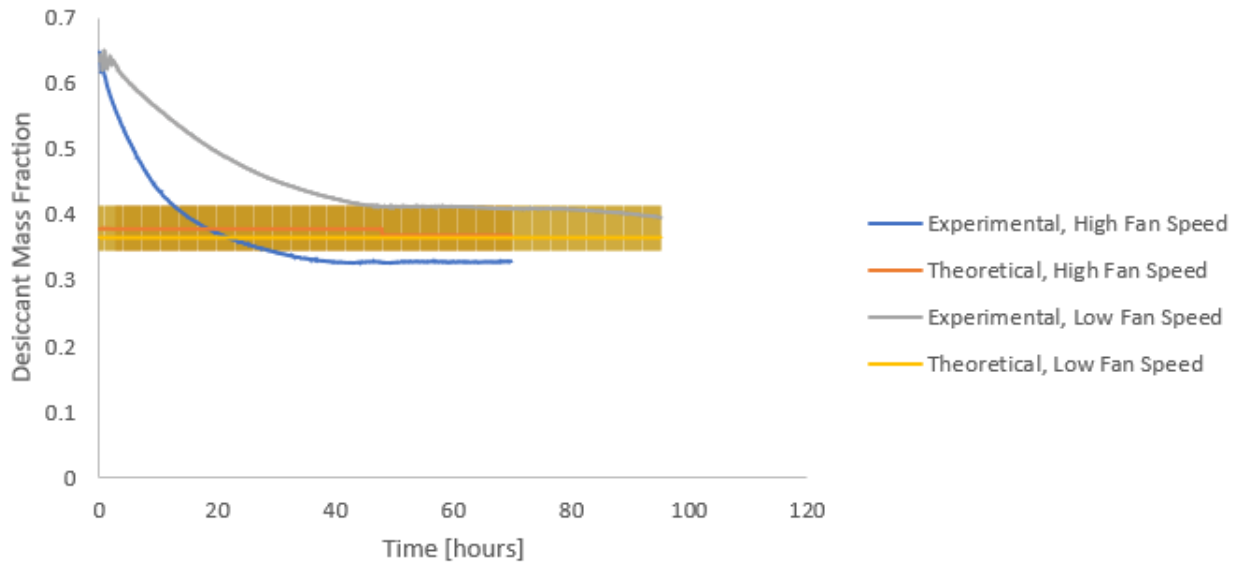


**Figure 29:** Desiccant mass fraction over time, comparing low and high fan speeds

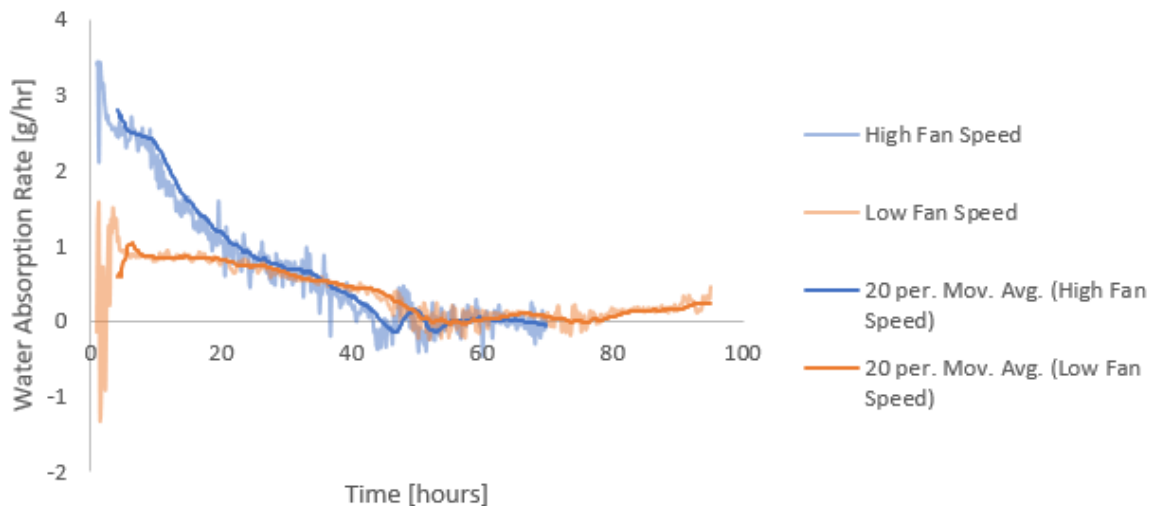


**Figure 30:** Water absorption rate over time, comparing low and high fan speeds

These figures show that a higher fan speed correlates to a higher water absorption rate. When comparing flow rate of water vapor through the fan to the water absorption rate by the desiccant, the water absorption rate is only 0.1% and 0.3% of the water vapor flow rate for the high fan speed and low fan speed tests respectively. These values show that the difference in water absorption rate is not due to a change in vapor concentration above the desiccant solution. This indicates that the difference in water absorption rate is being caused by additional mixing of the desiccant solution by the fan. For higher fan speeds, the desiccant will be mixed more and subsequently have a higher water absorption rate. A higher fan speed should be used when using a DAWG system.

Using a high fan speed to aid in mixing corresponds well to the gas-liquid mass transfer theories. These theories include the two-film theory, the penetration theory or “Higbie’s model”, and the surface renewal theory [55]. The surface renewal theory provides the best description of the results

of this test as it models a system where the rate of water absorption increases as the turbulence at the gas-liquid interface increases. Fast moving air from a fan at high speed causes more turbulence than slower moving air from a fan at low speed, leading to increased water absorption.

### Effect of desiccant type on water absorption

The effect of the type of desiccant on both the rate and total amount of water absorption was tested using the previously described testing setup. To do this, solutions each with an initial desiccant mass fraction of 0.6 were used in order to be consistent with the highest desiccant mass fraction from the thermodynamic analyses. Each had a solution depth of  $\frac{1}{4}$ ". A fan blew moist air on its high-speed setting, corresponding to an air speed of 16 mph as measured by a handheld anemometer. The desiccant solution was mixed during the testing.

The results comparing these tests for calcium chloride and lithium chloride are given in Figures 31 and 32. Figure 31 shows the mass of absorbed water over time, while Figure 32 shows the desiccant mass fraction over time.

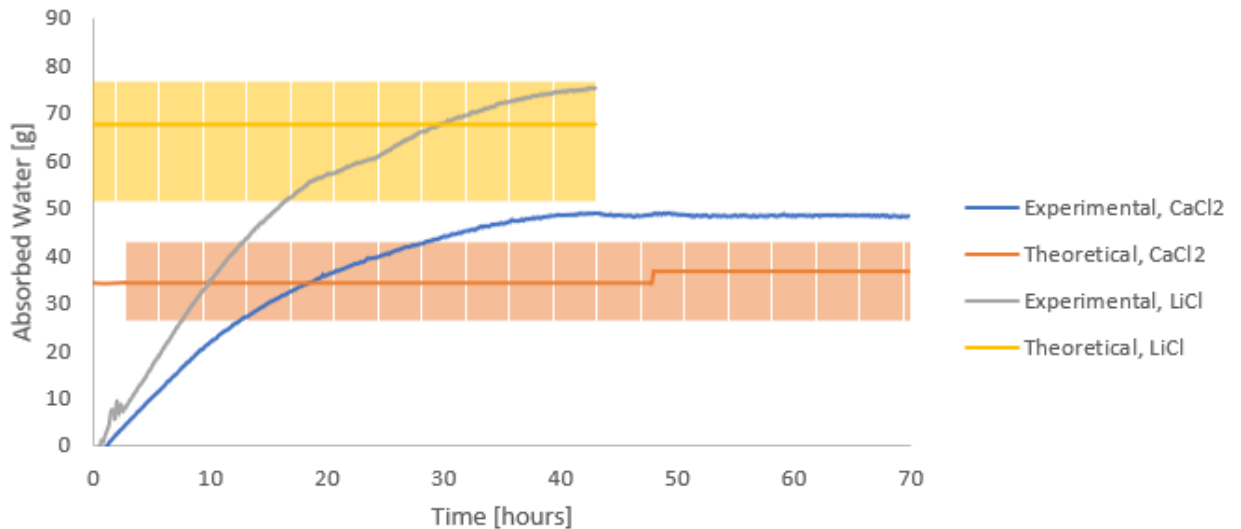


**Figure 31:** Mass of water absorbed over time, comparing CaCl<sub>2</sub> and LiCl

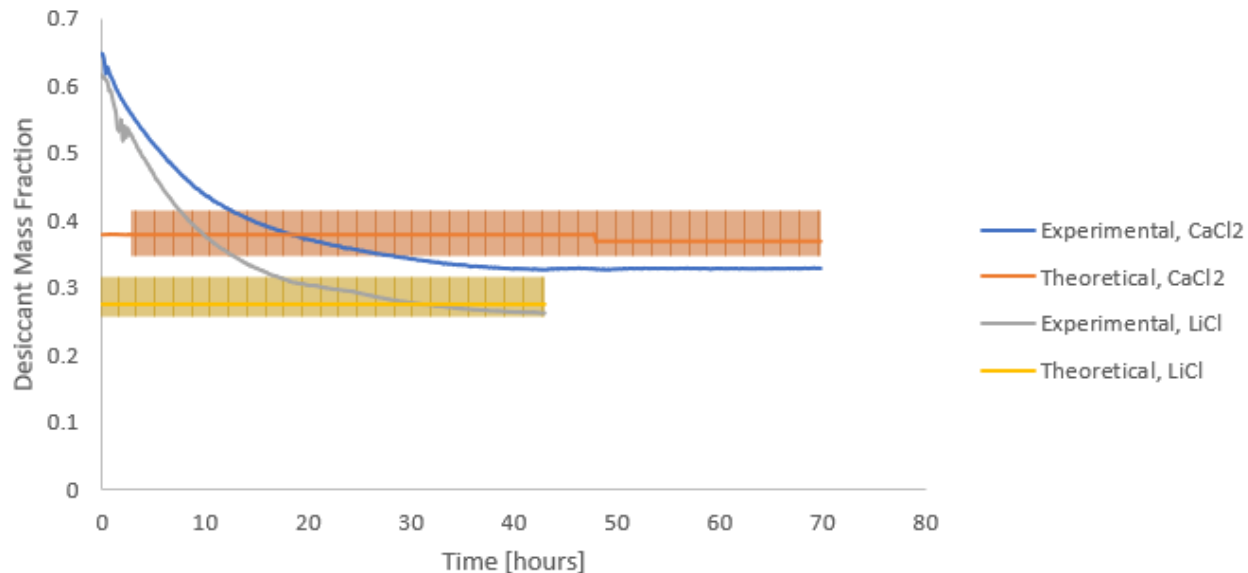


**Figure 32:** Desiccant mass fraction over time, comparing CaCl<sub>2</sub> and LiCl

In these tests, lithium chloride absorbed a greater amount of water. This was expected, since lithium chloride has a lower theoretical equilibrium mass fraction when at the same ambient conditions. This can be seen when comparing Figures 24 and 25. Therefore, it would require lithium chloride to absorb a greater amount of water to reach equilibrium.

One thing to note about these graphs is that when initially absorbing water, it is done at a nearly constant rate. However, as the desiccant solution approaches equilibrium the water absorption rate decreases. This agrees with surface renewable gas-liquid mass transfer theory [55]. In this theory, the mass transfer is proportional to the square root of the diffusion coefficient, while the diffusion coefficient is proportional to the desiccant concentration gradient between the vapor and liquid. When water vapor is being initially absorbed, it causes only a small percent change in the desiccant concentration gradient, leading to little variation in the water absorption rate. However, near equilibrium the absorption of water vapor causes a large percent change in the desiccant concentration gradient, leading to a larger variation in water absorption rate. The initial absorption rate, or initial slope of the graph, is higher for lithium chloride than calcium chloride. This higher initial absorption rate for lithium chloride is shown in Figure 33.

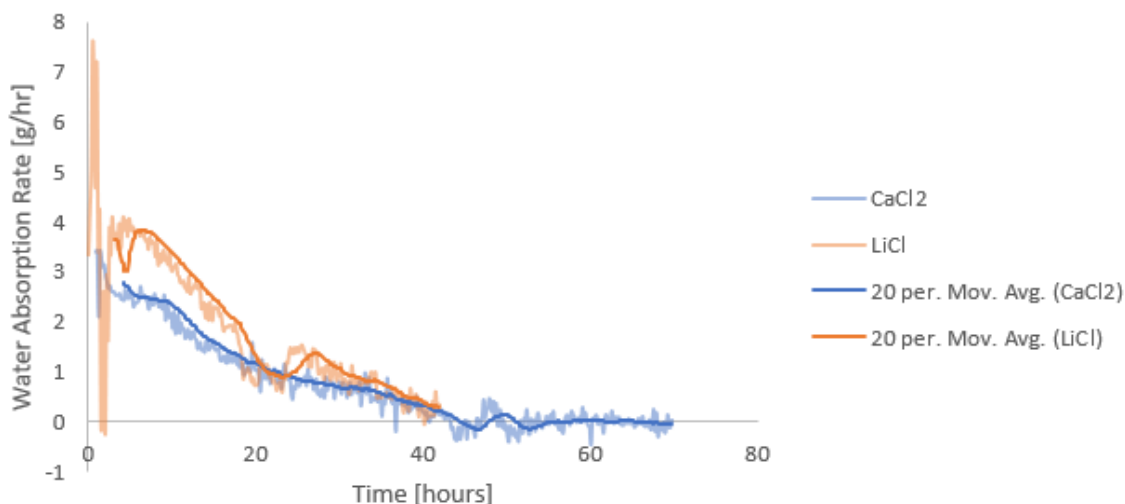


**Figure 33:** Water absorption rate, comparing CaCl<sub>2</sub> and LiCl

These tests show that lithium chloride has the advantage over calcium chloride when it comes to both total amount of water absorbed, as well as water absorption rate.

#### Effect of mixing on water absorption

The effect of mixing the desiccant solution on water absorption was tested. In these tests, a calcium chloride solution with an initial desiccant mass fraction of 0.6 was used. The initial depth of the solution was  $\frac{1}{4}$ ". The fan blew air on its high-speed setting, corresponding to 16 mph. Water vapor was absorbed until the solution reached equilibrium. The results of these tests for mixing vs. no mixing are shown in Figures 34 and 35. Figure 34 shows the mass of water absorbed over time, while Figure 35 shows the desiccant mass fraction over time.

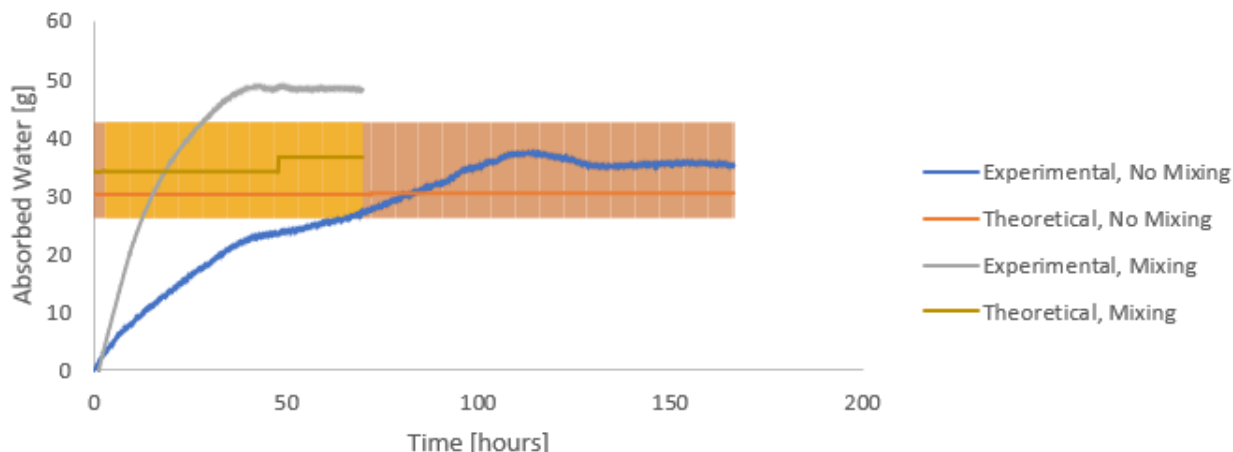


**Figure 34:** Mass of water absorbed over time, comparing mixing and no mixing

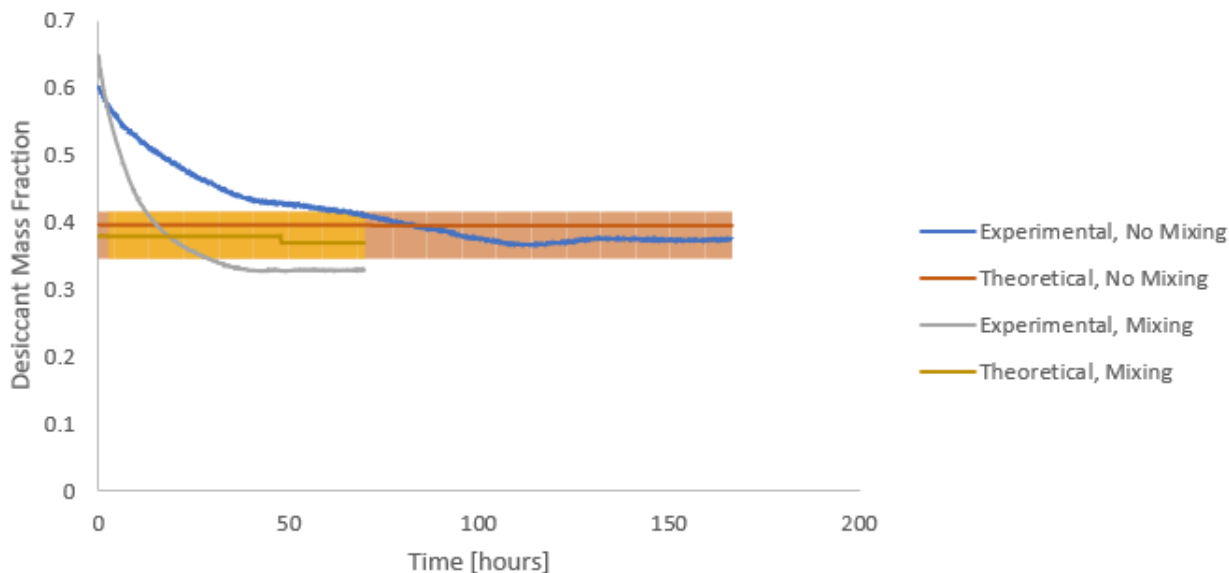


**Figure 35:** Desiccant mass fraction over time, comparing mixing and no mixing

These results show that mixing the desiccant solution has a great impact on the initial water absorption rate, allowing the desiccant solution to reach equilibrium more quickly. The equilibrium mass fraction of both solutions should be similar, only varying due to ambient conditions. This is because each solution was initially identical, so if all the desiccant gets dissolved into the solution by the end of the test, then the final mass fractions should be similar. The reason for a higher water absorption rate with mixing is because the calcium chloride is denser than water. When there is no mixing, the density gradient causes the calcium chloride to settle to the bottom of the petri dish. This causes the solution to become stratified, with a concentrated desiccant solution near the bottom and a more dilute desiccant solution near the top. The concentrated region of the solution often got so concentrated that the desiccant would crystalize and fall out of solution. The more dilute solution near the top is the portion in contact with the ambient air. Since this region is diluted, water isn't as attracted to the solution, which causes a decrease in water absorption rate. When the solution is mixed, the calcium chloride that had originally settled to the bottom is more evenly distributed



throughout the solution. This means that the top portion of the solution is more concentrated and allows for faster initial water absorption. This faster water absorption rate is seen in Figure 36.

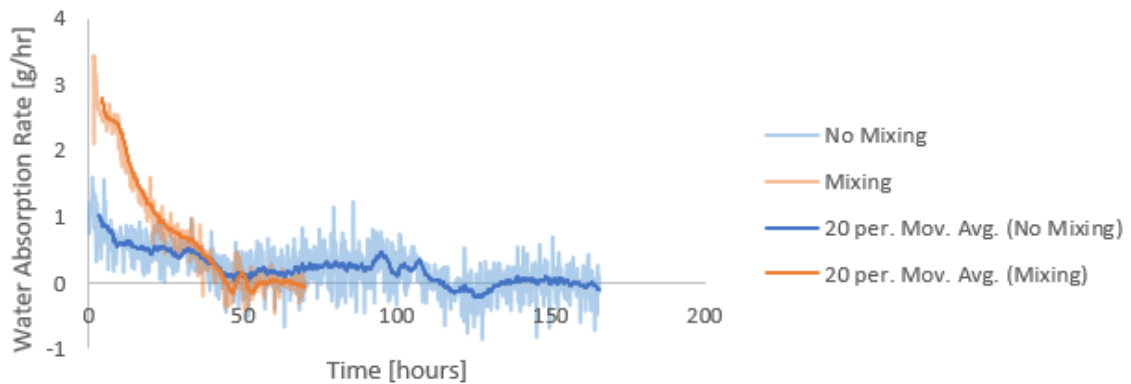


**Figure 36:** Water absorption rate, comparing mixing and no mixing

Of all the desiccant characteristics tested in Chapter 3, mixing the desiccant solution had the biggest impact on water absorption rate. When designing a DAWG system, a low-energy mixer should be used to aid in water absorption.

#### Effect of solution depth on water absorption

The effect of solution depth on water absorption was tested. Solutions with initial depths of  $\frac{1}{4}$ " and  $\frac{1}{2}$ " were tested. Each solution used calcium chloride with a 0.6 initial desiccant mass fraction. The fan blew air at its high-speed setting, corresponding to an air speed of 16 mph. The desiccant was not mixed during testing. Water vapor was absorbed until the solution reached equilibrium. The results of these tests are given in Figures 37 and 38. Figure 37 shows the desiccant mass fraction of the solution over time, while Figure 38 shows the water absorption rate over time.

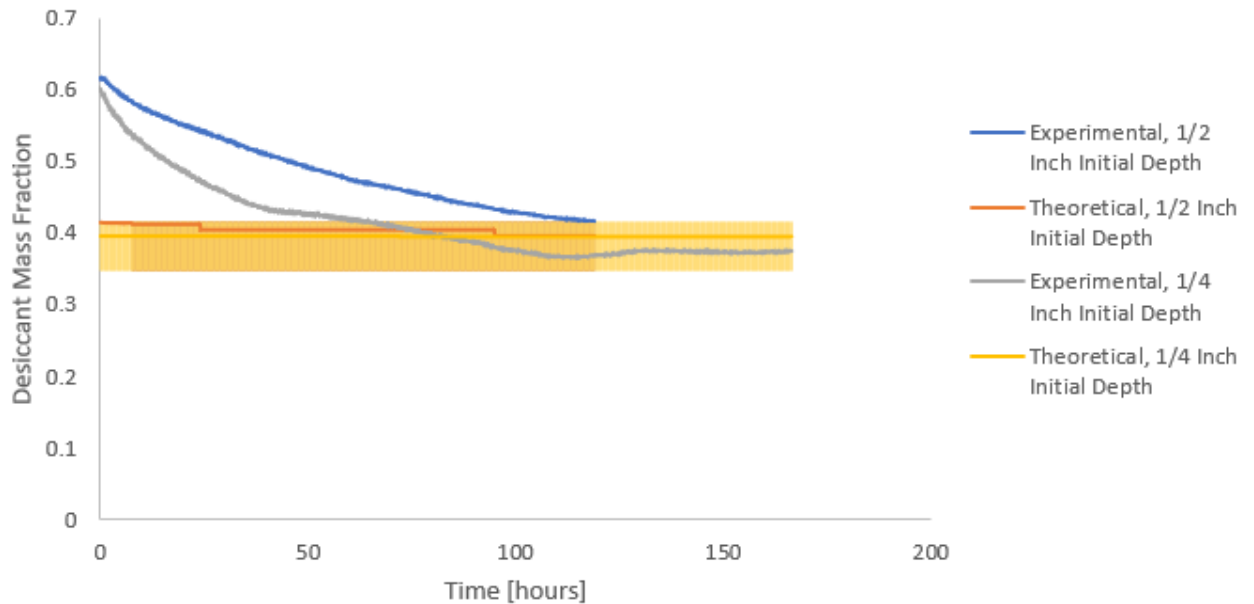


**Figure 37:** Desiccant mass fraction over time, comparing 1/4" and 1/2" solution depths

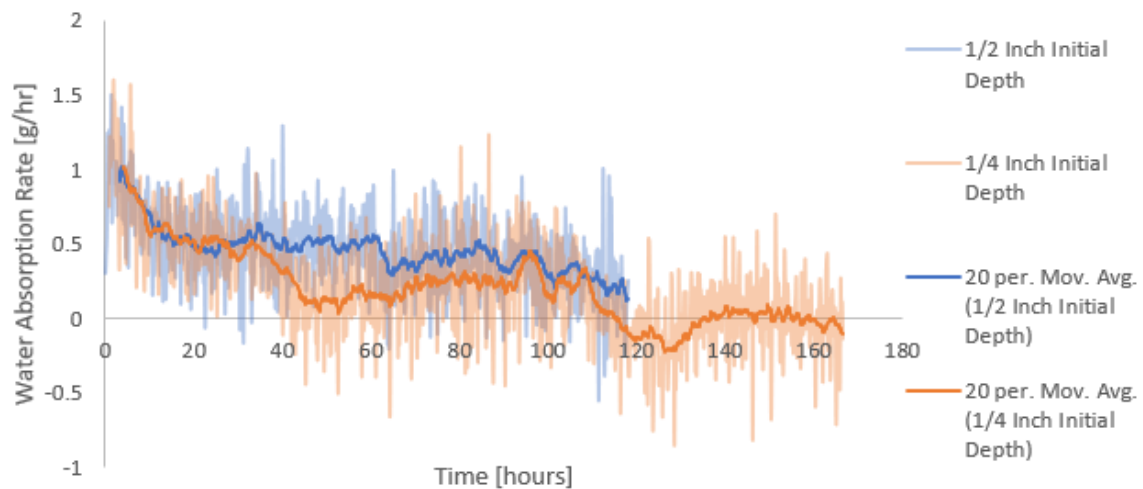


**Figure 38:** Water absorption rate over time, comparing 1/4" and 1/2" solution depths

These results show that the solution depth does not affect the initial water absorption rate. This can be seen in Figure 38. Since the deeper solution has more mass, it requires more water to be absorbed before reaching equilibrium. This means that the deeper solution will continue to absorb water vapor at its initial rate for a longer period of time, since it remains at a higher desiccant mass fraction for a longer period of time. These results further indicate that there is a limitation in the maximum mass transfer due to the solution surface area being fixed. These results are seen in Figure 37.

When considering how to set up the desiccant in a DAWG system, a deep desiccant solution depth is better than a shallow desiccant solution depth. This is because a deeper desiccant solution stays at a high water absorption rate for a longer period of time, as seen in Figure 38.

## Effect of solution surface area on water absorption

The effect of desiccant solution surface area on water vapor absorption rate was tested. A desiccant test was performed for two different dishes: a petri dish with a 3.5” diameter and a bowl with an 8.25” diameter. A calcium chloride solution with a 0.6 initial desiccant mass fraction and ¼” initial solution depth was used. A high fan speed was used, corresponding to an air speed of 16 mph. The solution was mixed during testing. The results of these tests are shown in Table 23.

**Table 23:** Water absorption versus solution surface area

Bowl Diameter [inch]	Solution Surface Area [in <sup>2</sup> ]	$\frac{surface\ area_{bowl}}{surface\ area_{petri\ dish}}$	Initial water absorption rate $\left[\frac{g}{hr}\right]$	$\frac{\dot{m}_{bowl}}{\dot{m}_{petri\ dish}}$
3.5	53.46	5.56	14.10	5.73
8.25	9.62		2.46	

These results indicate that water absorption varies linearly with surface area. This is expected since more desiccant solution at the same desiccant mass fraction is encountering the ambient air, and the interface between the desiccant solution and the ambient air is where the water absorption is occurring. If a DAWG system is being designed to absorb water quickly, the desiccant should be spread out over a large area. This is assuming that the fan is strong enough or there are enough fans in use to make sure that ambient air is being blown over the entire solution surface area.

When deciding whether to either widen or deepen the desiccant solution, widening will result in better water absorption. Doubling the surface area will double the water absorption rate for the entire test. Doubling the solution depth will result in the same initial water absorption rate, but this initial water absorption rate will be able to be held for a longer time. Assuming both solutions are mixed and homogenous, the solution with the higher surface area will reach equilibrium faster since it has a heightened water absorption rate for the entire test, whereas the deeper solution only has a heightened water absorption rate for the latter portion of the test. Additionally, wall effects may also be a factor in decreasing water absorption rate. A spread out and shallow solution will have less wall effects than a narrow and deep solution.

## Verification of equilibrium desiccant solution properties

For all the desiccant tests, a final experimental equilibrium desiccant mass fraction was calculated. Using the ambient temperature and relative humidity, the theoretical equilibrium desiccant mass fraction was determined using equations from literature [36]. The comparison of these mass fractions is given in Table 24.

**Table 24:** Theoretical and experimental equilibrium desiccant mass fractions

Test Number	Theoretical Equilibrium Desiccant Mass Fraction	Experimental Equilibrium Desiccant Mass Fraction	Percent Difference	Mixing [Yes/No]
1	$0.396 \pm 0.005$	$0.416 \pm 0.001$	4.9%	No
2	$0.394 \pm 0.005$	$0.374 \pm 0.001$	5.2%	No
3	$0.369 \pm 0.005$	$0.328 \pm 0.001$	11.8%	Yes
4	$0.365 \pm 0.005$	$0.395 \pm 0.002$	7.9%	Yes
5	$0.283 \pm 0.005$	$0.286 \pm 0.001$	1.1%	No
6	$0.282 \pm 0.005$	$0.239 \pm 0.002$	16.5%	No
7	$0.275 \pm 0.005$	$0.262 \pm 0.001$	4.8%	Yes

These results show that the solution may absorb more or less water than what is theoretically predicted. This indicates that the amount of water absorbed is greatly influenced by the solution mass fraction near the top of the solution, where the water absorption is occurring. When the solution is not mixed, a density gradient between the desiccant and water causes the desiccant to sink, causing the top of the desiccant to be more dilute. This leads to less water being absorbed than predicted.

On other tests when mixing occurred, the desiccant would be mixed and cause some of the desiccant to occasionally rise above the water level. Additionally, sometimes the desiccant would leave a salty scum on the walls of the dish when being mixed. Both conditions lead to a high desiccant concentration near the top of the solution. Since the top of the desiccant solution is where the moist air encounters the desiccant, the moist air will behave as if the solution has a high desiccant concentration, causing more water to be absorbed than predicted.

These tests did have some uncertainties when determining the experimental and theoretical desiccant mass fractions. The experimental desiccant mass fractions were calculated based off the solution mass measured by the desiccant. The solution is made using an initial mass of desiccant and water. The uncertainty in these masses,  $\delta_{m_{des}}$  and  $\delta_{m_{wat_i}}$ , are 0.1 g and 0.5 g respectively. The desiccant and petri dish are supported by stands whose masses are also recorded by the scale. The uncertainty in the support mass,  $\delta_{support}$ , is 0.1 g. The fan also exerts a downward force on the solution, which is detected by the scale. The uncertainty in the recorded mass due to the fan,  $\delta_{fan}$ , is 0.3 g. The scale also had an uncertainty due to the precision of its output values,  $\delta_{scale}$ , of 0.005 g.

The theoretical equilibrium desiccant concentration was based on the ambient pressure, temperature, and relative humidity. The ambient pressure was assumed to be constantly at atmospheric pressure, whereas small changes in ambient pressure occurred throughout the tests. This causes the uncertainty in the ambient pressure measurement,  $\delta_{pressure}$ , to be as high as 2000 Pa. The ambient air temperature and relative humidity were measured outside of the testing

enclosure and were assumed to be the same inside of the testing enclosure. The desiccant was assumed to be at the same temperature as the ambient air throughout the test, whereas it was most likely a little cooler than the ambient air temperature due to convective losses. The uncertainty in the solution temperature,  $\delta_{temp}$ , was assumed to be 1 °C. The uncertainty in the relative humidity inside of the testing enclosure,  $\delta_{RH}$ , was assumed to be 1% or 0.01. These uncertainties would alter the value of the theoretical equilibrium desiccant mass fraction.

Overall, the theoretical mass fractions may be used to accurately predict mass fractions of desiccant solutions. However, this assumes that the solution is well mixed and homogeneous. If the solution is not well mixed, then the solution may become stratified with different parts of the solution being more concentrated than other parts and with a different amount of water in the solution than predicted.

### Optimizing water absorption

In order to absorb the most water in a DAWG system, the system should have the following characteristics:

- The top surface area of the desiccant solution should be maximized, as water absorption rate scales linearly with solution surface area
- The desiccant solution should be mixed to ensure that the solution is homogenous, and that the desiccant doesn't settle
- A fan should be used which blows air across the desiccant solution at the highest fan speed to increase fluid turbulence at the gas-liquid interface, leading to increased water absorption
- Lithium chloride should be used rather than calcium chloride to allow for more water to be absorbed by the solution before reaching the equilibrium concentration

## Chapter 4: Prototype Development

A batch-style DAWG system prototype was designed and developed. Presented below are the design and operation aspects of the two prototypes that were designed. While two prototypes were designed, only the second prototype ended up being constructed. A second prototype needed to be designed because the initial prototype was too large for lab testing. Having a system that is too large would make it more difficult to heat during regeneration and to seal when operating under vacuum. Ultimately, the second prototype ended up being constructed and its operation tested in order to better understand the performance of a batch-style DAWG system and compare its performance to that predicted in the thermodynamic models.

### First System Prototype

The first system prototype was a large box-like design, measuring 27" x 9" x 15". The box would be made from 1/4" thick aluminum tooling plate. A Solidworks assembly model developed of the regenerator is shown in Figure 39. Schematics showing the entire system while operating with the water absorption and regeneration modes are shown in Figures 40 and 41 respectively.

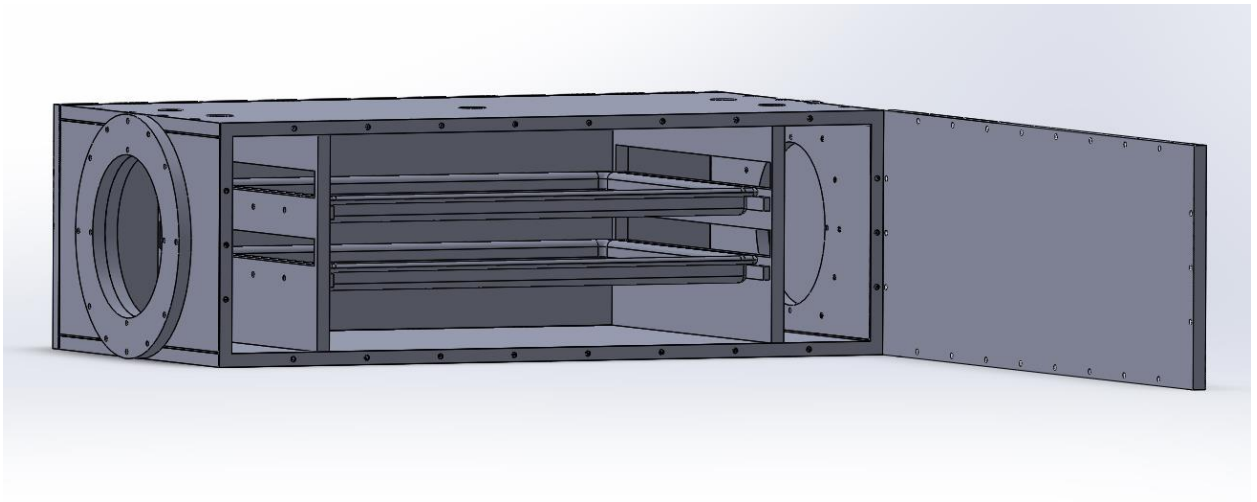


**Figure 39:** Regenerator Solidworks assembly model

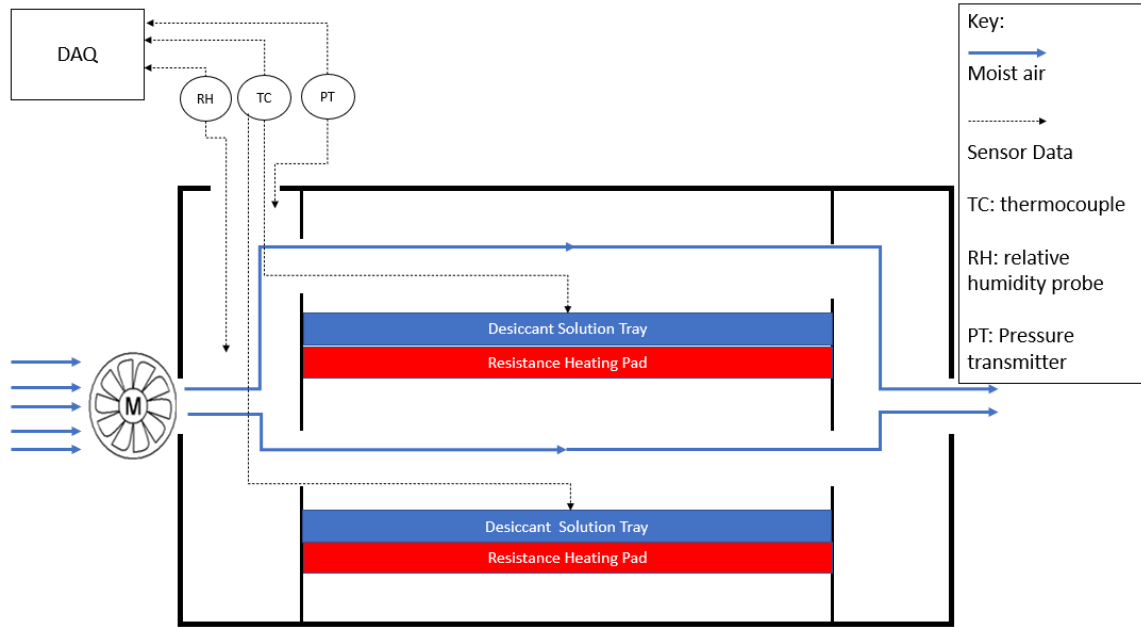


**Figure 40:** Schematic of first system prototype during water absorption

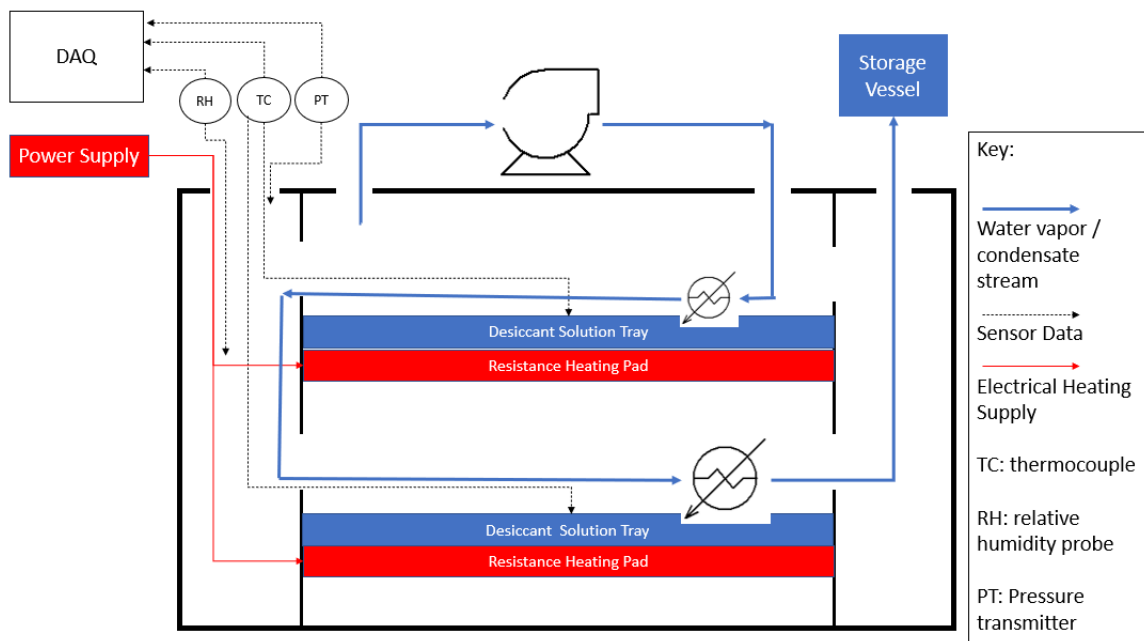


**Figure 41:** Schematic of first system prototype during regeneration

During regeneration, a fan would be mounted to the inlet side of the regenerator. The system was designed to allow either a fan or an aluminum cap to be supported on the regenerator during the absorption and desorption processes respectively. The fan would pass the ambient air through rectangular slots and over the top of trays which hold the desiccant solution. The outlet air would then pass through an opening on the outlet side of the regenerator.

When loading and unloading the desiccant solution, the front panel would be detached from the regenerator. This allows for the cookie sheets to be slid in and out of the regenerator, like an oven rack. Having the cookie sheets capable of being moved outside the regenerator makes it easier to load and unload the desiccant than if the cookie sheets were fixed inside the regenerator.

In order to ensure that the regenerator can hold a vacuum pressure, a thin silicone gasket would be used at each aluminum plate interface. Vacuum grease would also be used to ensure a leak-tight seal when operating at sub-atmospheric pressure.

In order to heat the regenerator, silicone pad heaters would be used. The heaters would be adhered to the bottom of the cookie sheets using high-temperature RTV silicone adhesive. Adhering the pad heater to the cookie sheet ensures good thermal contact and better heat transfer between the heater and the cookie sheet and subsequently the desiccant. The resistive heating wire connected to the pad heater would be fed out one of the ports on the regenerator's lid. Sealant tape is used to seal the port once the heating wire is fed through the port.

Type-J thermocouples would be used to measure several temperatures in the regenerator. These temperatures include the air temperature, desiccant solution temperature, cookie sheet temperature, and heating pad temperature. The wires for these thermocouples would go out of the same port as the heating wire. A model QPSH-AP-42 ProSense Pressure Transmitter would be used to measure the pressure within the regenerator. This pressure transmitter would screw into one of the tapped holes in the regenerator lid. The positioning of each of the sensors inside the regenerator are shown in Figure 42.

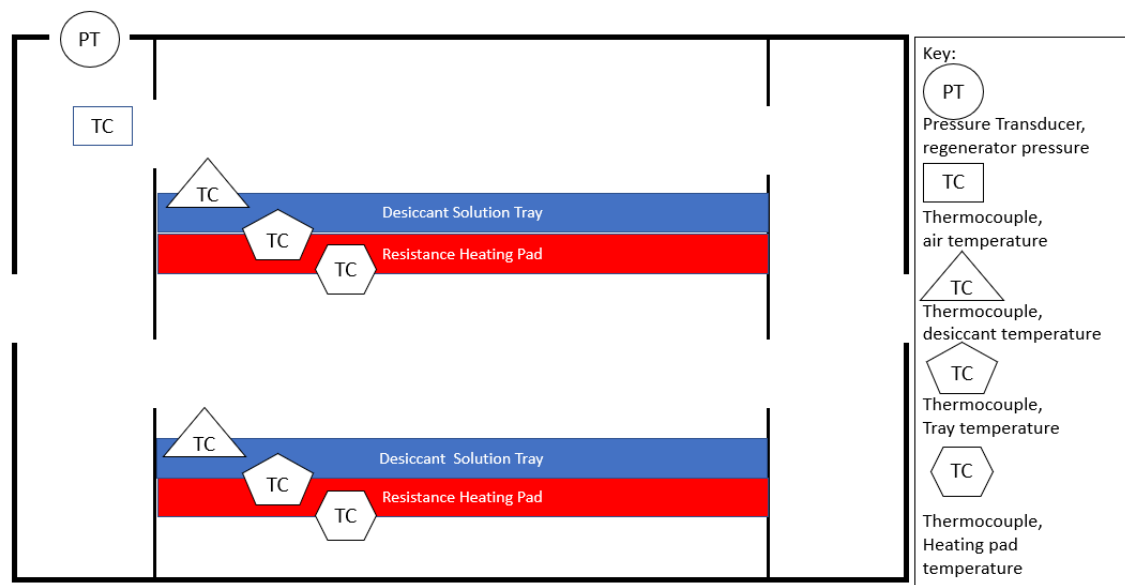


**Figure 42:** Positioning of sensors within the regenerator of the first system prototype

The temperature of the regenerator would be controlled using a model ICT-100VH Inkbird temperature controller. The desired regenerator temperature would be set using the temperature controller and controlled using the cookie sheet temperature measurement. The temperature controller would turn the power to the heating pad on and off depending on whether the desiccant temperature is below or above the set temperature respectively. Foam board would be used to



insulate the exterior of the regenerator. Adding insulation minimizes heat loss from the regenerator and allows the system to hold a constant regenerator temperature more easily.

Other temperatures measured during testing would be the ambient temperature and relative humidity. These values would be measured outside of the regenerator. These values, in addition to all the temperatures being measured within the regenerator, would be recorded using a National Instruments DAQ module and Signal Express software. An NI 9213 DAQ module would be used to record the thermocouple data while an NI 9201 DAQ module would be used to record the pressure transmitter and relative humidity probe data.

When conducting latent energy recovery, a compressor must be implemented in the system. One of the ports on the regenerator lid would be used for the inlet to the compressor, while another port would be for the outlet of the compressor to reinject compressed water vapor back into the regenerator, as shown in Figure 39. The compressor ports were located on the top of the regenerator since the water vapor rises in the regenerator once it has been vaporized, and since the compressor would sit on top of the regenerator during operation. When latent energy recovery is not being conducted and a compressor is not used, these ports would be sealed with a Swagelok pipe plug. During latent energy recovery, the reinjected water vapor would flow through a heat exchanger made from copper tubing. This copper tubing would be bent such that the tubing would go back and forth in a serpentine fashion through the desiccant solution. This would allow energy to be transferred from the compressed water vapor to the desiccant solution. Once the compressed water vapor has flowed through the latent energy recovery heat exchanger, it would exit out of the final lid port. If latent energy recovery is not performed, water vapor would also flow out of this outlet port.

The outlet water vapor would flow through another copper tube heat exchanger, which acts as a condenser. If the heat exchanger is sufficiently large enough, then the water vapor will condense due to natural convection before exiting the condenser. If the heat exchanger is too short, fins or a fan may be used to increase convective heat transfer and ensure all the water vapor condenses.

The condensate would flow into a custom stainless-steel storage vessel. The storage vessel uses quick-release KF cast clamps with KF centering rings to ensure the vessel can operate at sub-atmospheric pressure. The lid of the storage vessel would be modified to have an inlet port such that the condensate can flow into the storage vessel while still at sub-atmospheric pressure.

### Status of the First Prototype

The DAWG system using the first system prototype design was never constructed due to concerns about its performance. The regenerator has a relatively large volume, measuring 27" x 9" x 15". This large volume must be heated and cooled for each test. Due to the power output of the heating pads, it would take several hours to heat up the regenerator to the desired operating temperature. The required regeneration testing time versus power supplied by the resistance heater is shown in Figure 43. The power provided by the resistance heater in this figure goes towards the sensible and latent heating of the desiccant, as well as the sensible heating of the air and aluminum in the regenerator.

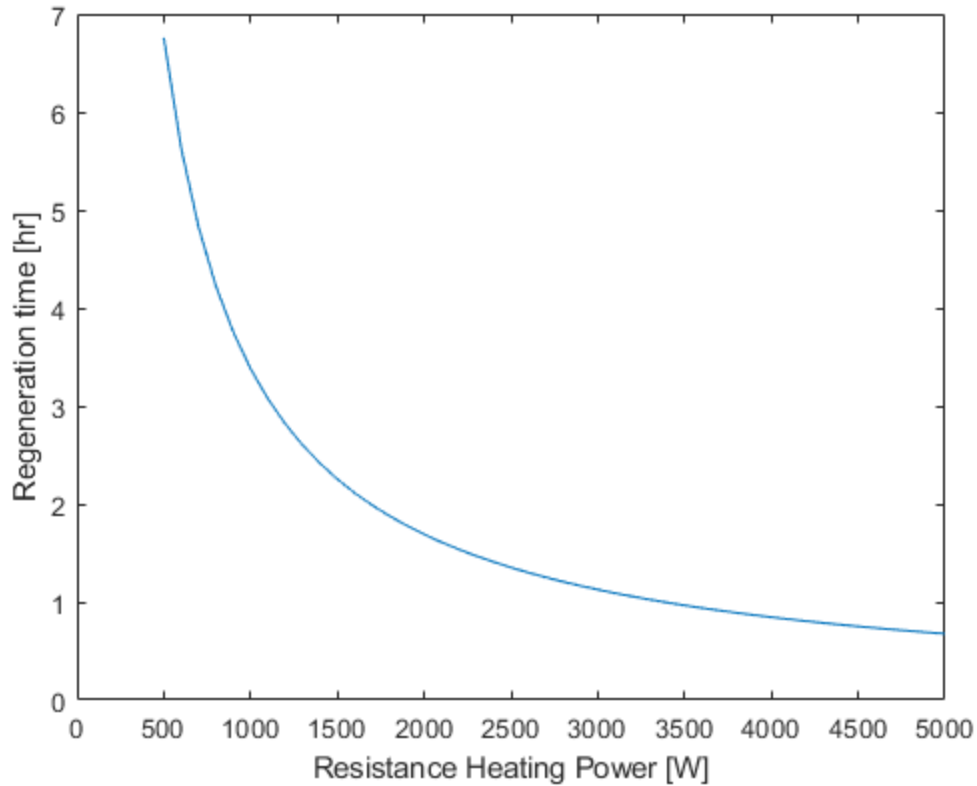


**Figure 43:** Correlation between resistance heating power and time to perform a regeneration test using the first system prototype

Convection losses were neglected for this calculation. However, the large surface area means that there would be several locations with convective losses, making it even harder for the system to maintain a constant regenerator temperature and requiring a longer time to perform a regeneration test.

The system would also require lots of machined components, which would have postponed the start of prototype testing. When running the system under vacuum, the system would need to be leak-tight. The large number of machined components comprising the outside of the regenerator would make the system very difficult to seal.

### Second System Prototype

A second system prototype was designed. This second prototype was much smaller than the first prototype. While this does mean it has a smaller desiccant solution carrying capacity, it also means that less energy is required to perform a regeneration test and the amount of convective losses is reduced. By having a lower thermal energy requirement, a heating pad can perform a regeneration test in less time than a regeneration test in a larger system. Additionally, the number of interfaces between different system components was reduced, making it easier to seal the system when it is operating under vacuum.

A schematic of the second system prototype testing setup operating under vacuum with no latent energy recovery is shown in Figure 44.

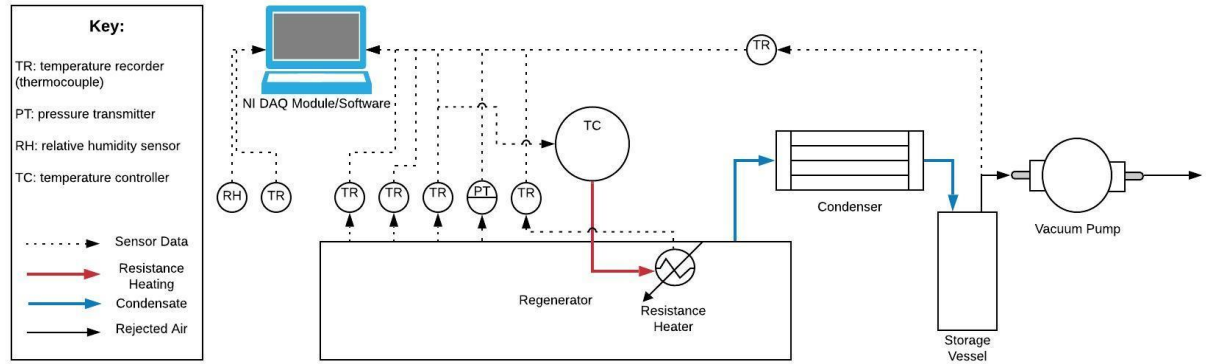


**Figure 44:** AWG system test setup schematic

A 10" diameter stainless-steel pot attained from a vacuum chamber was used as the regenerator. This pot has a much smaller volume than the previous design, so it takes less time to heat up and cool down. This helps regeneration tests occur faster and more frequently. Additionally, since the pot is all one piece rather than multiple panels like the previous design, there are less interfaces needed to be vacuum sealed and thus less chances for potential leaks.

The regenerator pot houses a smaller pan used for the desiccant solution. This steel desiccant pan has an 8.25" diameter, fitting snugly inside of the regenerator pot. A handle was fashioned out of metal wire, as shown in Figure 45, to allow the desiccant pan to be easily picked up and raised out of the regenerator pot. An electric pad heater is used to heat the regenerator. The pad heater is adhered to the bottom of the desiccant bowl using high temperature RTV silicone.



**Figure 45:** Regenerator desiccant pan wire handle

The regenerator is insulated in order to reduce convective losses. The exterior of the regenerator is insulated using Polyiso foam board. A small gap is present between the side of the regenerator and the side foam board. This gap is filled with a MaxWool 8# ceramic fiber to ensure for good thermal contact between the regenerator bowl and the exterior insulation. Ceramic fiber is also used on the interior of the regenerator pot between the pad heater and the bottom of the regenerator pot to minimize heat loss through the bottom of the regenerator. A schematic of the regenerator is shown in Figure 46.

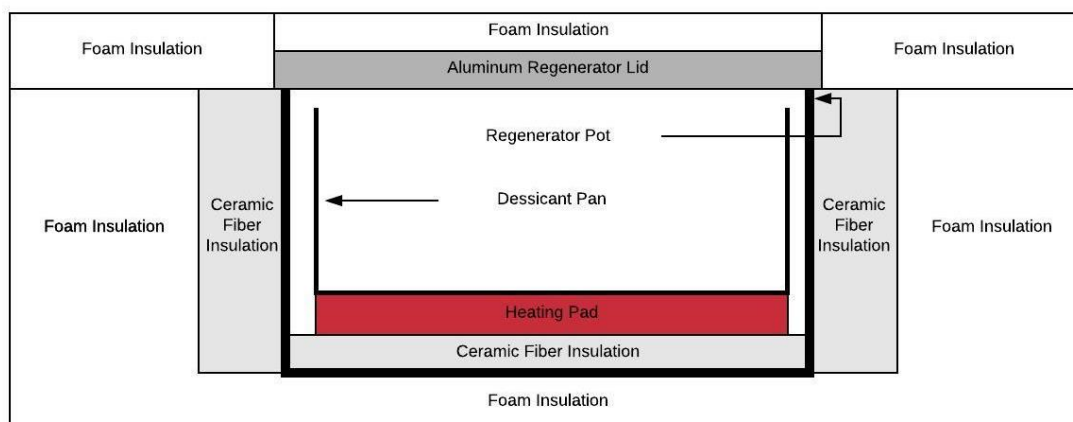


**Figure 46:** Regenerator layout

An acrylic lid was laser cut to be used when the desiccant is absorbing moisture. The lid has a hole cut out of the center and a fan mounted on top of it. This fan sucks ambient air in through a duct and blows it out onto the surface of the desiccant solution. The acrylic lid has small acrylic legs which prop the lid up about ½” off the lip of the regenerator pot. This allows for the ambient air to escape out the side of the regenerator once it has blown over the desiccant solution, as shown in Figure 47. The duct has a 3D-printed mount attached to it which allows for a Type-J thermocouple and Vaisala relative humidity probe to be positioned to measure the dry bulb temperature and relative humidity of the inlet ambient air. The fan setup using the acrylic lid is shown in Figure 48.

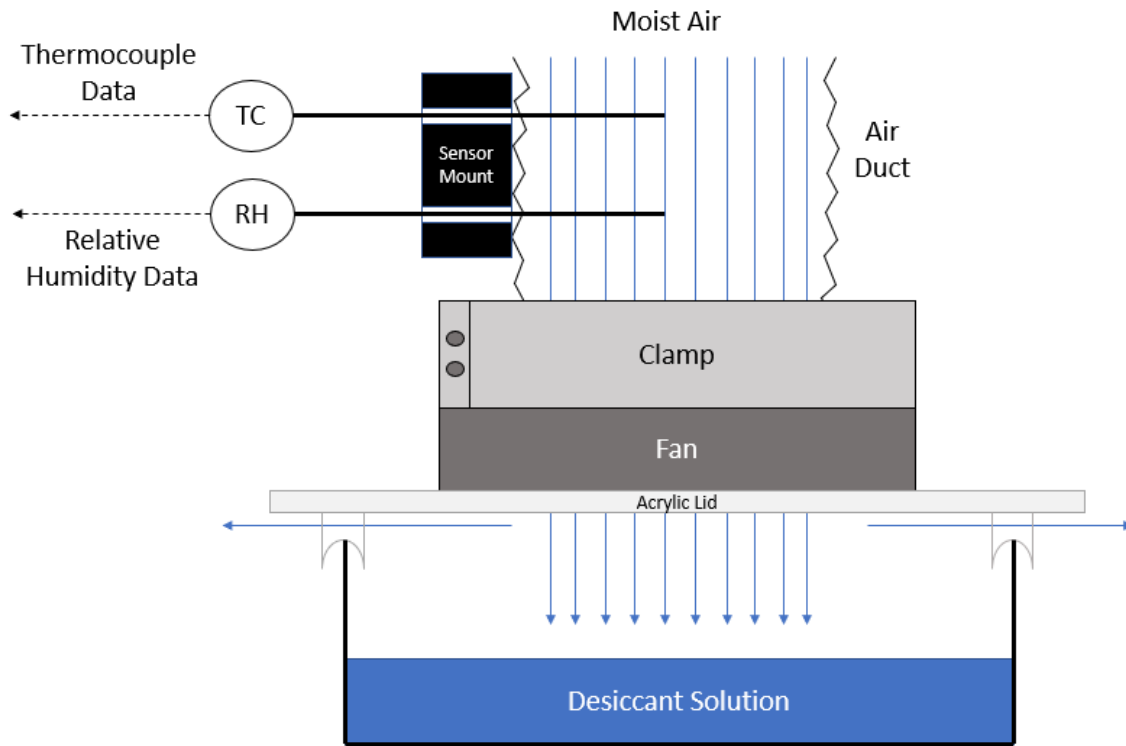


**Figure 47:** Ambient moist air flow through the system when the desiccant is absorbing moisture

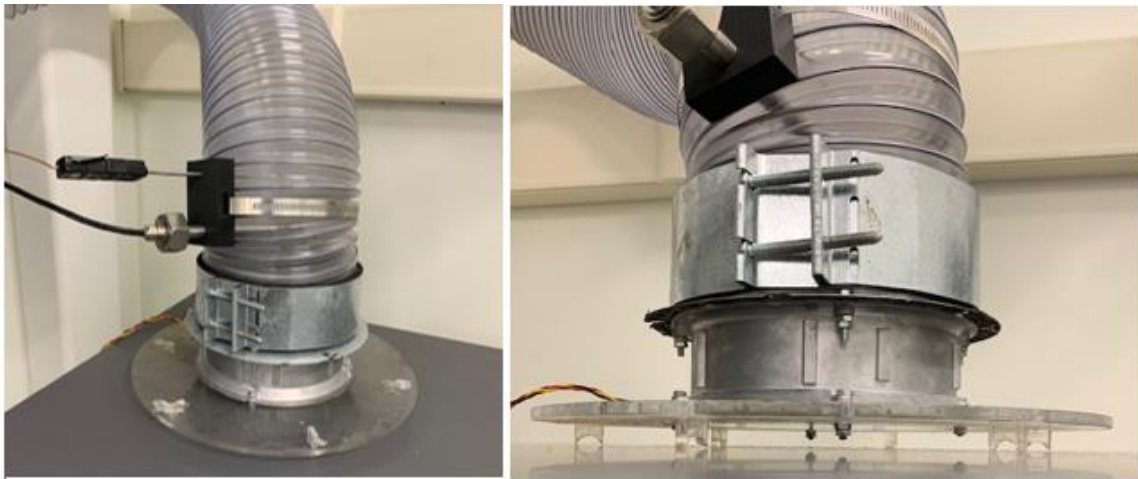


**Figure 48:** Fan setup with the acrylic lid used when the regenerator is absorbing moisture



An aluminum lid for the regenerator was designed and machined. This lid is used when the regenerator is vaporizing and regenerating the absorbed water vapor. The lid is insulated on the top and sides using foam board to limit the convective losses from the regenerator. This lid allows for the condensate to exit the regenerator, thermocouples and a pressure transmitter to be installed to monitor the system's performance, as well as allow a compressor to be attached when latent energy recovery is performed. This lid with the foam insulation and data sensors installed is shown in Figure 49, while the lid stripped of the sensor instrumentation and insulation while the Swagelok port connectors are exposed is given in Figure 50.

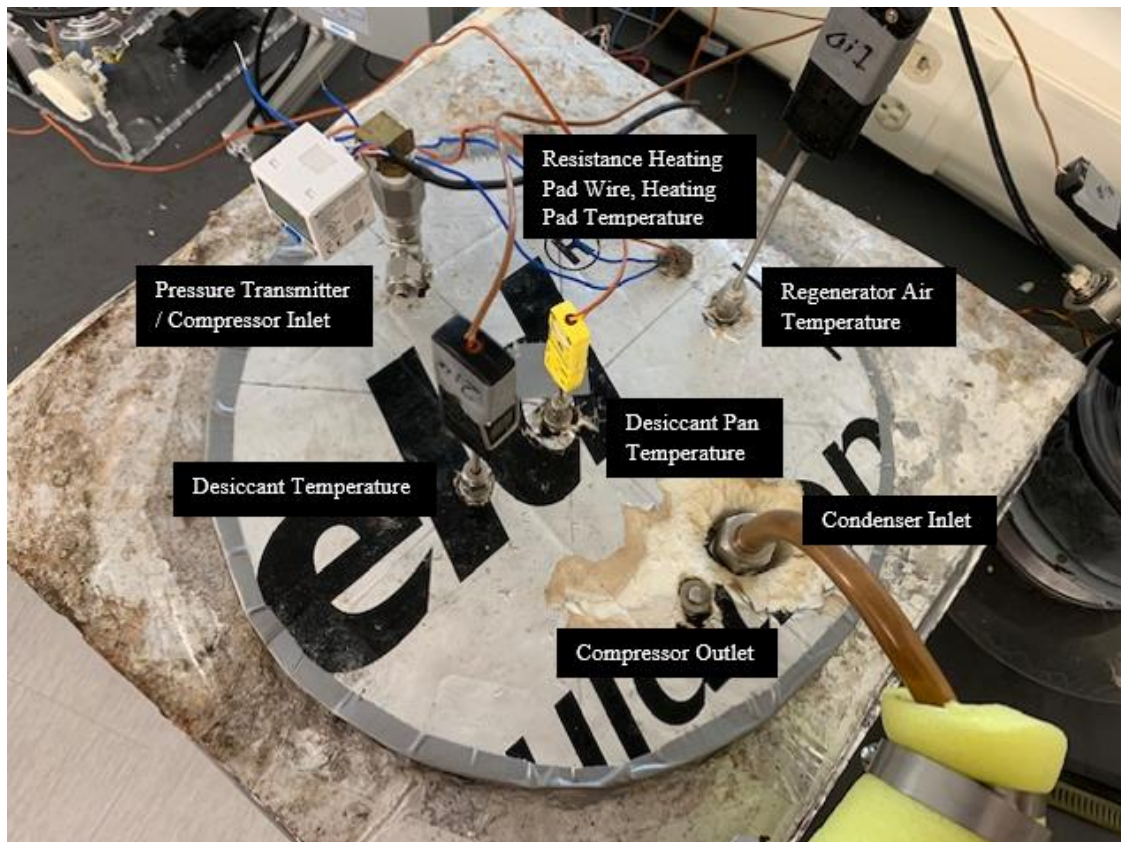


**Figure 49:** Aluminum regenerator lid with foam insulation and data collection hardware installed



**Figure 50:** Bare aluminum lid with Swagelok port connectors exposed

There are several ports in this lid. One port allows for the resistance heating wire to exit the system and plug into the temperature controller. This port is vacuum sealed using a high-temperature putty. The air temperature in the regenerator, liquid desiccant temperature, and desiccant pan temperature are all recorded using a combination of Type J and Type K thermocouples. Swagelok thermocouple ports are used to hold each thermocouple in place, while Teflon ferrules are used to provide a vacuum seal. The regenerator pressure may be measured using a model QPSH-AP-42 ProSense pressure transmitter. When latent energy recovery is being performed, a compressor may be used, in which case two of the ports would be used for water vapor inlet and outlet from the compressor. During latent energy recovery, a serpentine copper tube heat exchanger may be used inside of the regenerator to perform latent energy recovery. Another port is used for exiting steam to go to the condenser.

The interior lip of the aluminum lid is machined to allow for a thin gasket to be attached. This gasket is attached to the lid using vacuum grease to ensure a good seal. A high-temperature silicone gasket was initially used. However, it was determined that this material was too rigid to provide a good seal. Instead, an acrylic mold was constructed to allow a gasket to be made from Smooth-On Dragon Skin™ castable silicone. This new material is more elastic than the silicone of the old gasket. This allows for the regenerator lid to recess a little more into the gasket, enabling a better seal. Additionally, this new material allows the gasket to be more easily repositioned on the lid between tests if the gasket had previously shifted. The gasket sitting in the lip of the aluminum lid is shown in Figure 51.



**Figure 51:** Aluminum lid with a Dragon Skin™ silicone gasket

A condenser was constructed out of copper tubing with a  $\frac{3}{8}$ " and  $\frac{1}{2}$ " inner and outer diameter respectively. The condenser is cooled using a box fan to ensure that all the steam has condensed before exiting the condenser. A theoretical heat transfer analysis was performed on the condenser to determine the required condenser length using just natural convection to cool and condense the water vapor and find out whether a fan was required in order to use the 3-meter length of tubing that was available. The analysis showed that just using natural convection would not cool the water vapor enough to ensure that it all condenses. However, increasing the convective heat loss by a factor of 100, which models an external source like a fan aiding in convective heat transfer, would allow a condenser with a length as small as 1.9 meters to be used. This means that the 3-meter length of tubing would work for the DAWG system if additional convective heat transfer was enabled by something like a box fan.

At the outlet of the condenser, the temperature of the condensate is measured to ensure that all the condensate is being condensed. The condenser is tilted downward such that the storage vessel is below the regenerator. This allows for the condensate to drain via gravity into the storage vessel, as shown in Figure 52. The end of the condenser extends several inches into the storage vessel, as shown in Figure 53. By changing where the condensate enters the storage vessel from a port directly next to the vacuum pump line to a location several inches into the storage vessel, the condenser acts as a vapor-liquid separator since it makes it much more difficult for the vacuum pump to suck a large droplet of condensate into the vacuum line.





**Figure 52:** Condenser shape and orientation



**Figure 53:** Storage vessel and condenser positioning

The condensate flows into a stainless-steel storage vessel. The lid of the storage vessel is secured using KF quick-release cast clamps and sealed using a KF centering ring. This lid is modified to allow for the condenser outlet to go in through the lid. A Swagelok port with a hose barb is also attached to the lid.

Using the hose bars allows for a vacuum pump to be attached to the system so that regeneration can occur at sub-atmospheric pressure even when there is no compressor. The vacuum pump used during the sub-atmospheric pressure regeneration tests is a Welch DuoSeal 1400 vacuum pump [56]. This vacuum pump is shown in Figure 54.



**Figure 54:** Welch DuoSeal 1400 Vacuum Pump [56]

When undergoing regeneration, a temperature controller was used to control the power output to the resistance pad heater. An Inkbird ITC-100VH temperature controller was used to set the desired operating temperature. A Type-K thermocouple measuring the desiccant pan temperature was used to determine the operating temperature. The output of the temperature controller was connected to an Inkbird SSR-25 DA solid state relay. The solid-state relay was used to switch the power to the heater on and off, depending on the signal from the temperature controller. When the solid-state relay was connected, current could flow through the heating pad, subsequently heating up the regenerator. The electrical power being consumed by the temperature controller and resistance heater was monitored using a Kill-A-Watt meter. The temperature controller box is shown in Figure 55, while an electrical schematic of the temperature controller is shown in Figure 56.

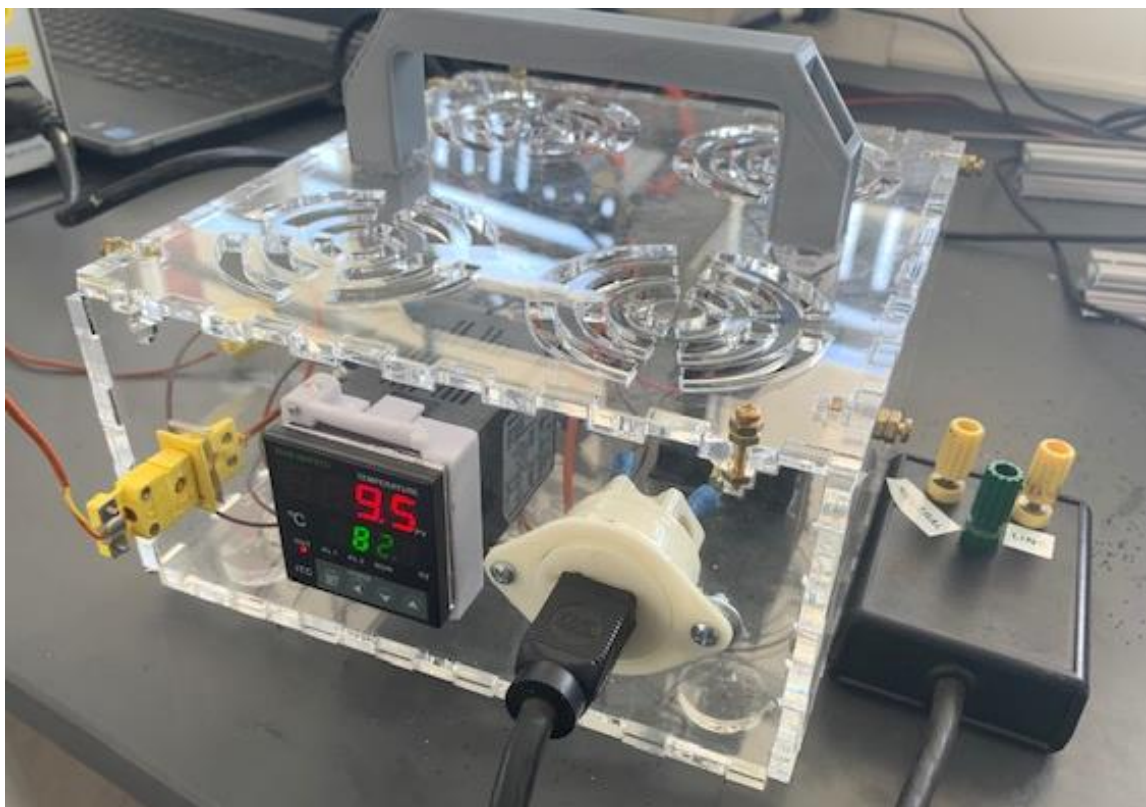


**Figure 55:** Temperature controller box

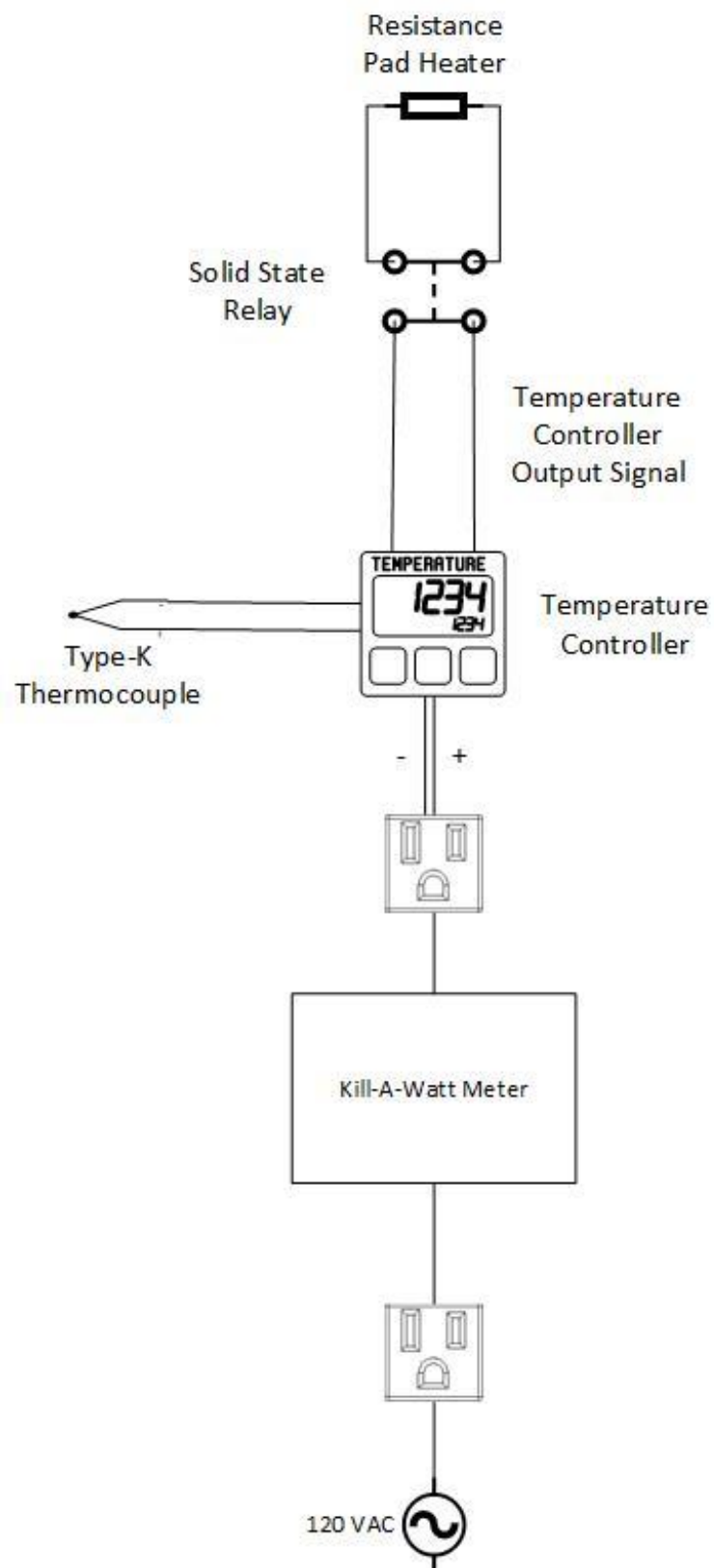


**Figure 56:** Temperature controller electrical schematic

The regenerator temperatures and pressure, condenser temperature, as well as the ambient temperature and relative humidity are all measured and recorded using National Instruments DAQ modules and Signal Express software. The thermocouple data was recorded using an NI 9213 module while the relative humidity and pressure data was recorded using an NI 9201 module. During testing, the power consumption of the heater and fan are also recorded using a Kill-a-Watt meter. An electrical schematic showing the DAQ system is given in Figure 57.

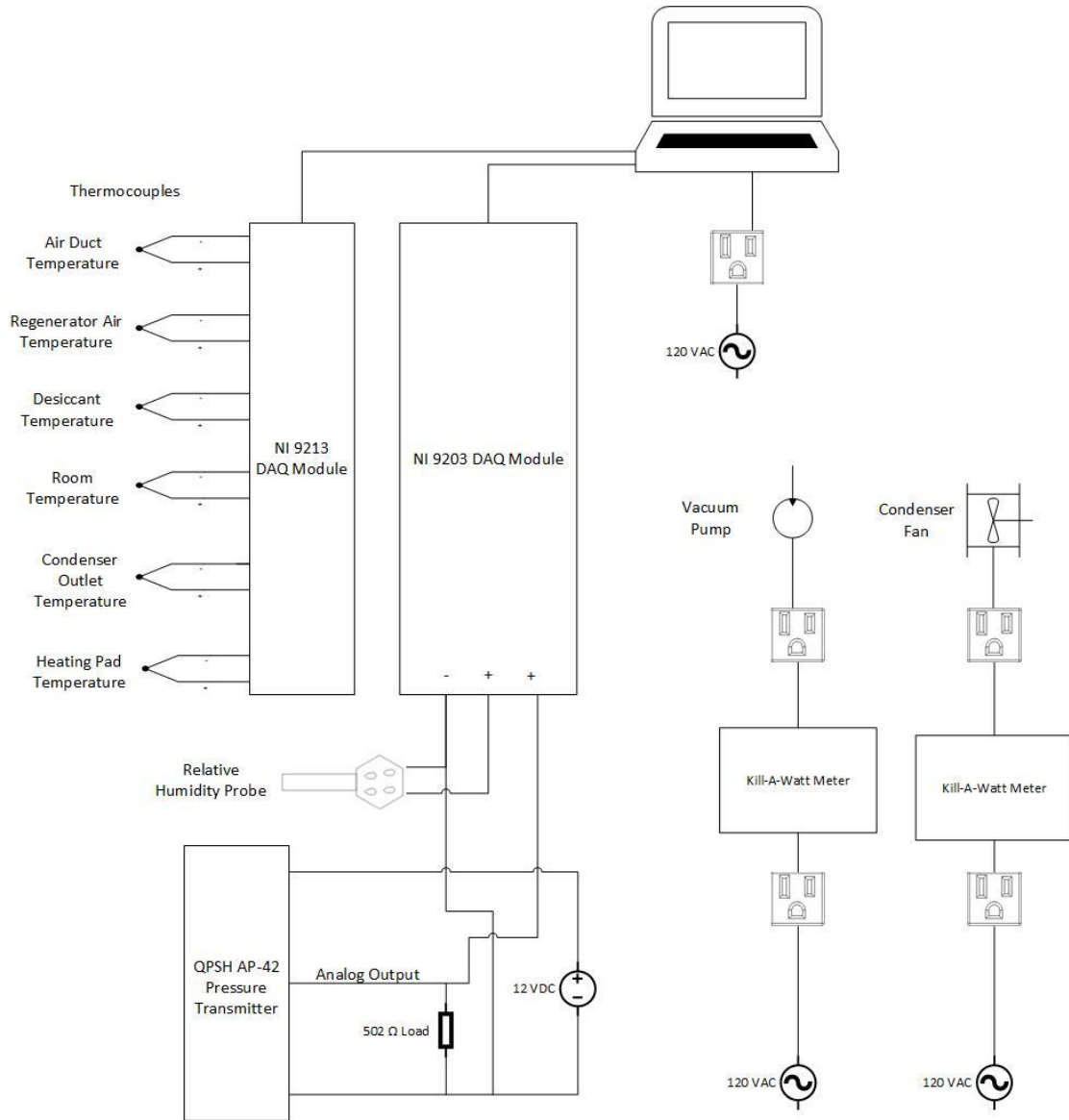


**Figure 57:** DAQ system electrical schematic



## Chapter 5: Prototype Evaluation and Modeling Validation

A DAWG system was run at atmospheric and sub-atmospheric pressure in order to measure the system energy consumption and condensate generation. By measuring the total energy consumption and condensate generation, an SEC value was calculated for each test and then compared to the theoretically predicted SEC value from the thermodynamic models operating under ideal conditions. Tests were run with both calcium chloride and lithium chloride desiccants. The energy flows into and out of the system were quantified for each test. Sometimes separate tests were run to verify some of these energy flows, such as the convective thermal losses. The condensate generated by these tests was subsequently evaluated using an Ion Chromatograph (IC) system and an Inductively Coupled Plasma Mass Spectrometer (ICP-MS) to test for desiccant loss and any contaminants in the water.

While a DAWG system with latent energy recovery was determined in the techno-economic analyses to be the optimal system configuration, latent energy recovery was not implemented in the system when testing the system's performance. This was due to difficulties in implementing a compressor that would be able to operate even if some water vapor were to condense while inside the compressor. Instead, a system with no energy recovery operating at either atmospheric or sub-atmospheric pressures was tested. Operating with these system configurations is still valuable as it shows whether the system can operate as predicted at a given regenerator temperature and pressure, and whether there are any additional system characteristics that should have been accounted for when performing the theoretical modeling.

### Convection Losses Testing

The main source of energy loss in the system is due to convective losses from the regenerator. This thermal load is one of the thermal energy loads being supplied by the resistance pad heater, with the sensible and latent heating energy loads being the others. These convective losses must be considered in order to know the sensible and latent energy loads of the system, which will ultimately be used to calculate the system's SEC.

When testing for convective losses, the system was completely sealed to ensure no mass flow into or out of the regenerator. A mass of ceramic particles was used to mimic the mass of desiccant solution in the regenerator. Desiccant solution could not be used during this test since the solution would boil and with the system sealed, the boiled water vapor would cause an increase in pressure, potentially turning the regenerator into a small bomb.

In order to test for convective losses, the system was heated until the system temperatures reached steady state, which indicates that the system is in equilibrium. The pad heater was supplied energy from a variable DC power supply. It was assumed that all the energy supplied by the variable DC power supply went into heating the regenerator and then exited the regenerator via convection. By varying the energy supplied to the pad heater, the system's convective losses at equilibrium and subsequently the equilibrium system temperatures would also be varied. Once the system reached equilibrium, the electric power, pad heater temperature, ceramic temperature, and air/lid temperature were recorded.

When modeling the heat loss, the regenerator was modelled as a cylinder with a known volume and surface area. Each surface of the cylinder was assumed to be isothermal. The bottom surface was held at the pad heater temperature, the sides were held at the desiccant/ceramic temperature, while the top surface was held at the air/lid temperature. Convection was facilitated at each of these surfaces due to a temperature gradient between the surface temperatures and the ambient temperature. This cylindrical model of the regenerator is shown in Figure 58.

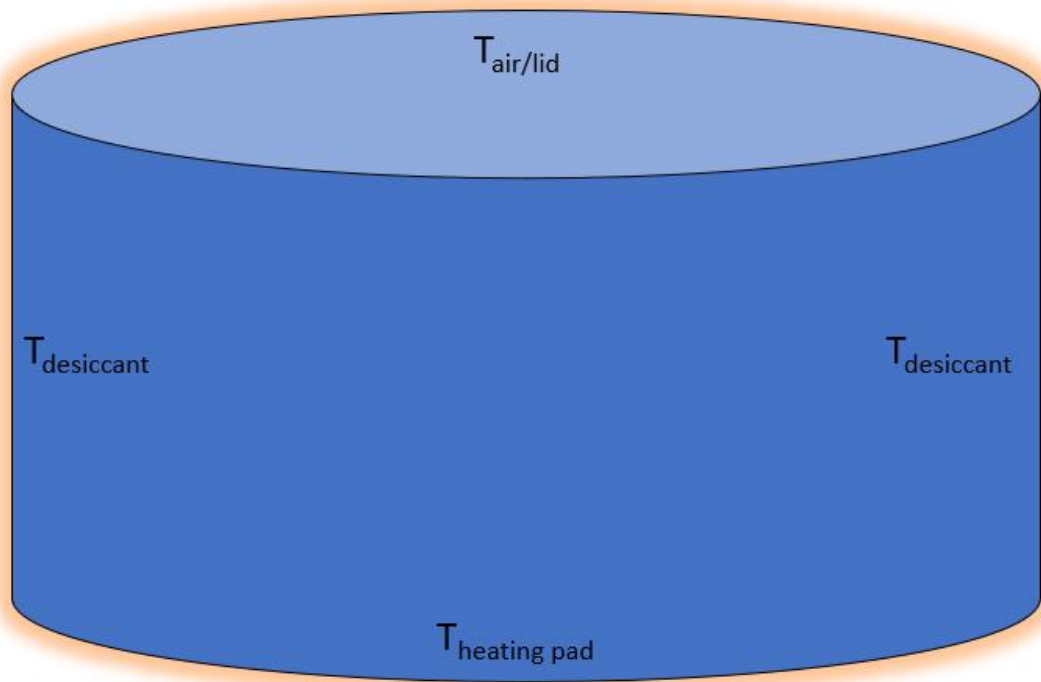


**Figure 58:** Cylindrical heat transfer model of the regenerator

In order to model the total convective loss from the regenerator, the value of the Overall Heat Transfer Coefficient,  $U$ , must be known. To find this value, an iterative approach was used to find the value of  $U$  which minimized the percent difference between the experimental and theoretical convective heat loss. Using this approach, the value of  $U$  was found to be  $1.923 \text{ W/m}^2\text{K}$ .

Once the overall heat transfer coefficient of the system is known, the model can be used to calculate the convective loss for a regeneration test, assuming the average heating pad, desiccant, and lid temperatures for the regeneration test are known. The equation used to model convective heat loss is given in Eq. 42.

$$Q_{conv} [W] = U \left( A_{bot}(T_{heating\ pad} - T_{amb}) + A_{side}(T_{desiccant} - T_{amb}) + A_{top}(T_{lid} - T_{amb}) \right) \quad (42)$$

### Prototype Testing – Atmospheric Pressure

For each test, regeneration occurred at atmospheric pressure. The desiccant solution would be regenerated between its dilute equilibrium desiccant mass fraction and a target concentrated desiccant mass fraction. This target concentrated desiccant mass fraction ranged between 0.45 –



0.6. Tests were run with both calcium chloride and lithium chloride desiccants. By knowing the desiccant type, regeneration pressure, and final mass fraction, a regeneration temperature could be calculated using equations from literature [36]. This regeneration temperature corresponds with the solution's saturation temperature while boiling at its highest mass fraction. A test matrix of the atmospheric pressure tests is shown in Table 25.

**Table 25:** Test matrix for tests conducted at atmospheric pressure

Target Desiccant Mass Fraction	Desiccant Type	Regeneration Temperature [°C]
0.4	CaCl <sub>2</sub>	117.3
0.45	CaCl <sub>2</sub>	123.5
0.5	CaCl <sub>2</sub>	130.5
0.55	CaCl <sub>2</sub>	138.0
0.6	CaCl <sub>2</sub>	145.8
0.45	LiCl	145.3
0.5	LiCl	154.3
0.55	LiCl	163.0
0.6	LiCl	171.1

## Testing Procedure

For each test, a regeneration test was performed. Regeneration involves a water absorption process and a water regeneration process. Diagrams showing the basic steps involved in both water absorption and regeneration are shown in Figures 59 and 60 respectively.

### Water Vapor Absorption Process

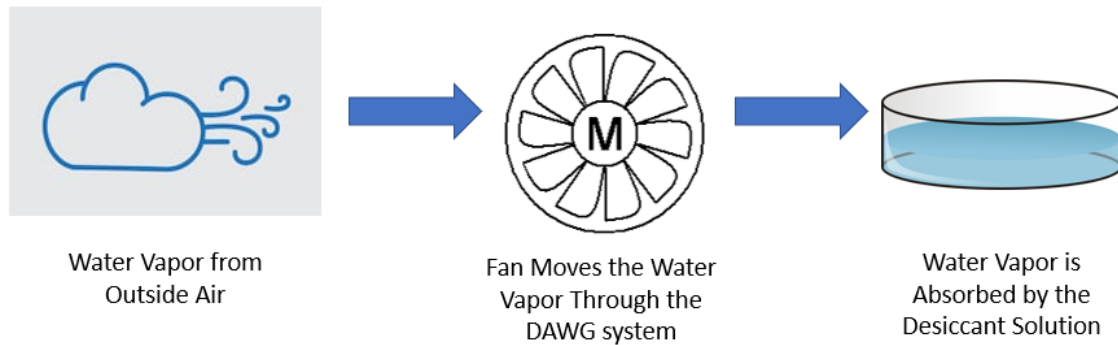


**Figure 59:** Diagram showing the process of water vapor absorption

## Water Vapor Regeneration Process

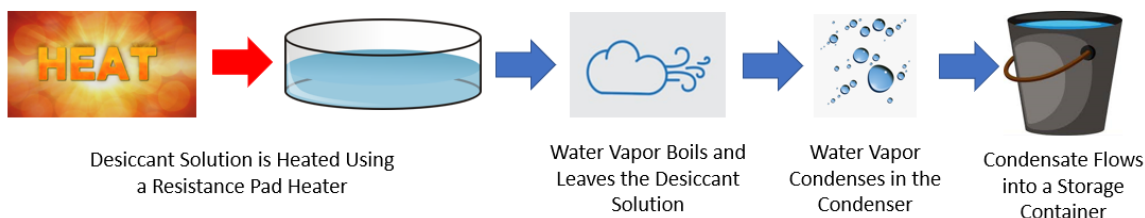


**Figure 60:** Diagram showing the process of water vapor regeneration

### *Initial Desiccant Solution Preparation*

When preparing the first batch of desiccant solution, a solution with known masses of desiccant and water was used. It was assumed in the analysis that the mass of desiccant in the solution does not change between each regeneration test. The amount of desiccant was chosen such that the predicted amount of condensate being generated would be less than the maximum amount of condensate that could be stored in the storage vessel.

### *Water Absorption*

A fan was run overnight blowing ambient outdoor air over the desiccant solution. By running the fan overnight, the desiccant solution was ensured to be at its equilibrium mass fraction by the time it undergoes regeneration. The fan used is powerful enough to both blow ambient moist air across the desiccant, as well as mix the desiccant solution. By partially enclosing the solution using the acrylic lid, the air swirled around above the solution, causing it to be mixed. The power consumption and run time are recorded in order to know the fan work required to blow the ambient air during the water absorption phase.

### *Initial Solution Property Measurement*

The density of the saturated desiccant solution is measured using a pycnometer and scale. The temperature of the solution is also measured. Using the density and temperature values, the initial mass fraction of the desiccant solution can be found using desiccant property relations found in literature [36]. Since the initial desiccant mass in the solution is known and is assumed to not change between tests, then the initial mass of water in the solution can also be calculated.

Several weather data measurements are recorded at the end of the water absorption process. These include the ambient dry bulb temperature, the ambient relative humidity, and the lab room dry bulb temperature. The local atmospheric pressure is found online using Weather Underground. Since the desiccant solution is boiled at this pressure, this pressure also corresponds to the solution vapor pressure.

### *Regeneration*

During each test, the desiccant solution was boiled until it reached a final target desiccant mass fraction. This final target desiccant mass fraction was different for each test, varying from 0.4 – 0.6. Using the solution vapor pressure and the final target mass fraction, the final desiccant saturation temperature could be found using relations from literature [36]. This saturation temperature corresponds to the temperature the solution will boil at once it reaches the final target mass fraction. Since this saturation temperature is the hottest temperature the desiccant should reach, this temperature is used as the target temperature set on the temperature controller. The

relationship between saturation temperature, vapor pressure, and desiccant mass fraction for calcium chloride solutions is shown using an Othmer chart like that in Figure 61. A similar figure for lithium chloride solutions is shown in Figure 62. In these figures, the blue lines show solutions of constant desiccant mass fraction while the red line shows the crystallization point of the solution.

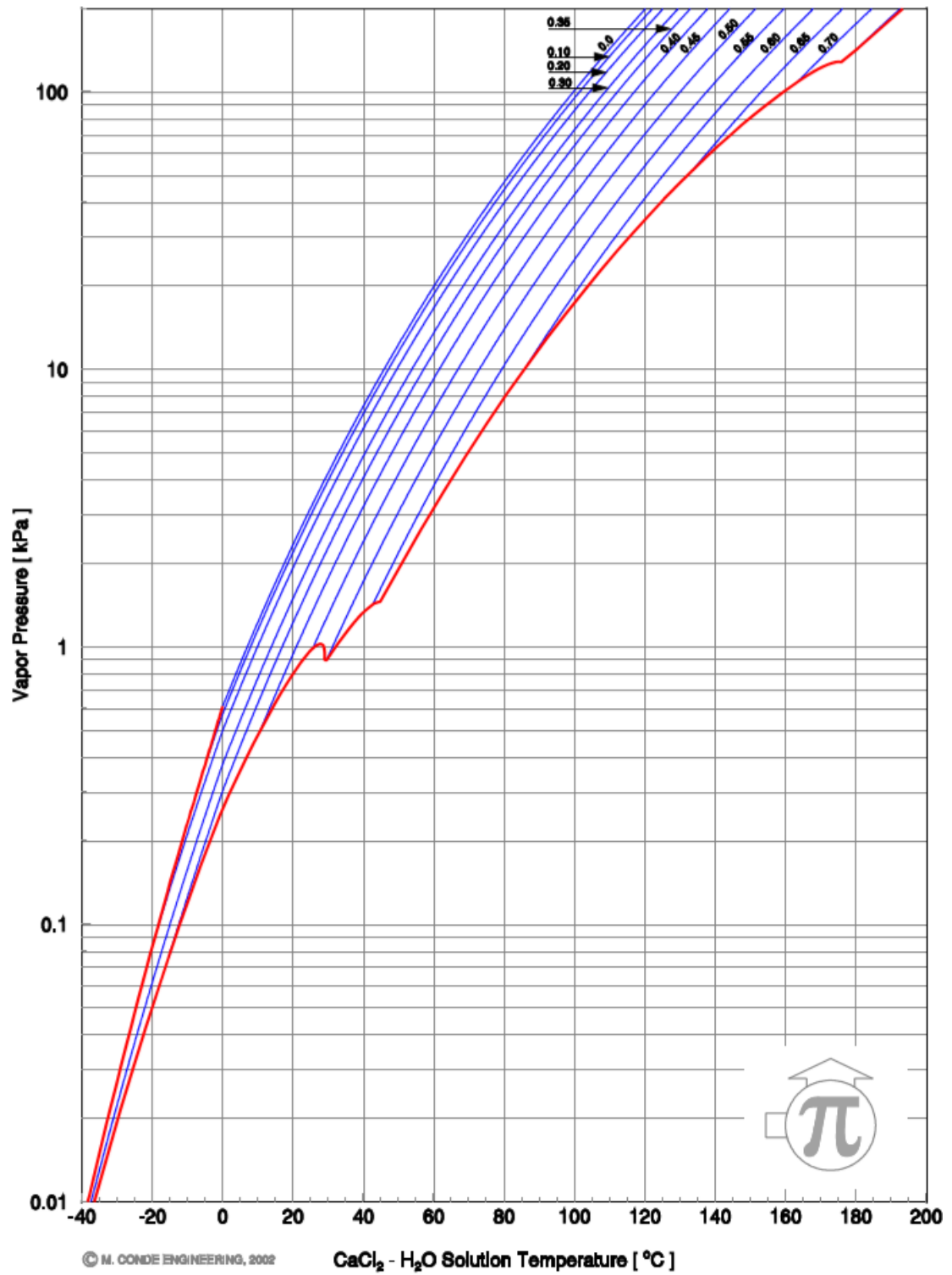


**Figure 61:** Othmer chart showing relation between solution temperature, vapor pressure, and desiccant mass fraction for  $\text{CaCl}_2$  solutions [36]

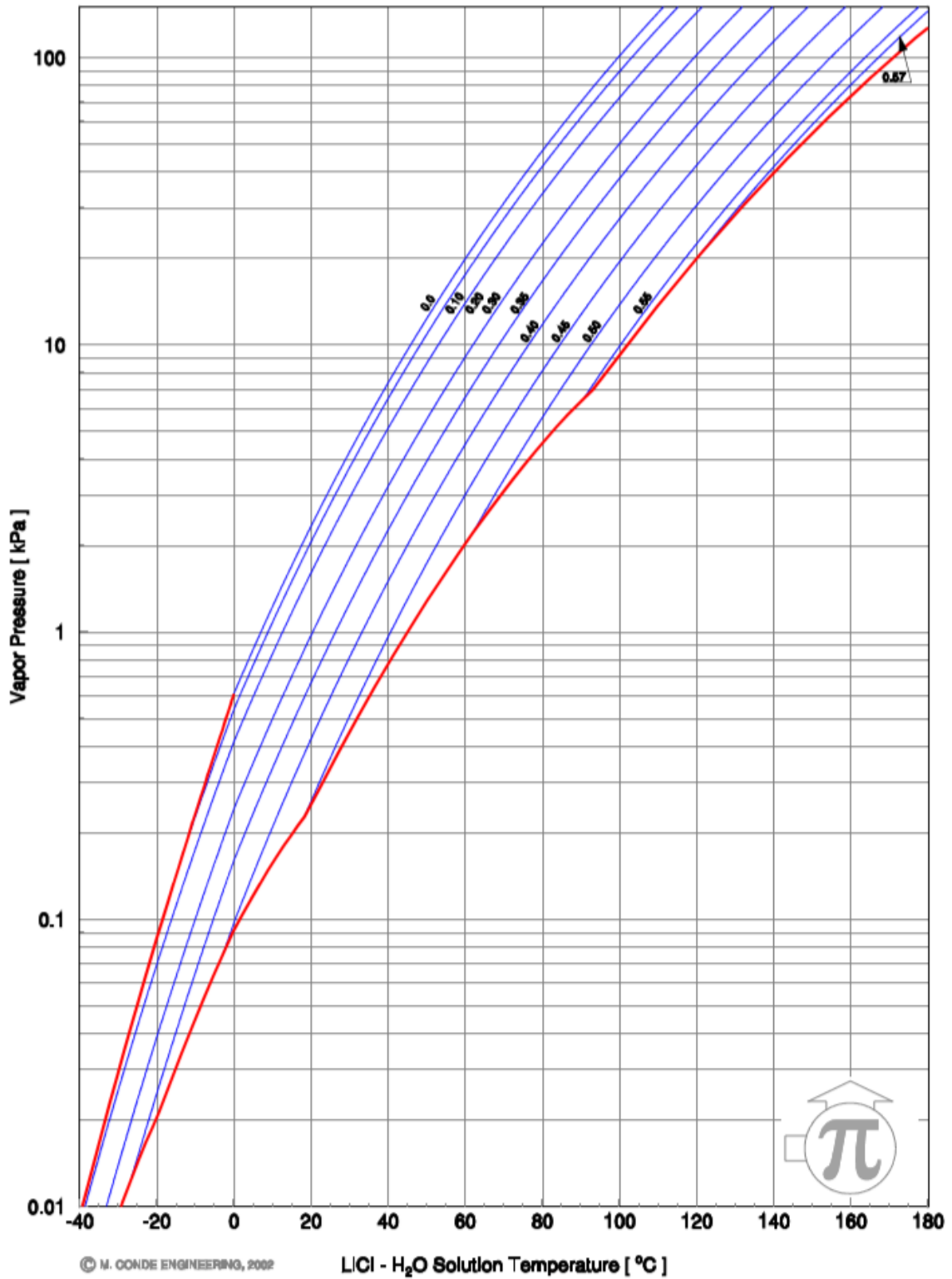


**Figure 62:** Othmer chart showing relation between solution temperature, vapor pressure, and desiccant mass fraction for LiCl solutions [36]

Once the system is set up to perform a regeneration test, the heater is plugged into the outlet on the temperature controller and the box fan cooling the condenser coils is plugged into a wall outlet. At each of these outlets, a Kill-A-Watt meter is used to measure the electrical energy usage at each outlet since the start of the regeneration test.

The system then heats up and boils off the absorbed water vapor. During this regeneration test, a DAQ system records the temperature of the heating pad, desiccant pan, desiccant solution, and air in the regenerator. The heater may be unplugged for portions of this heating phase in order to prevent the heating pad from overheating. Once the desiccant solution was at steady state, the heater and fan are unplugged. It was determined the solution was at steady state once its temperature leveled off to a constant temperature, which could be seen using the Signal Express DAQ interface. The final heater and fan electric work consumption as well as the maximum desiccant solution temperature are all recorded at this time. The regenerator is let to cool for several minutes to try and minimize the amount of steam that billows out of the regenerator and into the face of the person handling the system when the regenerator lid is eventually removed.

The condenser and storage vessel are removed together from the regenerator lid. Once the condenser and storage vessel are separated from one another, air is blown through the condenser to get out and remaining condensate. This remaining condensate also goes to the storage vessel. The mass of all the condensate collected is then measured.

#### *Final Solution Property Measurement*

Multiple methods were used to determine the final solution desiccant mass fraction. In any given test, typically two or three of these methods would be employed. One method involved measuring the solution density using the pycnometer to determine the solution's final mass fraction. This method is the most accurate method for determining mass fraction. However, this method does not work if the crystallization temperature of the desiccant solution is too high. If the crystallization temperature is too high, then the top layer of the desiccant solution will start to crystallize as it cools since it is the coldest region of the cooling solution. This can sometimes cause a layer of crystallized desiccant to cover the entire solution, as seen in Figure 63. If the solution is crystallizing then the solution is much more difficult to work with, since a pipette cannot be used to transfer the solution to the pycnometer without some of the desiccant crystallizing and clogging up the pipette.



**Figure 63:** Desiccant crystalizing after a regeneration test

The second method for determining the final solution desiccant mass fraction involves using the regenerator pressure and the maximum desiccant solution temperature. Using these values, a corresponding solution mass fraction can be used using fitted equations from literature [36]. This method does not work well if the desiccant solution hasn't yet reached equilibrium. If the desiccant solution hasn't held its maximum equilibrium temperature long enough, then the solution doesn't have enough time to allow all the water to vaporize, leading to this method measuring a final desiccant mass fraction that is too high.

The third method for determining the final solution desiccant mass fraction involves using the difference between the calculated water mass in the initial desiccant solution and the collected condensate mass to determine the mass of water in the final desiccant solution. Assuming no desiccant is lost from the solution during regeneration, then the final mass fraction can be calculated. If any condensate leaks out of the system or the water vapor doesn't make its way to the condenser and storage vessel, then the final desiccant mass fraction will be off when using this method.

A comparison of the final desiccant mass fraction values calculated using each of these methods over the course of both the atmospheric and sub-atmospheric pressure tests is given in Table 26.

**Table 26:** Comparison of final desiccant mass fraction measurement methods

MF target	MF from density	MF from temperature	MF from condensate mass
0.4	0.405	0.41	0.361
0.299	0.257	0.242	0.195
0.45	0.358	0.457	0.360
0.45	0.371	0.473	0.352
0.45	0.503	0.489	0.476
0.45	0.309	0.478	0.293
0.45	0.409	0.444	0.402
0.45	0.363	0.449	0.288
0.45	0.433	0.456	0.414
0.45	0.419	0.448	0.381

### Testing Results

The total SEC was calculated for each of the experiments run and compared to the theoretical SEC for the given ambient conditions. This SEC value was broken into its sensible and latent energy components, similarly to the thermodynamic AWG analyses. A fan for cooling the condenser as well as a fan for blowing and mixing the ambient air across the concentrated desiccant were used, and the effect of their electrical work on the total SEC is also shown. The results showing the SEC for the atmospheric DAWG tests with calcium chloride are shown in Figure 64.

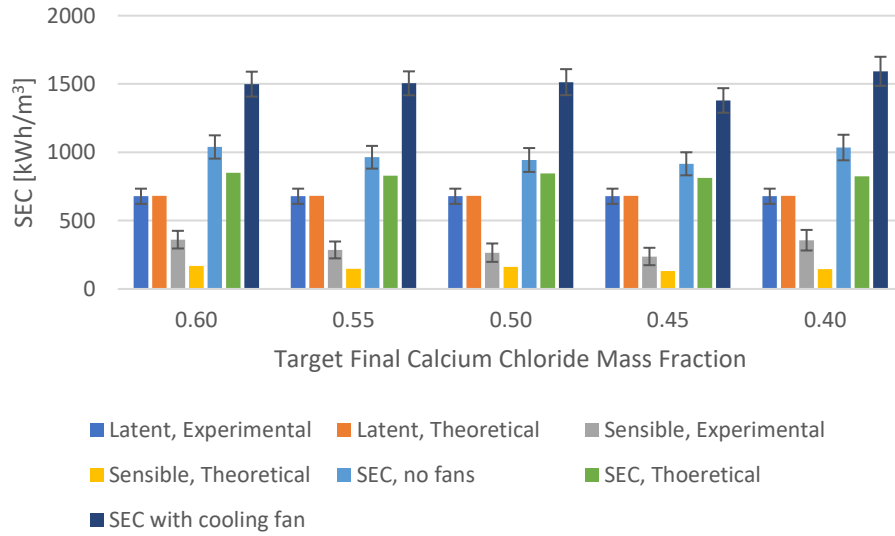
**Figure 64:** Experimental SEC breakdown for CaCl<sub>2</sub> at atmospheric pressure

Figure 64 shows the experimental SEC associated with the latent and sensible thermal energy loads and how they compare to the theoretical thermal energy loads. The thermal energy loads are supplied entirely from the resistance heating pad. The breakdown of the experimental thermal energy loads is given in Eq. 43.

$$Q_{heater} = Q_{sensible} + Q_{latent} + Q_{convective} = Q_{sensible} + m_{condensate}h_{fg} + Q_{convective} \quad (43)$$



The heater energy is known from the electrical energy supplied across the Kill-A-Watt meter. The latent energy load is known from the amount of condensate that is generated each test. The convective thermal losses are known by correlating the regenerator temperatures to the temperatures from the convection losses tests. Eq. 43 is then used to find the sensible thermal energy load.

The total theoretical SEC only accounts for the thermal energy loads. The equivalent experimental SEC is the SEC where the fan work is ignored, which is shown by the value of  $SEC_{no\ fans}$ . When incorporating the work associated with the box fan cooling the condenser, the total SEC becomes  $SEC_{with\ cooling\ fan}$ .

The results for the atmospheric DAWG tests with lithium chloride are shown in Figure 65.

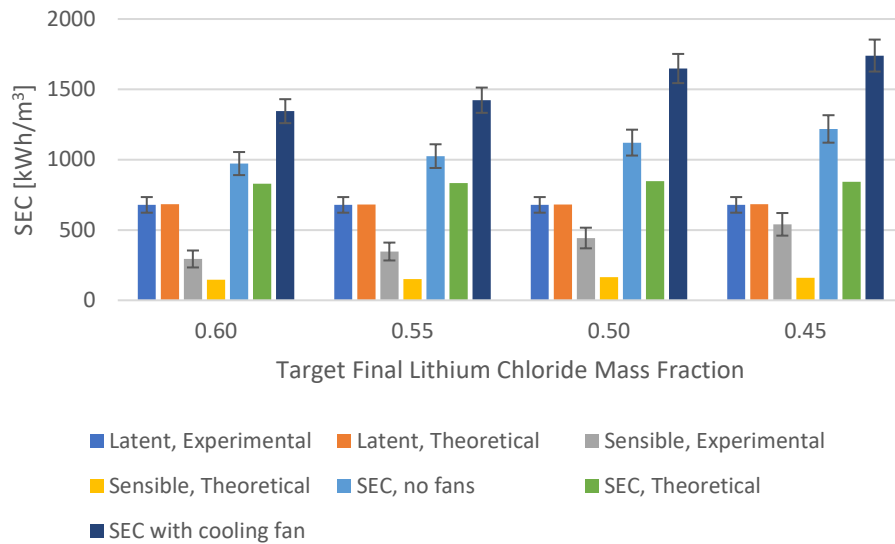


**Figure 65:** Experimental SEC breakdown for LiCl at atmospheric pressure

The results show that the latent energy load is the largest thermal energy load, as expected from the theoretical models. Additionally, the theoretical SEC is close in value to the experimental SEC, which is given by the value of  $SEC_{no\ fan}$ . The theoretical SEC is always a slightly less than the experimental SEC. This can be due to additional unaccounted thermal losses in the system.

Figures 62 and 63 show that the addition of a box fan to aid in heat transfer across the condenser causes a considerable increase in SEC. If the tubing of the heat exchanger were much longer, then the heat transfer across the condenser would be able to be performed via natural convection and a box fan would not be required. In this system configuration the cost of the box fan and its energy consumption is being traded for the material cost of additional heat exchanger tubing. The system SEC would then be better modeled as the value of  $SEC_{no\ fan}$ .

The fan being used during the water absorption phase operated at 32.4 W (12 V, 2.7 A) during each regeneration phase. This fan was oversized for the operation, as it was both blowing moist air across the desiccant and blowing hard enough to mix the desiccant solution. Additionally, the fan was run overnight or over the course of a few days between regeneration tests. However, the fan was powerful enough that a new regeneration test could have been performed after approximately 4-8 hours of water absorption. Using these reduced water absorption times, the mixing fan would

increase the system SEC by an additional 450-900 kWh/m<sup>3</sup>. While a smaller fan with a lower electrical power consumption could be used, it would come at the cost of a reduction of moist air flow rate. Reducing the flow rate of moist air would cause the water absorption phase to take longer, as well as make it more difficult to mix the desiccant solution to keep the water absorption rate high.

## Prototype Testing – Sub-Atmospheric Pressure

Several regeneration tests were also conducted at sub-atmospheric pressure. The purpose of the sub-atmospheric pressure tests was to ensure that the energetic performance of the system can be predicted by the thermodynamic models. In future tests, latent energy recovery may be implemented in the system, which would require the system to run at sub-atmospheric pressure. The performance of the system during those tests may be compared to the results of the sub-atmospheric pressure tests with no latent energy recovery in order to quantify the energetic benefit of performing latent energy recovery.

For each test, regeneration occurred at sub-atmospheric pressure, and the desiccant would be regenerated between its equilibrium desiccant mass fraction and a final target concentrated desiccant mass fraction of 0.45. A target final desiccant saturation temperature was chosen for each test, ranging from 80 – 95 °C. This corresponds to the target regeneration temperature. However, sometimes this target saturation temperature was slightly altered to have a corresponding regeneration pressure that could be achieved by the vacuum pump. Tests were run with both lithium chloride and calcium chloride desiccants. By knowing the desiccant type, final desiccant mass fraction, and final solution saturation temperature, a corresponding vapor pressure was determined for each test using equations from literature [36]. This vapor pressure corresponds with the regeneration pressure. A test matrix for the sub-atmospheric tests is given in Table 27.

**Table 27:** Test matrix for tests conducted at sub-atmospheric pressure

Desiccant Type	Regeneration Temperature [°C]	Regeneration Gauge Pressure [kPa]
CaCl <sub>2</sub>	95	-65.5
CaCl <sub>2</sub>	90	-71.4
CaCl <sub>2</sub>	85	-78.5
CaCl <sub>2</sub>	80	-83.5
LiCl	95	-85.1
LiCl	90	-88.7
LiCl	87.3	-91.0
LiCl	82.7	-93.0

## Testing Procedure

### *Initial Desiccant Solution Preparation*

The initial desiccant solution was prepared like the previous tests using a desiccant solution with a known initial mass of desiccant and water. The amount of desiccant used was chosen such that the amount of condensate generated each test would not be more than the maximum amount of condensate that could be stored in the storage vessel.

### *Water Absorption*

A fan is run overnight to ensure that the desiccant solution is saturated to its equilibrium mass fraction by the time regeneration occurs the next day. The power consumption and operating time of the fan are recorded in order to calculate the electric work consumed by the fan during the water vapor absorption phase.

### *Initial Solution Property Measurement*

The density and temperature of the desiccant solution are recorded in order to calculate the initial desiccant mass fraction. Since the desiccant mass is known and assumed to not change between tests, then the initial mass of water in the desiccant solution can be calculated.

Several weather data measurements are recorded including ambient dry bulb temperature, room temperature, and relative humidity. The local ambient pressure is found online using Weather Underground.

### *Regeneration*

For each test, water was regenerated from the solution until a final desiccant mass fraction of 0.45 was achieved. The final saturation temperature was varied for each test, ranging from 80 – 95 °C. This saturation temperature is the set temperature of the temperature controller. Using the final mass fraction and saturation temperature, the final saturation pressure could be calculated using fitted equations from literature [36]. This saturation pressure corresponds to the regenerator operating pressure for the regeneration test.

Once the system is set up to perform the regeneration test, the vacuum pump is turned on. Vacuum is pulled on the system until the desired regenerator pressure is reached. If the system were truly vacuum sealed, then the vacuum pump would only be turned on until the regenerator pressure is reached, at which point the system would hold its pressure and the vacuum pump could be turned off. However, the system has a small number of vacuum leaks which require the vacuum pump to be on for the entire regeneration test to ensure the regenerator maintains the desired pressure. Since the vacuum pump is always on, a throttling needle valve is used to create a pressure drop between the regenerator and the vacuum pump. By adjusting the opening of the needle valve, the pressure drop across the valve and subsequently the regenerator operating pressure can be adjusted.

Once the regenerator pressure is attained, then the heater and condenser fan are turned on. The Kill-A-Watt meters measuring the electrical energy going to the temperature controller, condenser fan, and vacuum pump are all reset at this time. The regeneration test occurs until the final saturation temperature is achieved. At this point the heater, condenser fan, and vacuum pump are turned off. The electrical work from the Kill-A-Watt meters, as well as the highest desiccant temperature are all recorded.

Once the regeneration test is complete, the regenerator is allowed to cool before opening the regenerator lid. The condenser and storage vessel are removed from the system. The mass of the collected condensate from the storage vessel and condenser is then measured. Air is blown through the condenser to ensure any condensate is blown out of the condenser and into the storage vessel.

### *Final Solution Property Measurement*

The final desiccant solution mass fraction is then determined using a combination of the three previously described methods. These include the density-based approach using the pycnometer, the theoretical temperature-based approach using the equilibrium desiccant temperature, or the mass-based approach using the mass of condensate collected.

### Drying Out the Vacuum Pump

After each regeneration test, the vacuum pump is sealed and turned on in order to boil off any water vapor that was sucked into the pump. The condensate in the storage vessel has a non-zero vapor pressure. This means there is some amount of vapor that is present above the liquid level in the storage vessel. Since the vacuum pump sucks out all the air in the regenerator, this pressure is caused by non-condensed water vapor. This water vapor is sucked into the tubing between the storage vessel and the vacuum pump. If there is enough of a temperature difference between the vapor and the ambient air, then the water vapor will condense in the tubing and fall back into the storage vessel. If there is not enough of a temperature difference or there is not enough length of tubing, then some of this vapor can end up in the vacuum pump, causing a decrease in pump performance. By boiling off any water vapor at the end of the test, the maximum vacuum pump performance can be retained for the next regeneration test.

### Testing Results

The SEC was calculated for the regeneration tests run at sub-atmospheric pressure. The breakdown of the SEC from the tests using calcium chloride is shown in Figure 66. The breakdown of the SEC from the tests using lithium chloride is shown in Figure 67.

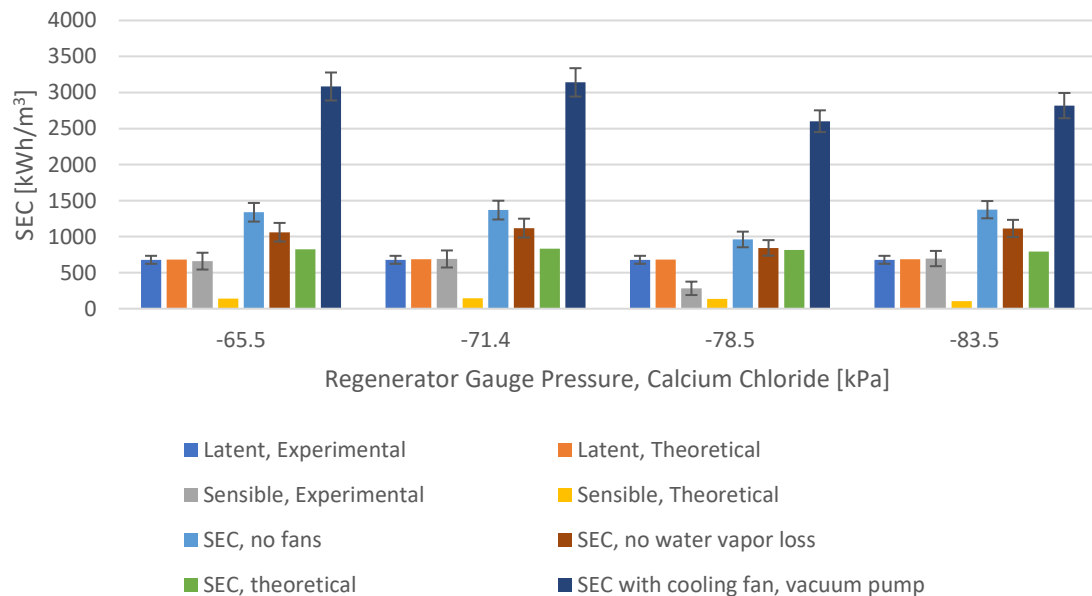


**Figure 66:** Experimental SEC breakdown for  $\text{CaCl}_2$  at sub-atmospheric pressure

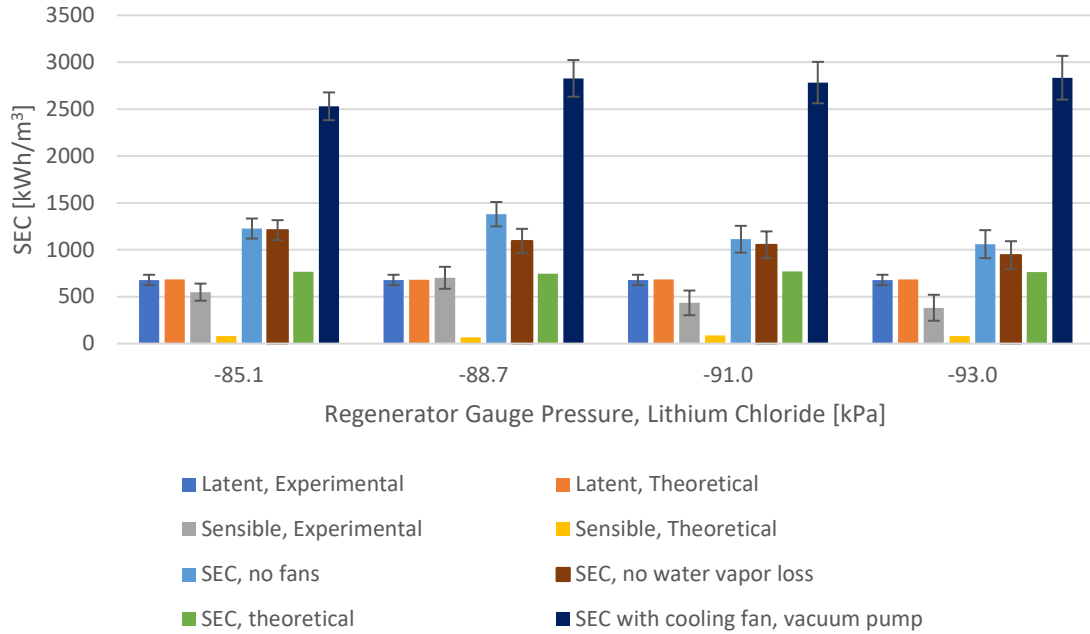


**Figure 67:** Experimental SEC breakdown for LiCl at sub-atmospheric pressure

Figures 66 and 67 show that the theoretical system SEC,  $SEC_{theoretical}$ , is always less than the corresponding experimental SEC,  $SEC_{no\ fans}$ . This can be explained by unaccounted thermal losses, as well as a loss in water vapor mass due to it getting sucked into the vacuum pump. During these sub-atmospheric pressure tests, an average of 16% of the regenerated water vapor mass was sucked into the vacuum pump rather than staying in the storage vessel, with some tests seeing as much as a 26% loss in water vapor mass through the vacuum pump. The effect of the water vapor loss on the SEC can be seen by comparing the values of  $SEC_{no\ fans}$  and  $SEC_{no\ water\ vapor\ loss}$ .

The results show that when incorporating the electric energy consumption of the cooling box fan and vacuum pump, the SEC more than doubles for each test. If the condenser were long enough to allow the water vapor to condense via natural convection, then the energy consumption of the cooling box fan would be eliminated. Similarly, if the system were able to hold its sub-atmospheric pressure without the vacuum pump continuously running, then the energy consumption of the vacuum pump would be nearly eliminated. In order to be able to hold a regeneration pressure, the system would need to be redesigned with better vacuum seal. Additionally, by not running the vacuum pump continuously, the amount of water vapor that gets sucked into the vacuum pump would be nearly eliminated, causing a slight decrease in the system's SEC.

## Modeling Validation

The comparison of the theoretical and experimental SEC values show that the thermodynamic model of the batch-style DAWG system was able to predict the system's performance, thus validating the model. While the actual experimental SEC was typically much higher than the theoretical SEC, the increase in SEC can be explained by differences between the experimental system and the theoretically modeled system.

One cause for differing SEC values was the use of a vacuum pump that operated continuously when operating at sub-atmospheric pressure. If the system had better vacuum seals, then the vacuum pump would only need to operate at the very beginning of the regeneration test in order to get the system to the desired regeneration pressure, rather than operating continuously throughout the entire regeneration test. This reduction in vacuum pump work would lead to a reduction in the system's SEC, leading to a better match between the experimental and theoretical SEC values.

Another cause for differing SEC values was the use of a box fan to cool the condenser and aid in convective heat transfer. If the condenser was longer, then the water vapor would be able to condense via natural convection rather than require the box fan for additional cooling. This would eliminate the work of the box fan and would lead to a further reduction in the system's SEC, leading to a better match between the experimental and theoretical SEC values.

A final cause for differing SEC values is unaccounted thermal losses and water vapor losses. Unaccounted thermal losses may be due to an oversimplified convective loss model which causes the amount of the convective heat loss to be underestimated. Another thermal loss may be due to the length of resistance heating wire that is heated before entering the regenerator. One source of unaccounted water vapor loss includes any water vapor that is sucked into the vacuum pump during regeneration. Additionally, if some of the water vapor stays in the regenerator rather than flowing into the condenser tubing or condenses on the lid of the regenerator rather than inside the condenser, this would cause an unaccounted water vapor loss. All these losses would lead to an increase in the experimental SEC and cause a worse match between the experimental and theoretical SEC values.

### Evaluation of Desiccant Loss

The condensate generated in the DAWG batch processes was analyzed to determine the extent of desiccant loss from the desiccant solution through the regeneration process. When calculating the desiccant mass fractions, it was assumed that the mass of desiccant in the solution was constant between tests. By verifying that there is a minimal amount of ions in the condensate associated with each desiccant, then the assumption of negligible desiccant loss can be upheld.

In order to determine the desiccant loss, a Dionex Model ICS-1500 and Model ISC-1600 Ion Chromatograph (IC) was used to measure  $\text{Ca}^{2+}$  and  $\text{Cl}^-$  loss, while an iCAP RQ Inductively Coupled Plasma Mass Spectrometer (ICP-MS) was used to measure  $\text{Li}^+$  loss. Condensate generated from a calcium chloride solution was tested for  $\text{Ca}^{2+}$  and  $\text{Cl}^-$  ions. Condensate generated from a lithium chloride solution was tested for  $\text{Li}^+$  and  $\text{Cl}^-$  ions.

When calculating the  $\text{Ca}^{2+}$  ion concentration, several cation standards were used to calibrate the IC. Five cation standards were used with concentrations of 0.5, 1, 5, 10, and 25 parts per million (ppm). When calculating  $\text{Cl}^-$  ion concentration, five anion standards were used to calibrate the IC with concentrations of 0.5, 1, 5, 10, and 25 ppm.

When calculating the  $\text{Li}^+$  ion concentration, several standards were used to calibrate the ICP-MS. Three standards were used with concentrations of 10, 25, and 50 parts per billion (ppb).

$\text{Ca}^{2+}$  ions had a concentration in the condensate of 8.68 ppm. When calculating desiccant loss, it was assumed that each  $\text{Ca}^{2+}$  ion corresponded on the loss of an entire  $\text{CaCl}_2$  molecule from the desiccant solution. Under these assumptions, it was calculated that 0.048 g  $\text{CaCl}_2$  was lost over the

course of all the atmospheric pressure regeneration tests using  $\text{CaCl}_2$  desiccant, which corresponds to a 0.025% loss in desiccant. The calculation of these values is given in Eqs. 44-46.

$$m_{\text{Ca}^{2+} \text{ loss}} = \left( \frac{8.68 \text{ g Ca}^{2+}}{10^6 \text{ mL H}_2\text{O}} \right) \left( \frac{1 \text{ mL H}_2\text{O}}{1 \text{ g H}_2\text{O}} \right) (1986.7 \text{ g H}_2\text{O}) = 0.017 \text{ g Ca}^{2+} \text{ lost} \quad (44)$$

$$m_{\text{CaCl}_2 \text{ loss}} = 0.017 \text{ g Ca}^{2+} \left( \frac{1 \text{ mol Ca}^{2+}}{40.08 \text{ g Ca}^{2+}} \right) \left( \frac{1 \text{ mol CaCl}_2}{1 \text{ mol Ca}^{2+}} \right) \left( \frac{110.98 \text{ g CaCl}_2}{1 \text{ mol CaCl}_2} \right) = 0.048 \text{ g CaCl}_2 \quad (45)$$

$$\text{CaCl}_2 \text{ loss [\%]} = \left( \frac{0.048 \text{ g CaCl}_2 \text{ lost}}{193.5 \text{ g CaCl}_2 \text{ used}} \right) * 100 = 0.025\% \text{ CaCl}_2 \text{ lost} \quad (46)$$

$\text{Cl}^-$  ions had a concentration in the condensate generated from  $\text{CaCl}_2$  desiccant of 6.49 ppm. When calculating desiccant loss, it was assumed that the loss of two chloride ions corresponded to the loss of one entire  $\text{CaCl}_2$  molecule from the desiccant solution. Under these assumptions, it was calculated that 0.020 g  $\text{CaCl}_2$  was lost over the course of all the atmospheric pressure regeneration tests using  $\text{CaCl}_2$  desiccant, which corresponds to a 0.010% loss in desiccant. The calculation of these values is given in Eqs. 47-49.

$$m_{\text{Cl}^- \text{ loss}} = \left( \frac{6.49 \text{ g Cl}^-}{10^6 \text{ mL H}_2\text{O}} \right) \left( \frac{1 \text{ mL H}_2\text{O}}{1 \text{ g H}_2\text{O}} \right) (1986.7 \text{ g H}_2\text{O}) = 0.013 \text{ g Cl}^- \text{ lost} \quad (47)$$

$$m_{\text{CaCl}_2 \text{ loss}} = 0.013 \text{ g Cl}^- \left( \frac{1 \text{ mol Cl}^-}{35.45 \text{ g Cl}^-} \right) \left( \frac{1 \text{ mol CaCl}_2}{2 \text{ mol Cl}^-} \right) \left( \frac{110.98 \text{ g CaCl}_2}{1 \text{ mol CaCl}_2} \right) = 0.020 \text{ g CaCl}_2 \quad (48)$$

$$\text{CaCl}_2 \text{ loss [\%]} = \left( \frac{0.020 \text{ g CaCl}_2 \text{ lost}}{193.5 \text{ g CaCl}_2 \text{ used}} \right) * 100 = 0.010\% \text{ CaCl}_2 \text{ lost} \quad (49)$$

$\text{Cl}^-$  ions had a concentration in the condensate generated from  $\text{LiCl}$  desiccant of 3.49 ppm. When calculating desiccant loss, it was assumed that the loss of each  $\text{Cl}^-$  ion corresponded to the loss of an entire  $\text{LiCl}$  molecule from the desiccant solution. Under these assumptions it was calculated that 0.0059 g  $\text{LiCl}$  was lost over the course of all the atmospheric pressure regeneration tests using  $\text{LiCl}$  desiccant, which corresponds to a 0.007% loss in desiccant. The calculation of these values is given in Eqs. 50-52.

$$m_{\text{Cl}^- \text{ loss}} = \left( \frac{3.49 \text{ g Cl}^-}{10^6 \text{ mL H}_2\text{O}} \right) \left( \frac{1 \text{ mL H}_2\text{O}}{1 \text{ g H}_2\text{O}} \right) (1408.3 \text{ g H}_2\text{O}) = 0.0049 \text{ g Cl}^- \text{ lost} \quad (50)$$

$$m_{\text{LiCl loss}} = 0.0049 \text{ g Cl}^- \left( \frac{1 \text{ mol Cl}^-}{35.45 \text{ g Cl}^-} \right) \left( \frac{1 \text{ mol LiCl}}{1 \text{ mol Cl}^-} \right) \left( \frac{42.39 \text{ g LiCl}}{1 \text{ mol LiCl}} \right) = 0.0059 \text{ g LiCl} \quad (51)$$

$$\text{LiCl loss [\%]} = \left( \frac{0.0059 \text{ g LiCl lost}}{79.9 \text{ g LiCl used}} \right) * 100 = 0.007\% \text{ LiCl lost} \quad (52)$$

$\text{Li}^+$  ions had a concentration in the condensate generated from  $\text{LiCl}$  desiccant of 741 ppb. When calculating desiccant loss, it was assumed that the loss of each  $\text{Li}^+$  ion corresponded to the loss of an entire  $\text{LiCl}$  molecule from the desiccant solution. Under these assumptions it was calculated that 0.0064 g  $\text{LiCl}$  was lost over the course of all the atmospheric pressure regeneration tests using  $\text{LiCl}$  desiccant which corresponds to a 0.008% loss in desiccant. The calculation of these values is given in Eqs. 53-55.

$$m_{\text{Li}^+ \text{ loss}} = \left( \frac{741 \text{ g Li}^+}{10^9 \text{ mL H}_2\text{O}} \right) \left( \frac{1 \text{ mL H}_2\text{O}}{1 \text{ g H}_2\text{O}} \right) (1408.3 \text{ g H}_2\text{O}) = 0.0010 \text{ g Li}^+ \text{ lost} \quad (53)$$

$$m_{\text{LiCl loss}} = 0.0010 \text{ g Li}^+ \left( \frac{1 \text{ mol Li}^+}{6.941 \text{ g Li}^+} \right) \left( \frac{1 \text{ mol LiCl}}{1 \text{ mol Li}^+} \right) \left( \frac{42.39 \text{ g LiCl}}{1 \text{ mol LiCl}} \right) = 0.0064 \text{ g LiCl} \quad (54)$$

$$LiCl \text{ loss } [\%] = \left( \frac{0.0064 \text{ g } LiCl \text{ lost}}{79.9 \text{ g } LiCl \text{ used}} \right) * 100 = 0.008\% \text{ } LiCl \text{ lost} \quad (55)$$

Each of these results show that there was a minimal amount of desiccant loss over the course of the regeneration tests. Therefore, the assumption of a constant desiccant mass in the desiccant solution between regeneration tests is reasonable.

## Condensate Contaminant Testing

The condensate was tested using the iCAP RQ ICP-MS in order to determine the concentration of different metal ion contaminants in the condensate. In addition to measurements for calcium, lithium, and chloride concentrations, measurements were also made to detect the concentrations of copper, iron, and lead in the condensate. Copper was chosen to be analyzed since the condenser is made of copper. Iron was chosen to be analyzed because the storage vessel and regenerator both contain stainless steel. Lead was chosen to be analyzed in case there was high levels of lead in any tap water or materials used throughout the tests.

The concentrations of these ions were compared to the Primary Drinking Water Standards set by the Environmental Protection Agency (EPA) as well as other levels discussed in literature [57] [58] [59] [60]. Primary Drinking Water Standards are regulations on the level of contaminants which may pose a health risk when in the drinking water supply. Two of these primary drinking water standards are the Maximum Contaminant Level (MCL) and Maximum Contaminant Level Goal (MCLG) [59]. The MCL is an enforceable standard which sets the highest level of a contaminant that is allowed in drinking water. The MCLG is a non-enforceable health benchmark goal which is set at a level at which no known or anticipated adverse effect on a person's health is expected. The comparison of the different ion concentrations in the condensate to the concentration levels found in literature is shown in Table 28.

**Table 28:** Comparison of condensate contaminant concentrations (ppb) to contaminant limits from literature

Contaminant	Condensate from CaCl <sub>2</sub>	Condensate from LiCl	MCL	MCLG	Other limits from literature
Lithium	26.935	741.334	-	-	700
Chloride	6492.9	3488.7	-	250,000	-
Calcium	8682.8	790	-	-	30,000
Iron	6.953	48.81	-	300	-
Copper	389.822	266.922	1300	1000	-
Lead	13.919	1.93	15	-	-

These results show the only contaminant concentration that is high is that of lithium in the condensate generated from LiCl. The limit for lithium is an estimate from literature and is not a limit which is enforced by the EPA. This literature value for the limit in LiCl concentration is related to the lowest observable effect level (20 mg/kg/day) that was observed in long-term studies and treatments of humans using lithium [61]. This value was used as a reference dose of lithium which, when dissolved in water, results in a limit of 700 ppb. The literature limit for calcium is that for soft water. Since the concentration of calcium is below this limit, a water softener would not be necessary with the condensate. The concentration of lead is high, and may pose an issue, especially if a trigger level for lead of 10 ppb becomes standard.



A survey scan of several other elements was performed by the ICP-MS during the condensate testing. This scan indicated that the concentration of nearly all other elements tested were lower than their respective MCL or MCLG. However, the scan did indicate a high level of silver in both condensate samples when compared to the MCLG for silver (100 ppb). Future tests may investigate the concentration of silver in the condensate to verify this result.

## Chapter 6: Conclusions and Future Work

Several AWG systems were analyzed in order to determine whether AWG is a feasible method of water generation which could be used in combatting water stress. In order to effectively combat water stress, AWG must be implemented in such a way which minimizes the energetic and economic cost of water production. The performance of each analyzed AWG system was compared using the metrics of SEC and LCOW, which measure the energetic and monetary cost of the water produced. The thermodynamic analyses found the operation point for each system configuration that would produce the lowest SEC. The economic analyses used the operating point of minimum SEC for each system and calculated its LCOW. These analyses showed that the optimal system configuration is a batch-style DAWG system with latent energy recovery, which has an SEC of 210 kWh/m<sup>3</sup> and an LCOW as low as 3.34 \$/m<sup>3</sup>. Future analyses may look to evaluate all the system operating points to find the one with the lowest LCOW, rather than only evaluating the operating point with the lowest SEC. Additionally, desiccants other than lithium chloride and calcium chloride may be analyzed to determine whether they have properties which result in a better theoretical system performance.

In order to best develop a DAWG system, the properties of the desiccant being used were analyzed to determine how to optimize both the rate and total amount of water absorption. These tests showed that the amount of desiccant solution being used should be maximized, with the solution being more spread out in order to increase the contact area between the desiccant solution and the moist air. Additionally, the desiccant solution should be mixed in order to ensure that the desiccant solution is homogenous, and the desiccant doesn't settle. Future work may involve developing different methods for mixing the desiccant solution. The current method of mixing involves using an oversized fan to swirl air above the desiccant solution. The development of other mixing methods should be explored which maintain the level of water absorption but reduce the energetic cost of mixing. Low-energy mixing will be particularly important if desiccant solutions with high desiccant concentrations continue to be used.

A prototype of a batch-style DAWG system with no energy recovery was developed in order to test and compare the system's performance to that predicted from the thermodynamic analyses. The results of the prototype testing demonstrated that the thermodynamic models can predict the performance of a batch-style DAWG system operating at a given temperature and pressure. Any inconsistencies between the theoretical and experimental SEC values can be explained by differences between the experimental system and the modeled system, as opposed to an error in the modeling approach.

When operating the system at sub-atmospheric pressure, the vacuum pump needed to be continuously operating in order to maintain the desired pressure. Without operating continuously, the system would slowly leak in ambient air and increase the system's pressure. Future redesigns of the system should look at minimizing the number of leaks in the system. This may be done by developing better approaches to sealing the system, as well as minimizing the number of interfaces that need to be sealed.

When condensing the water vapor, a box fan was needed for providing additional convective heat transfer for the water vapor to condense. If the condenser tubing was long enough, then the water vapor would be able to condense using just natural convection and a box fan would not be required. Future redesigns of the system should look at designing an affordable heat exchanger which can provide the necessary heat transfer via natural convection to condense the water vapor.

Future work also involves the design and implementation of a compressor and heat exchanger to perform latent energy recovery. One of the main challenges with implementing the compressor is

ensuring that the compressor will not be damaged or have its performance suffer if water vapor condenses while inside the compressor. This is made extra challenging due to the extremely high relative humidity at the inlet of the compressor. Additionally, oil shouldn't be used in the compressor to ensure that oil particulates don't end up in the condensate which may eventually be consumed. One possible solution may be the design of oil-less positive displacement compressor. Challenges with the latent energy recovery heat exchanger include optimizing heat transfer while choosing a heat exchanger material that will not corrode when in contact with a desiccant solution.

## References

- [1] K. Park, S. S. Chhatre and S. Srinivasan, "Optimal Design of Permeable Fiber Network Structures for Fog Harvesting," *Langmuir*, vol. 29, no. 43, pp. 13269-13277, 2013.
- [2] P. Gandhidasan and H. I. Abualhamayel, "Modeling and Testing of a Dew Collection System," *Desalination*, vol. 180, no. 1-3, pp. 47-51, 2005.
- [3] V. P. Starr, D. A. Anati and D. A. Salstein, "Effectiveness of controlled convection in producing precipitation," *Journal of Geophysical Research*, vol. 79, no. 27, pp. 1896-1977, 20 September 1974.
- [4] R. V. Wahlgren, "Atmospheric Water Vapour Processor Designs for Potable Water Production: A Review," *Water Research*, vol. 35, no. 1, pp. 1-22, 2001.
- [5] A. El-Ghonemy, "Fresh Water Production from/by Atmospheric Air for Arid Regions, Using Solar Energy: Review," *Renewable and Sustainable Energy Reviews*, vol. 16, no. 8, pp. 6384-6422, October 2012.
- [6] European Environment Agency, "Water Glossary," 2019. [Online]. Available: <https://web.archive.org/web/20190710174955/https://www.eea.europa.eu/themes/water/glossary>.
- [7] P. H. Gleick, "Basic Water Requirements for Human Activities: Meeting Basic Needs," *Water International*, vol. 21, no. 2, pp. 83-92, 1996.
- [8] M. Falkenmark, "The Massive Water Scarcity Now Threatening Africa: Why Isn't It Being Addressed?," *Ambio*, vol. 18, no. 2, pp. 112-118, 1989.
- [9] International Water Management Institute, "World water supply and demand. Colombo, Sri Lanka: International Water Management Institute," 2000.
- [10] D. Seckler, U. Amarasinghe, D. Molden, R. de Silva and R. Barker, "World water demand and supply, 1990 to 2025: Scenarios and issues. Research Report 19.," *International Water Management Institute*, 1998.
- [11] World Resources Institute, "Physical and Economic Water Scarcity," January 2009. [Online]. Available: <https://web.archive.org/web/20180820050400/http://www.wri.org/resource/physical-and-economic-water-scarcity>.
- [12] M. J. Moran, H. N. Shapiro, D. D. Boettner and M. B. Bailey, *Fundamentals of Engineering Thermodynamics*, 8 ed., 2014, p. 1030.
- [13] Ecoblue, "Ecoblue Water is Life," 2019. [Online]. Available: <https://web.archive.org/web/20190713191117/https://ecobluecorp.com/>.

- [14] B. L. Spletzer, D. S. Callow, L. C. Marron and J. R. Salton, "Method and apparatus for extracting water from air". Albuquerque, NM (US) Patent US6360549B1, 26 March 2002.
- [15] A. Dash and A. Mohapatra, "Atmospheric Water Generator: To meet the drinking water requirements of a household in coastal regions of India," 2015.
- [16] H. Kim, S. Yang, S. R. Rao and S. Narayanan, "Water harvesting from air with metal-organic frameworks powered by natural sunlight," *Science*, vol. 356, no. 6336, pp. 430-434, 28 April 2017.
- [17] H. Kim, S. R. Rao and E. A. Kapustin, "Adsorption-based atmospheric water harvesting device for arid climates," *Nature Communications*, vol. 9, no. 1191, 2018.
- [18] F. Fathieh, M. J. Kalmutzki and E. A. Kapustin, "Practical water production from desert air," *Science Advances*, vol. 4, no. 6, 8 June 2018.
- [19] K. Oshima, M. Yamazaki, T. Takewaki, H. Kakiuchi and A. Kodoma, "Application of novel FAM adsorbents in a desiccant system," *Kagaku Kogaku Ronbunshu*, vol. 32, no. 6, pp. 518-523, 2006.
- [20] M. Kumar and A. Yadav, "Comparative study of solar-powered water production from atmospheric air using different desiccant materials," *International Journal of Sustainable Energy*, vol. 9, no. 6, pp. 393-400, 26 June 2016.
- [21] M. Sultan, I. I. El-Sharkawy, T. Miyazaki, B. B. Saha and S. Koyoma, "An overview of solid desiccant dehumidification and air conditioning systems," *Renewable and Sustainable Energy Reviews*, vol. 46, pp. 16-29, June 2015.
- [22] J. Wang, J. Liu, R. Wang and L. Wang, "Experimental investigation on two solar-driven sorption based devices to extract fresh water from atmosphere," *Applied Thermal Engineering*, vol. 127, pp. 1608-1616, 25 December 2017.
- [23] G. William, M. Mohamed and M. Fatouh, "Desiccant system for water production from humid air using solar energy," *Energy*, vol. 90, no. 2, pp. 1707-1720, October 2015.
- [24] A. S. Inc., "System and Method for Producing Water". Patent US20080135495A1, 12 June 2008.
- [25] P. Gandhidasan and H. Abualhamayel, "Water recovery from the atmosphere," *Renewable Energy*, vol. 9, no. 1-4, pp. 745-748, September-December 1996.
- [26] P. Gandhidasan and H. Abualhamayel, "Investigation of humidity harvest as an alternative water source in the Kingdom of Saudi Arabia," *Water and Environmental Journal*, vol. 24, no. 4, 28 October 2010.
- [27] H. Abualhamayel and P. Gandhidasan, "A method of obtaining fresh water from the humid atmosphere," *Desalination*, vol. 113, no. 1, pp. 51-63, November 1997.

- [28] A. M. Hamed, "Absorption-regeneration cycle for production of water from air-theoretical approach," *Renewable Energy*, vol. 19, no. 4, pp. 625-635, April 2000.
- [29] J. Winkler, "Laboratory Test Report for Fujitsu 12RLS and Mitsubishi FE12NA Mini-Split Heat Pumps," Golden, CO, 2011.
- [30] D. O'Connor, J. K. S. Calautit and B. R. Hughes, "A Review of Heat Recovery Technology for Passive Ventilation Applications," *Renewable and Sustainable Energy Reviews*, no. 54, pp. 1481-1493, 2016.
- [31] D. Seker, H. Karatas and N. Egrican, "Frost formation on fin-and-tube heat exchangers. Part I - Modeling of frost formation on fin-and-tube heat exchangers," *International Journal of Refrigeration*, vol. 27, pp. 367-374, 2004.
- [32] K. Prölss and G. Schmitz, "Modeling of Frost Growth on Heat Exchanger Surfaces," *energy*, vol. 10, pp. 509-516, 2006.
- [33] D. Bergmair, S. Metz, H. de Lange and A. van Steenhoven, "System analysis of membrane facilitated water generation from air humidity," *Desalination*, vol. 339, pp. 26-33, 15 April 2014.
- [34] D. T. Bui, M. K. Ja, J. M. Gordon, K. C. Ng and K. J. Chua, "A thermodynamic perspective to study energy performance of vacuum-based membrane dehumidification," *Energy*, vol. 132, pp. 106-115, 1 August 2017.
- [35] Y. Yang, D. Rana, C. Q. Lan and T. Matsuura, "Development of Membrane-Based Desiccant Fiber for Vacuum Desiccant Cooling," *ACS Applied Materials & Interfaces*, vol. 8, no. 24, pp. 15778-15787, 2 June 2016.
- [36] M. R. Conde-Petit, "Aqueous solutions of lithium and calcium chlorides: -Property formulations for use in air conditioning equipment design," M. Conde Engineering, Zurich, Switzerland, 2014.
- [37] H. El-Dessouky, H. I. Shaban and H. Al-Ramadan, "Steady-state analysis of multi-stage flash desalination process," *Desalination*, vol. 103, no. 3, pp. 271-287, December 1995.
- [38] C.-C. Chen, H. I. Britt, J. F. Boston and L. B. Evans, "Local Composition Model for Excess Gibbs Energy of Electrolyte Systems," *AIChE Journal*, vol. 28, no. 4, pp. 588-596, July 1982.
- [39] K. S. Spiegler and Y. M. El-Sayed, A desalination primer: introductory book for students and newcomers to desalination, 1994.
- [40] Lazard, "Lazard's Levelized Cost of Energy Analysis - Version 12.0," 2018.
- [41] National Renewable Energy Laboratory, "High-Concentration III-V Multijunction Solar Cells," U.S. Department of Energy, [Online]. Available: <https://web.archive.org/web/20190508135020/https://www.nrel.gov/pv/high-concentration-iii-v-multijunction-solar-cells.html>. [Accessed 2019].

- [42] H. Goodwin, T. C. Jellicoe, N. J. Davis and M. L. Bohm, "Multiple exciton generation in quantum dot-based solar cells," *Nanophotonics*, vol. 7, no. 1, pp. 111-126, 1 1 2018.
- [43] SupplyHouse.com, "Compressor Refrigeration," 2019. [Online]. Available: <https://web.archive.org/web/20191212020840/https://www.supplyhouse.com/>.
- [44] ACR News, "Compressors: Don't blame the compressor!," 1 November 2009. [Online]. Available: <https://web.archive.org/web/20171014014529/http://www.acr-news.com/compressors-dont-blame-the-compressor--->.
- [45] Cole-Parmer, "Low-Flow Positive Displacement Flexible Impeller Pump, 120 VAC," 2019. [Online]. Available: <https://web.archive.org/web/20191211205418/https://www.coleparmer.com/>.
- [46] Cat Pumps, "How long will a Cat Pump last? - Preventative Maintenance".
- [47] Department of Energy (DOE) Office of Energy Efficiency and Renewable Energy (EERE), *Solar Desalination. Funding Opportunity Announcement (FOA) Number: DE-FOA-0001778*.
- [48] The Home Depot, "Baseboard and Floor Heaters," 2019. [Online]. Available: <https://web.archive.org/web/20191212035343/https://www.homedepot.com/>.
- [49] Square One, "Getting to know electric baseboard heaters," [Online]. Available: <https://web.archive.org/web/20191212201847/https://www.squareoneinsurance.com/us/electric-baseboard-heaters>.
- [50] EComfort, "M-Series Wall Mounted Air Conditioning System," Mitsubishi Electric - Cooling and Heating, [Online]. Available: <https://web.archive.org/save/https://www.ecomfort.com/Mitsubishi-MZ-GL12NA/p65348.html>.
- [51] Hannabery HVAC, "Heat Pumps 101," 2019. [Online]. Available: <https://web.archive.org/web/20191212201955/https://www.hannabery.com/heat-pumps101-faqs.shtml>.
- [52] U. Caldera, D. Bogdanov, S. Afanasyeva and C. Breyer, "Role of seawater desalination in the management of an integrated water and 100% renewable energy based power sector in Saudi Arabia," *Water*, vol. 10, no. 1, p. 3, 2018.
- [53] PaintingValley.com, Artist, *Petri Dish Sketch*. [Art]. Painting Valley, 2019.
- [54] profiCAD, Artist, *Fan*. [Art]. profiCAD, 2019.
- [55] B. I. Morsi and O. M. Basha, "Mass Transfer in Multiphase Systems, Mass Transfer - Advancement in Process Modelling," IntechOpen, 2015.
- [56] Welch Vacuum, "Welch DuoSeal 1400," 2019. [Online]. Available: <https://web.archive.org/save/https://welchvacuum.com/products/duoseal-1400>.

- [57] B. Oram, "Lithium in Drinking Water," Water Research Center, 2014.
- [58] B. L. Balentine, "Permissible Limits for Metals," [Online]. Available: <https://web.archive.org/web/20191212201716/https://www.occeweb.com/og/metals-limits.pdf>.
- [59] Office of Water, "2018 Edition of the Drinking Water Standards and Health Advisories Tables," Washington, DC, 2018.
- [60] P. Sengupta, "Potential Health Impacts of Hard Water," *International Journal of Preventative Medicine*, vol. 4, no. 8, pp. 866-875, 2013.
- [61] Virginia Department of Health, "Fact Sheet on Lithium," 1997.